

**Democratic and Popular Republic of Algeria
Ministry of Higher Education and Scientific Research**



**ABOU BAKR BELKAID UNIVERSITY
DEPARTMENT OF TELECOMMUNICATION
LABORATORY OF TELECOMMUNICATION
Faculty of Engineering Sciences**



**Doctoral Thesis
Option: Telecommunications**

Title of the Thesis

**NONLINEAR PROPAGATION OF AN ULTRASHORT
LASER PULSE IN TITANIUM SAPPHIRE**

Presented by:

M^f: KHELLADI Mounir

Promoter:

P: O .SEDDIKI

Members of the Examination committee

Professor: K.E. GHAF FOUR

Chairperson

Professor: M. CHIKH BLED

Professor: G. BASSOU

Professor: R. NAOUM

Academic year 2009-2010

Abstract:

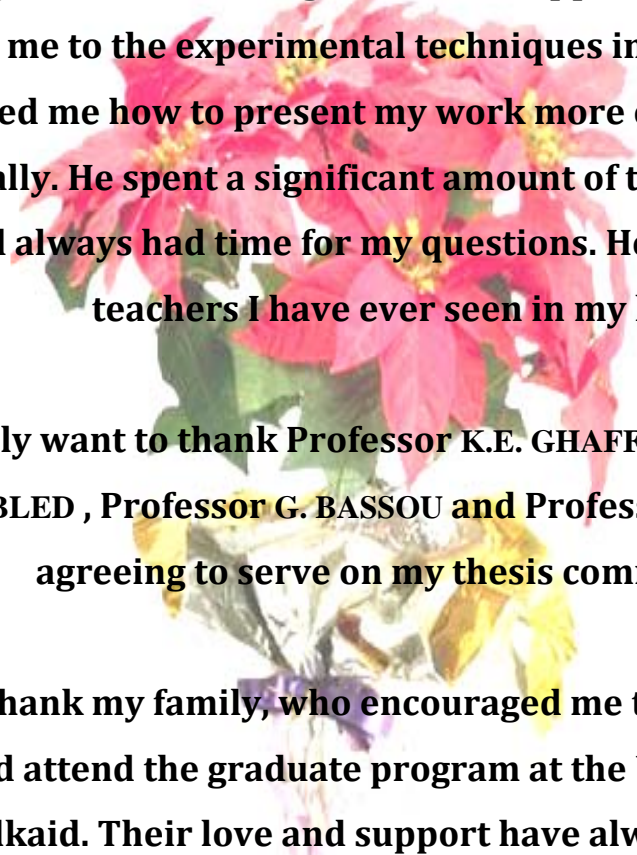
Wave propagation in dispersive nonlinear media has become a topic of intense research activities, in part stimulated by its potential application to optical fiber communication systems. Propagation of optical pulses in Titanium Sapphire is mainly influenced by the group velocity dispersion and the refractive index nonlinearity. Rapid progress in ultra short time laser technology has made it possible that optical pulses with durations comparable to the carrier oscillation cycle can be generated. The propagation of such ultra short and intense pulses is then affected by additional physical mechanisms, where especially higher order effects become important. Highly nonlinear operating conditions or the interplay between the different linear and nonlinear effects can result in dramatic changes of the temporal and spectral properties of the pulse.

The propagation of an ultra short pulse is governed by a generalized nonlinear Schrödinger equation (NLSE), which can be derived from the underlying Maxwell equations within the slowly varying envelope approximation. We solve numerically a generalized Schrodinger equation by using a split step Fourier method. Effects such as the impacts of group velocity dispersion (GVD), third order dispersion (TOD), self phase modulation (SPM), wave breaking (WB), self steepening (SS), and intrapulse stimulated Raman scattering (ISRS) are demonstrated in detail. Examples for the above effects are demonstrated, as well as their interplay in the context of soliton propagation. The numerical method therefore presents an advantage tool for describing the ultra short pulse laser propagation in Titanium sapphire.

Keywords: Titanium sapphire, ultra short laser pulse, Generalized Nonlinear Schrodinger Equation, Group Velocity Dispersion, Self Phase modulation, Soliton.

ACKNOWLEDGEMENTS

I would like to give special thanks to my advisor Dr. Omar Seddiki, for his guidance, encouragement and support. Not only did he introduce me to the experimental techniques in optics, but he also showed me how to present my work more effectively and professionally. He spent a significant amount of time supervising this work and always had time for my questions. He is one of the best teachers I have ever seen in my life.



I especially want to thank Professor K.E. GHAF FOUR , Professor M. CHIKH BLED , Professor G. BASSOU and Professor R. NAOUM for agreeing to serve on my thesis committee.

I want to thank my family, who encouraged me to travel away from home and attend the graduate program at the University of Abou Bakr Belkaid. Their love and support have always given me the energy to work.

Finally, I would like to express my sincere regards to the great physicist of all times, Elbert Einstein, for what he accomplished in science in general and physics in particular.

TABLE OF CONTENTS

General Introduction	0
Chapter I: Titanium Sapphire Theory	5
1.1. Optoelectronics	6
1.2. Sapphire and Ti: sapphire.....	7
1.2.1. Overview.....	7
1.2.2. Structure of sapphire and Ti: Sapphire.....	8
1.2.3. Spectroscopy of sapphire and Ti-doped sapphire.....	9
1.2.4. Influence of Ti ⁴⁺ and defects on Ti: sapphire spectroscopy.....	10
1.3. Refractive Index.....	12
1.3.1. Chromatic Dispersion.....	13
1.4. Fiber Nonlinearities.....	15
1.4.1. Nonlinear Refraction.....	16
1.5. Chapter Summary	17
Chapter II: Ultra short Laser Pulse Generation and Compression	19
2.1. Introduction.....	20
2.1.1. Definitions.....	22
2.1.1.1. Absorption.....	22
2.1.1.2. Spontaneous Emission.....	22
2.1.1.3. Stimulated Emission.....	22
2.1.2. Longitudinal Modes.....	22
2.1.2.1. Pulsed Operation.....	25
2.1.3. Mode-locking techniques.....	25
2.1.3.1. Active Mode-Locking.....	28
2.1.3.2. Passive Mode-Locking.....	30
2.1.3.3. Kerr Lens Mode-Locking.....	32
2.1.4. Applications.....	35
2.1.4.1. Mode-Locked Rhodamine 6G Dye Lasers.....	35
2.1.4.2. The Mode-locked Laser Oscillator.....	36
2.2. Ultrashort Lasers Pulses	37
2.2.1. Mathematical Description of Laser Pulses.....	39
2.2.1.1. Time Domain Description.....	40
2.2.1.2. Frequency Domain Description.....	41
2.2.2. Propagation of a Light Pulse in Transparent Medium.....	42
2.2.3. Dispersion Parameter of a Transparent Medium.....	44
2.2.3.1. Temporal study of the widening of ultra-short pulses introduced by the elements of the cavity.....	45
2.2.4. Time-Frequency Decomposition.....	46
2.2.4.1. Wavelet Theory.....	46
2.2.4.2. Wavelet Techniques.....	47
2.2.4.3. Simulations and Comparison with silica fiber.....	49
2.3. Cavity Alignment.....	52
2.3.1. Group Velocity Dispersion.....	52
2.3.2. Self Phase Modulation.....	53
2.3.3. Prismatic Group Delay Dispersion Compensator.....	54
2.3.4. Time-Compression with a Pair of Gratings.....	56
Chapter III: Nonlinear Effects Modeling	59
3.1. Maxwell's Equations.....	60
3.2. Fiber Modes.....	63

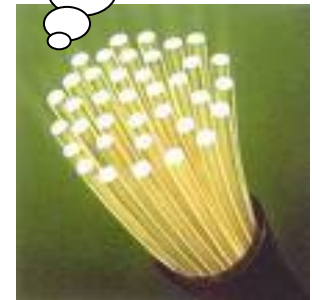
3.2.1. Eigen value Equation.....	63
3.2.2. Single-Mode Condition.....	66
3.2.3. Characteristics of the Fundamental Mode.....	66
3.3. Pulse-Propagation Equation.....	68
3.3.1. Nonlinear Pulse Propagation.....	68
3.3.2. Higher-Order Nonlinear Effects.....	70
3.4. Numerical Method.....	72
3.4.1. Introduction.....	72
3.4.2. Split-Step Fourier Method.....	73
3.5. Chapter Summary.....	73
Chapter IV: Group Velocity Dispersion.....	75
4.1. Different Propagation Regimes.....	76
4.2. Dispersion-Induced Pulse Broadening.....	78
4.2.1. Gaussian Pulses.....	79
4.2.2. Chirped Gaussian Pulses.....	82
4.2.3. Hyperbolic-Secant Pulses.....	84
4.2.4. Super-Gaussian Pulses.....	85
4.3. Third-Order Dispersion.....	86
4.3.1. Changes in Pulse Shape.....	87
4.4. Dispersion Compensation.....	89
4.4.1. Compensation of Third-Order Dispersion.....	90
Chapter V: Self Phase Modulation.....	93
5.1. SPM-Induced Spectral Broadening.....	94
5.1.1. Nonlinear Phase Shift.....	95
5.1.2. Changes in Pulse Spectra.....	97
5.1.3. Effect of Pulse Shape and Initial Chirp.....	99
5.2. Effect of Group-Velocity Dispersion.....	102
5.2.1. Pulse Evolution.....	102
5.2.2. Optical Wave Breaking.....	104
5.2.3. Effect of Third-Order Dispersion.....	109
5.3. Higher-Order Nonlinear Effects.....	112
5.3.1. Self-Steepening.....	113
5.3.2. Effect of GVD on Optical Shocks.....	116
5.3.3. Intrapulse Raman Scattering.....	118
5.4. Chapter Summary.....	118
Chapter VI: Generalized Nonlinear Schrodinger Equation.....	120
6.1. Modulation Instability.....	121
6.1.1. Linear Stability Analysis.....	121
6.2. Fiber Solitons.....	122
6.2.1. Fundamental Soliton.....	123
6.2.2. Higher-Order Solitons.....	125
6.3. Higher-Order Effects.....	127
6.3.1. Third-Order Dispersion.....	128
6.3.2. Self-Steepening.....	130
6.3.3. Intrapulse Raman Scattering.....	133
6.4. Propagation of Femtosecond Pulse.....	136
Conclusion General.....	140
Appendices, Lists of Publications, Sigles and Acronyms.....	144

GENERAL INTRODUCTION

I am thinking about
some interesting
materials; but is a
series which is titanium
sapphire



Are there any
materials that react
correctly to an 800
nm wavelength?



Let's see if this
material can verify
that condition



GENERAL INTRODUCTION

In recent years, optical fibers have increasingly replaced the traditional coax cable for long distance telecommunication, and transmission speeds of over $1Tbits/s$ can now be achieved over one single optical fiber. Accompanied with the rapid growth in optical telecommunications, the spectroscopy studies of rare-earth ions doped material hosts have become very important as it lightens the enormous potentialities to optical sources and amplifiers operating at wavelengths compatible with fiber communications technology.

Optical and laser technologies have expanded considerably over the last few decades however there is considerable effort to miniaturize such devices. Ti:sapphire has excellent physical and spectral properties which make it a very attractive lasing/optoelectronic material and is widely tunable giving rise to specific applications. Single crystal sapphire is also extremely hard, chemically inert and has excellent thermal conductivity and high electrical resistivity. Sapphire may be synthetically grown, with a well advanced process owing to its demand as an electrically insulating substrate for microelectronic devices. With the advent of the Ti:sapphire laser, the growth of high quality Ti-doped materials and its spectroscopic properties were investigated to the extent that the laser rapidly became commercially viable. To realize a Ti:sapphire waveguide laser, it is proposed that Ti^{3+} is introduced into a nominally pure sapphire wafer by high energy ion implantation.

The field of ultrashort laser physics has existed for nearly four decades. It can be considered a fairly mature field and the generation, manipulation, measurement and usage of ultrashort pulses are at the frontiers of laser research today. Mode-locked fiber lasers have made huge advances over recent years and are being researched to replace bulky solid-state lasers in the future. Fiber lasers can generate high average powers and a good beam quality, however at present there is no fiber laser capable of replacing the Ti:Sapphire laser in the region of 700 – 1100 nm. The future progress in the field of ultrashort laser pulse generation can only unlock new applications. Currently Ti:Sapphire cannot be

GENERAL INTRODUCTION

bettered as an ultrafast laser and it is KLM Ti: sapphire lasers that have produced pulses of 6 fs in duration. The progress in the field of ultrashort laser pulse generation has been rapid and continuous, and has a long lifetime ahead. Laser powers should increase and intensities should be regularly pushed over 10^{21} W/cm². Research continues into discoveries for new gain media in the hope of improving on the excellent Ti: Sapphire and will continue for as long as ultrashort laser pulses remain useful, which, judging by the numerous and varied applications, will be for many years to come. Of course, as the technology continues to develop, more applications will be found for it. Lasers should become cheaper to build as technologies and design improve, making them further compacted, and cheaper to buy as further applications call for them.

Nonlinear optics is a field that has become important since the invention of the laser. It is providing us with a fundamental understanding of the nature of light and revealed to us a world of applications. Franken and his staff observed the first nonlinear optical properties in 1961. Radiation with wavelength $\lambda = 3471$ Å and the power of the order of 1mW was observed in the transmitted light. Franken observed a second harmonic generation, that is, a doubling of the frequency of light. The effect of the wavelength dependence of gain, nonlinearity and dispersion to the propagation of short pulses in high-gain efficiency silica fiber was studied. It resulted in asymmetric spectrum and chirp, and reduction of the pulse broadening. Wavelength dependence of the nonlinearity was demonstrated to have the most effect, compared to that of dispersion or gain.

Many nonlinear effects have been studied extensively using optical fibers as a nonlinear medium, despite the fact that the strengths of the nonlinearities in fused silica are relatively low compared to many other materials. Another reason for using optical fibers to study nonlinear effects is because they have small core areas, which results in high intensity in the core. For more intense laser radiation, the polarization is composed of a linear part and an intensity dependent

nonlinear part. Therefore, most nonlinear effects present in Titane-Sapphire are induced. These effects include elastic processes such as self-phase modulation (SPM), self-steepening, third-harmonic generation, intrapulse Raman scattering.

Chapter I is devoted to the theory of Titanium and the Titanium-Doped Sapphire Crystal.

Chapter II gives the necessary background for the generation and compression of ultrashort laser pulses.

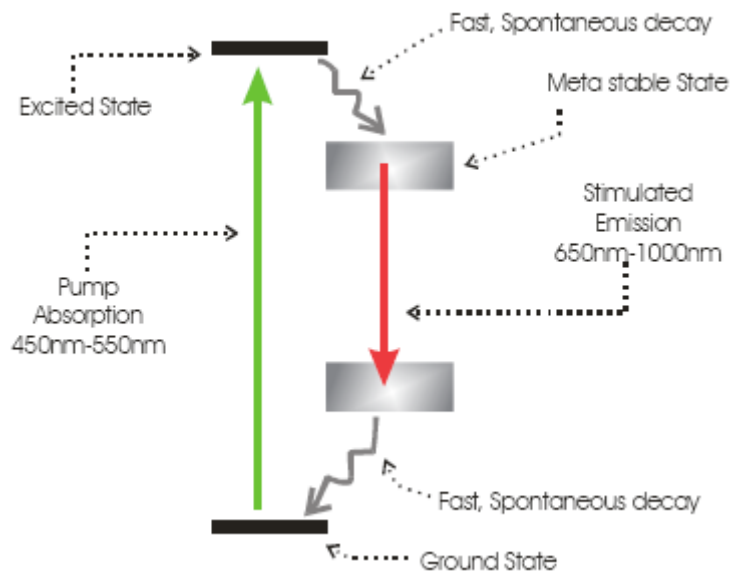
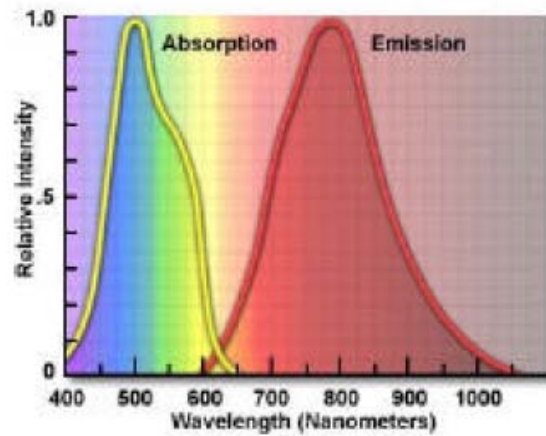
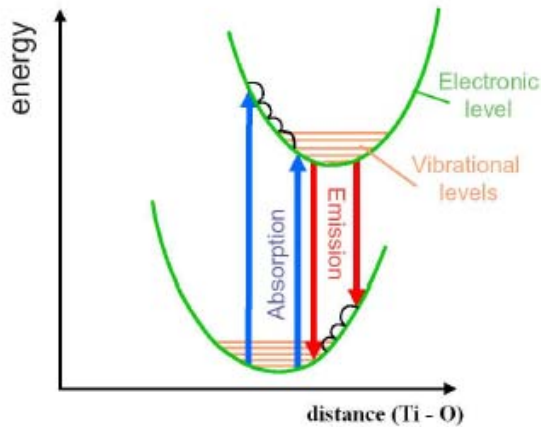
In chapter III we establish the background theories for propagation of light in single-mode optical fibers. We give an overview of the scalar nonlinear Schrodinger equation which governs the propagation of the envelope of an optical pulse in a single-mode optical fiber.

In chapter IV we describe the pulse-propagation problem by treating fibers as a linear optical medium. We discuss the conditions under which the GVD effects dominate over the nonlinear effects by introducing two length scales associated with GVD and SPM.

In chapter V we consider SPM as a simple example of the nonlinear optical effects that can occur in optical fibers. We also discuss the case of pure SPM by neglecting the GVD effects. Then, we introduce the case of both effects: GVD and SPM.

In chapter VI we present an analytical study of pulse splitting in Titanium-Sapphire, basing our study on the generalized nonlinear of Schrödinger equation.

CHAP I TITANIUM SAPPHIRE THEORY



1.1 Optoelectronics

Optical and laser technologies have changed the way the world shops, communicates, heals, learns and is entertained over a few short decades. The expansion of waveguide optical technologies into areas previously the domain of electronics, can be attributed to the volume/speed/reliability of processing/transfer/analysis and the advent of the optical fiber and the semiconductor laser. The growth and improvement in the world's long distance communication systems is probably the most apparent example of this evolution. However optical technologies play an increasingly important role in more and more facets of modern society. Currently, considerable research is being undertaken to realize an integrated optical circuit to guide, switch, generate and amplify light in the same way that semiconductor devices process electrical information.

The invention of the laser in the 1960's provided a source of high intensity monochromatic and coherent light and its availability spawned new exciting fields of scientific research. Many systems reached mature design, and after experiences with the often hazardous dye lasers which were also susceptible to chemical degradation, there was considerable interest, in both scientific and industrial communities, regarding the prospects for a tunable solid-state laser. Moulton announced lasing in the Ti: sapphire material over the wavelength range 660 – 1180 *nm* in 1982 [2], and this quickly became the most widely used tunable laser system after its introduction in 1988.

As previously stated, the miniaturization of such a laser would herald an exciting progression in the systems development and it could yield a portable, low power, more efficient, less expensive, robust and highly tunable laser source. Such a device would be ideal for remote laser spectroscopy which requires tuning to scan across a wavelength range for applications such as pollution detection, environmental monitoring and other forms of remote sensing from aircrafts or satellites and under conditions of appropriately high output power. The waveguide laser could provide a more economical option for femtosecond time scale pulse research [3].

1.2 Sapphire and Ti: sapphire

1.2.1 Overview

Since the reporting of laser action by Moulton in 1982 [4], the Ti: sapphire laser has been the subject of extensive investigations and has become the most widely used tunable solid-state laser. The Ti: sapphire system combines a broad tuning range of about 400nm with a relatively large gain cross section.

In this lasing material, a Ti^{3+} ion is substituted for an Al^{3+} ion in Al_2O_3 . These crystals are typically grown by a number of methods and typically consist of sapphire doped with $0.10\text{ Ti}_2\text{O}_3\%$ by weight. Crystals of Ti: Al_2O_3 exhibit a broad absorption band, located in the blue-green region of the visible spectrum with a peak around 490 nm . A relatively weak absorption band is observed in the infra-red region. This residual infra-red absorption interferes with efficient laser operation, particularly in the case of flash-lamp pumping. Optimized crystal growth techniques and additional annealing processes have drastically reduced this absorption band compared to earlier crystals. The great interest in this material arises from the broad vibronic fluorescence band which allows tunable laser output between $660 - 1180\text{ nm}$, with the peak of the gain curve around 800 nm . The energy level diagram of Ti: sapphire with the absorption and emission spectra are shown in Figure 1.1 [5]. Besides having favorable spectroscopic and lasing properties, another advantage of Ti: Al_2O_3 arises from the material properties of sapphire itself, namely very a high thermal conductivity, an exceptional chemical inertness and a mechanical rigidity.

Titanium sapphire is commercially available in sizes up to 3.5cm across by 15cm long and, due to the well-developed growth technology of sapphire, of good optical quality. Ti: sapphire lasers have been pumped with a number of sources such as argon and copper vapor lasers, frequency doubled Nd: YAG and Nd: YLF lasers, as well as flash-lamps. Flash-lamp pumping is very difficult to achieve in Ti: sapphire because a very high pump flux is required.

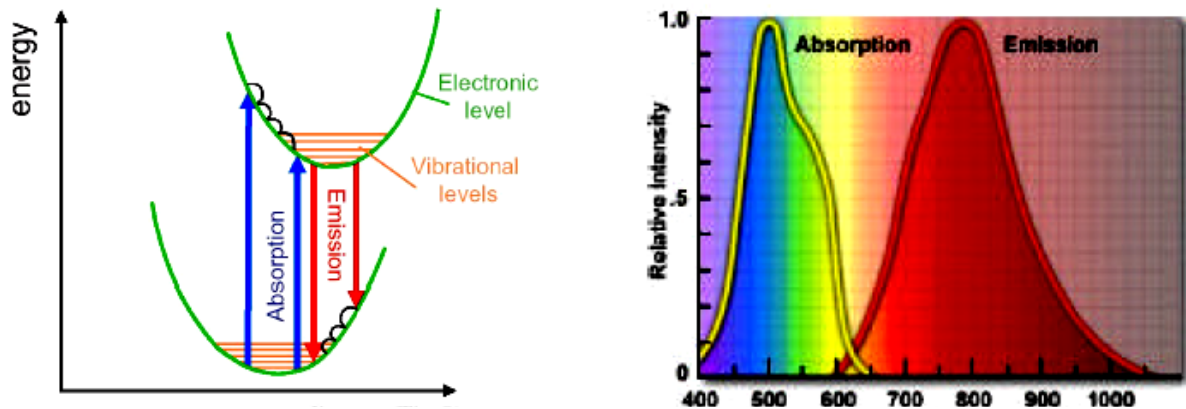


Figure 1.1: The energy level diagram of Ti: sapphire together with the absorption and emission spectra. Interaction of the titanium electron with Al_2O_3 produces the wide spreading of the energy levels and results in broad tuning [4, 5, 8]

1.2.2 Structure of sapphire and Ti: sapphire

The natural alumina Al_2O_3 (corundum) structure is comprised of hexagonally close packed oxygen anions with two thirds of the octahedral sites in between the oxygen planes occupied by Al cations, as shown in Figure 1.2.a. Only two out of every three aluminum sites are filled, to maintain overall charge neutrality. The orientations of the common crystal planes are shown in Fig. 1.2.b, together with the corresponding crystallographic axes, defined in a direction perpendicular to the planes. High quality sapphire crystals are routinely grown and are readily available in wafer form, with one or two sides polished to high optical quality. Ti-doped sapphire crystals (referred to as 'bulk-doped Ti: sapphire') are formed by introducing Ti_2O_3 into the melt during crystal growth. The Ti^{3+} ion is incorporated on the Al lattice site, in place of an Al^{3+} ion, and forms the (3+) oxidation state that is necessary for lasing. The Ti^{3+} impurity will cause some local distortion of the lattice due to the difference in size, since the atomic radius of Al is about two thirds that of Ti.

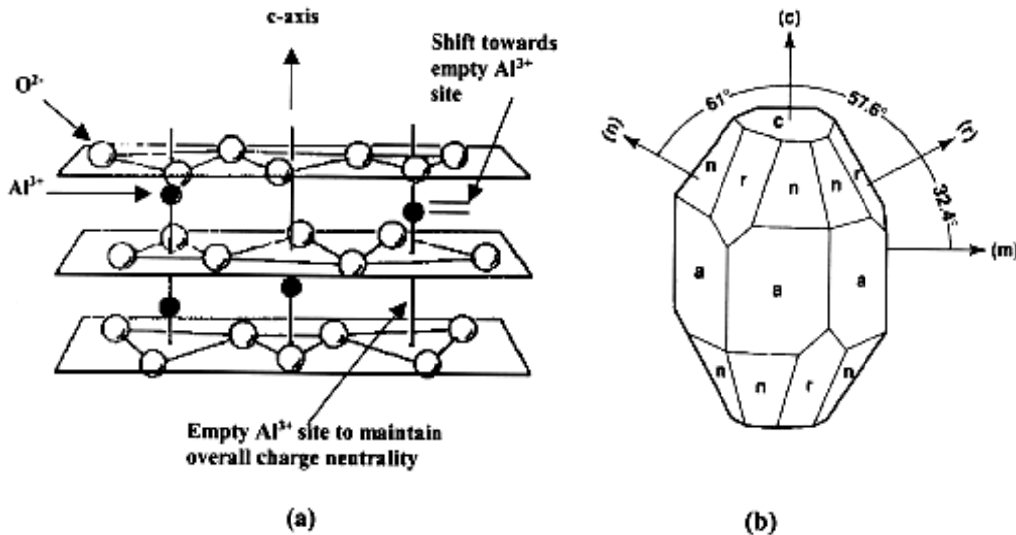


Figure 1.2: a) 3-D view of the structure of sapphire. Between each layer of closed packed oxygen ions, are aluminum sites, although only two out of every three are occupied. b) Diagram of the common crystal planes in the sapphire lattice [14]

The incorporation of other valence states of Ti will require a mechanism to compensate for the local imbalance of charge and correspondingly, the solubility of Ti³⁺ is significantly greater than that of Ti⁴⁺ in sapphire [6].

1.2.3 Spectroscopy of sapphire and Ti-doped sapphire

Pure single crystal sapphire has a high transparency to wavelengths between $0.2 \mu\text{m}$ to about $5 \mu\text{m}$ in the infra-red, as shown in Fig.1.3. The presence of defects and impurities in the lattice will affect the electronic structure and may allow optical transitions to occur. For example, optical absorption at wavelengths in the ultra-violet accompanies electron transitions that are related to the presence of defects in the Al₂O₃ lattice. Impurities, particularly transition metal ions, give rise to characteristic absorption and often yield brightly colored crystals [11].

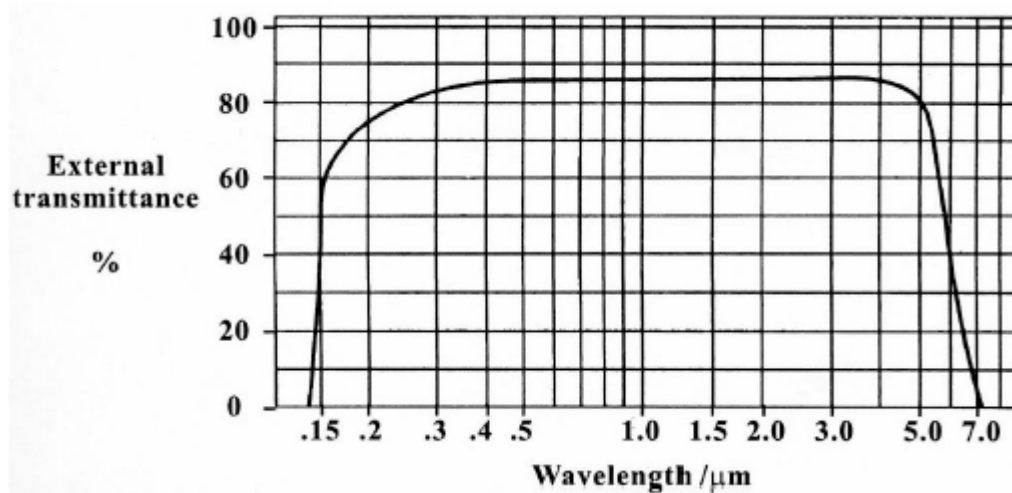


Figure 1.3: Transmission of a 1mm thick sapphire wafer over a large optical range [16]

For Ti^{3+} -doped sapphire, optical absorption and fluorescence are related to electronic transitions of the Ti^{3+} ion incorporated by substitution on the Al lattice. The origin of the optical transitions has been extensively studied, with an interest motivated by the advent of the Ti: sapphire laser and the need for high quality crystals [7].

1.2.4 Influence of Ti^{4+} and defects on Ti: sapphire spectroscopy

Although Ti^{3+} is more soluble in sapphire than is Ti^{4+} , trace quantities of Ti^{4+} may be included in the sapphire lattice. The inclusion of Ti^{4+} is detrimental to laser performance as the resulting distortions to the lattice and the inclusion of associated defects causes a shift in the absorption of the nearby Ti^{3+} ion from blue-green to the near infra-red. The shift to longer wavelengths is attributed to a weakened local crystal field as a result of interaction with a nearby Al vacancy and/or Ti^{4+} ion [8]. The absorption shown in Figure 1.4 overlaps the fluorescence band associated with the laser emission. In a laser configuration, this would increase the round-trip cavity losses and limit the laser performance. The absorption band peaks at around 800nm and extends well into the infra-red. The polarization dependence is in contrast with the absorption characteristic of the Ti^{3+} ion, as the σ polarized absorption is greater than the π polarized absorption.

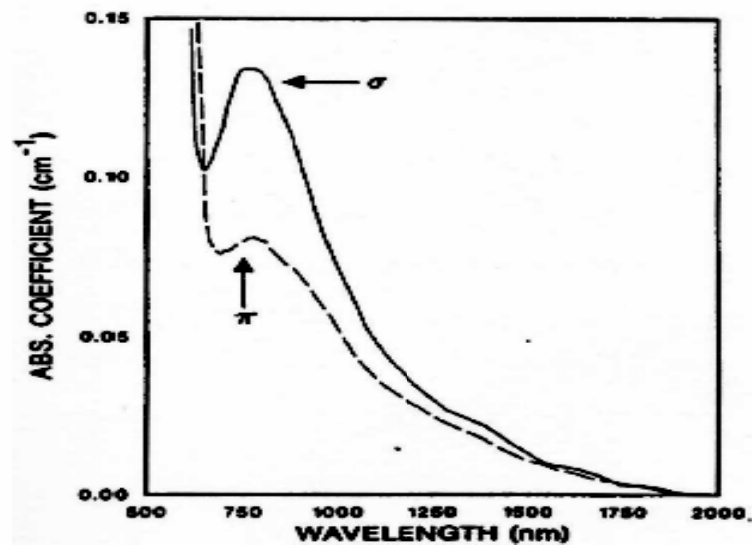


Figure.1.4: Absorption at wavelengths in the near infra-red [5]

The titanium ion in the sapphire lattice is in the trivalent state as it occupies the site of a trivalent ion, aluminum, and due to lattice defects, it is probable that traces of Ti^{4+} exist in the crystal. The ion induces a distortion in the lattice field and causes a shift in absorption of nearby Ti^{3+} ions towards the infrared. This shift in absorption results in an overlap with the emission band of the laser [28, 29]. Figure 1.4 shows the absorption due to the (Ti^{3+} - Ti^{4+}) pairs which can be seen to have a peak near . This effect limits the performance of the laser as it increases the losses in the cavity. An important characteristic of a titanium-doped sapphire crystal is the ratio of peak absorption in the blue-green region () to the parasitic peak absorption near . This ratio is called Figure of Merit (FOM) and characterizes the quality of the crystal. Today, crystals with FOM near 1000 can be fabricated, although they are highly priced.

1.3 Refractive Index

The crystal of Ti: Sa is a uniaxial birefringent crystal. For λ , the difference in index of refraction $n_e - n_o$ between the ordinary index and the extraordinary index is about 10^{-4} . The refraction index n in the visible and infra red regions can be modeled using Sellmer’s equation [9]:

$$n^2(\lambda) = n_\infty^2 + \frac{A_1}{\lambda^2 - \lambda_1^2} + \frac{A_2}{\lambda^2 - \lambda_2^2} + \frac{A_3}{\lambda^2 - \lambda_3^2} \tag{1.1}$$

Where the three couples (λ_i, A_i) are deduced empirically by adjusting the experimental measurements in the visible field (see figure 1.5).

T=295 K

Ordinary axis	(0.0033, 1.077)	(0.0114, 1.025)	(151.2, 5.04)
Extraordinary axis	(0.0004, 1.041)	(0.0141, 1.03)	(123.8, 3.55)

Table 1.1: Values of the couples (λ_i, A_i) for Ti:Sa à T= 295 K[4]

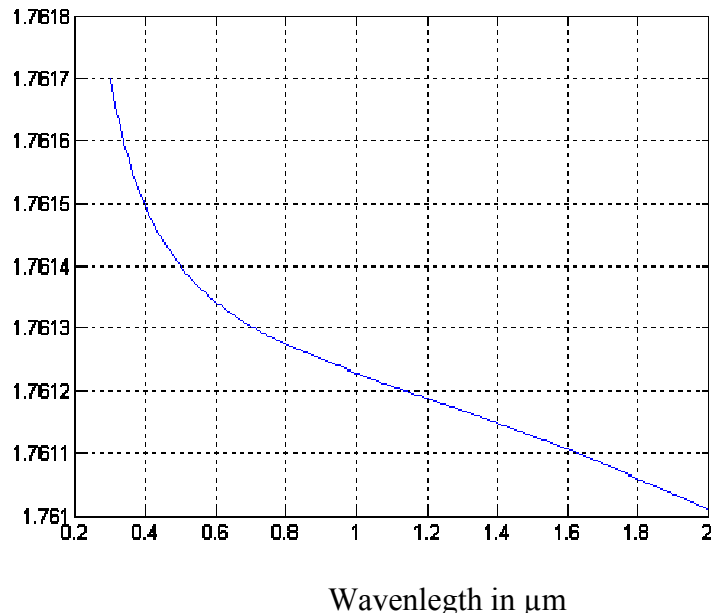


Figure.1.5: Curves of dispersion of the indexes of ordinary and extraordinary refraction of *Ti: Sa* according to the wavelength in the visible field, deduced from the expression (1.1)

In the wavelength range $[700nm - 900nm]$, which corresponds to the field of operation of the power channels Ti: Sa, the index of refraction is around 1.76 for the ordinary index and 1.755 for the extraordinary index (see figure 1.5).

1.3.1 Chromatic Dispersion

When an electromagnetic wave interacts with the bound electrons of a dielectric, the medium response, in general, depends on the optical frequency. This property, referred to as chromatic dispersion, manifests through the frequency dependence of the refractive index $n(w)$. On a fundamental level, the origin of chromatic dispersion is related to the characteristic resonance frequencies at which the medium absorbs the electromagnetic radiation through oscillations of bound electrons. Far from the medium resonances, the refractive index is well approximated by the Sellmeier equation.

Fiber dispersion plays a critical role in propagation of short optical pulses because different spectral components associated with the pulse travel at different speeds given by $c/n(w)$. Even when the nonlinear effects are not important, dispersion-induced pulse broadening can be detrimental for optical communication systems.

In the nonlinear regime, the combination of dispersion and nonlinearity can result in a qualitatively different behavior, as discussed in later chapters. Mathematically, the effects of fiber dispersion are accounted for by expanding the mode-propagation constant β in a Taylor series about the frequency w_0 at which the pulse spectrum is centered:

$$\beta(w) = n(w) \frac{w}{c} = \beta_0 + \beta_1(w - w_0) + \frac{1}{2}\beta_2(w - w_0)^2 + \frac{1}{6}\beta_3(w - w_0)^3 + \dots,$$

where

$$\beta_m = \left(\frac{d^m \beta}{dw^m} \right)_{w=w_0} \quad (m = 0, 1, 2, \dots) \quad (1.2)$$

The parameters β_1, β_2 and β_3 are related to the refractive index n and its derivatives through the relations

$$\beta_1 = \frac{1}{v_g} = \frac{n_g}{c} = \frac{1}{c} \left(n + w \frac{dn}{dw} \right),$$

$$\beta_2 = \frac{1}{c} \left(2 \frac{dn}{dw} + w \frac{d^2n}{dw^2} \right),$$

$$\beta_3 = \frac{1}{c} \left(3 \frac{d^2n}{dw^2} + w \frac{d^3n}{dw^3} \right), \quad (1.3)$$

where n_g is the group index and v_g is the group velocity. Physically speaking, the envelope of an optical pulse moves at the group velocity while the parameter β_1 represents the group velocity of the pulse and β_2 represents the dispersion of the group velocity and is responsible for pulse broadening. This phenomenon is known as the group-velocity dispersion (GVD), and β_2 is the GVD parameter. The parameter β_3 given by Eq.(3) represents the Dispersion Slope (Ds) or Third Order Dispersion (TOD) which is responsible for asymmetry.

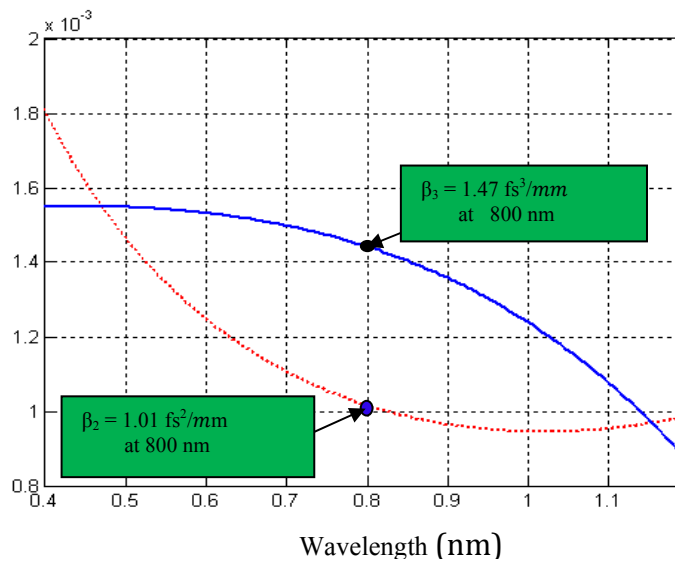


Figure.1.6: Variation of β_2 and β_3 with wavelength for Ti: Sa crystal.

The dispersion parameter D that what is commonly used in the fiber-optics literature in place of β_2 . It is related to β_2 by the relation

$$D = \frac{d\beta_1}{d\lambda} = -\frac{2\pi c}{\lambda^2} \beta_2 \approx -\frac{\lambda}{c} \frac{d^2 n}{d\lambda^2} \quad (1.4)$$

This total GVD represents the pulse broadening in time [ps] by a fiber length of L [Km] for a pulse with a spectral width of $\delta\lambda$ [nm] as follows.

$$\Delta t[\text{ps}] = L[\text{Km}] \cdot \delta\lambda [\text{nm}] \cdot D \left[\frac{\text{ps}}{\text{nm.Km}} \right] \quad (1.5)$$

The effect of GVD on the Bit-rate B can be estimated by

$$B \cdot \Delta t = B \cdot L \cdot \delta\lambda |D| < 1 \quad (1.6)$$

Therefore, the BL product for single mode fibers can be increased by operating at the ZDW and using a pulse with narrow spectral width [10].

1.4 Fiber Nonlinearities

The response of any dielectric to light becomes nonlinear for intense electromagnetic fields, and optical fibers are no exception. On a fundamental level, the origin of nonlinear response is related to anharmonic motion of bound electrons under the influence of an applied field. As a result, the total polarization \mathbf{P} induced by electric dipoles is not linear in the electric field \mathbf{E} , but satisfies the more general relation

$$\mathbf{P} = \varepsilon_0 (\chi^{(1)} \cdot \mathbf{E} + \chi^{(2)} : \mathbf{E}\mathbf{E} + \chi^{(3)} \vdots \mathbf{E}\mathbf{E}\mathbf{E} + \dots). \quad (1.7)$$

where ε_0 is the vacuum permittivity and $\chi^{(j)}$ ($j = 1, 2, \dots$) is the j th order susceptibility. In general, $\chi^{(j)}$ is a tensor of rank $(j + 1)$. The linear susceptibility $\chi^{(1)}$ represents the dominant contribution to \mathbf{P} . Its effects are included through the refractive index n and the attenuation coefficient α . The second-order susceptibility $\chi^{(2)}$ is responsible for such nonlinear effects as second-harmonic generation and sum-frequency generation. However, it is nonzero only for media that lack an inversion symmetry at the molecular level. As SiO_2 is a symmetric molecule, $\chi^{(2)}$ vanishes for silica glasses.

1.4.1 Nonlinear Refraction

The lowest-order nonlinear effects in optical fibers originate from the third order susceptibility $\chi^{(3)}$, which is responsible for phenomena such as third harmonic generation, four-wave mixing, and nonlinear refraction. Unless special efforts are made to achieve phase matching, the nonlinear processes that involve generation of new frequencies (e.g. third-harmonic generation and four-wave mixing) are not efficient in optical fibers. Most of the nonlinear effects in optical fibers therefore originate from nonlinear refraction, a phenomenon referring to the intensity dependence of the refractive index. In its simplest form, the refractive index can be written as

$$\tilde{n}(w, |E|^2) = n(w) + n_2|E|^2 \quad (1.8)$$

where $n(w)$ is the linear part given by Eq. (1.1), $|E|^2$ is the optical intensity inside the fiber, and n_2 is the nonlinear-index coefficient related to $\chi^{(3)}$ by the relation (see Section 3.3).

$$n_2 = \frac{3}{8n} \text{Re}(\chi_{xxxx}^{(3)}) \quad (1.9)$$

The tensorial nature of $\chi^{(3)}$ can affect the polarization properties of optical beams through nonlinear birefringence. The intensity dependence of the refractive index leads to a large number of interesting nonlinear effects; the most widely studied is self-phase modulation (SPM). Self-phase modulation refers to the self-induced phase shift experienced by an optical field during its propagation in optical fibers. Its magnitude can be obtained by noting that the phase of an optical field changes by

$$\Phi = \tilde{n}k_0L = (n + n_2|E|^2)k_0L \quad (1.10)$$

where $k_0 = 2\pi/\lambda$ and L is the fiber length. The intensity-dependent nonlinear phase shift $\Phi_{NL} = n_2k_0L|E|^2$ is due to SPM. Among other things, SPM is responsible for spectral broadening of ultrashort pulses and formation of optical solitons in the anomalous-dispersion regime of fibers [11].

Table 1: Active medium physical and laser properties

Chemical formula	Ti ³⁺ :Al ₂ O ₃
Crystal structure	Hexagonal
Lattice constants	a =4.748, c = 12.957
Laser action	4 Level Vibronic
Fluorescence lifetime	3.2 μ s (T=300 K)
Tuning range	660 – 1050 nm
Absorption range	400 – 600 nm
Emission peak	795 nm
Absorption peak	488 nm
Refractive index	1.76 à 800 nm
Nonlinear index effect n_2	3.2.10 ⁻¹⁶ cm ⁻² .w
Absorption cross section	9.3.10 ⁻²⁰ cm ²
Mass density (grams/cm)	3.965
Atomic density (atoms/cm)	1.17.10 ²³

Tableau.2: Titanium Doped Sapphire Crystal Characteristics

1.5 Summary of Chapter

Sapphire is a strong, robust, resistant and optically transparent crystal with numerous commercial applications. The solid-state Ti: sapphire material has a simple energy level diagram, high absorption cross section and is very widely vibronically broadened. A very important characteristic of sapphire is that it is the second hardest material that can be found in nature after diamond and it is chemically inert to any etchant at room temperature [1-2].

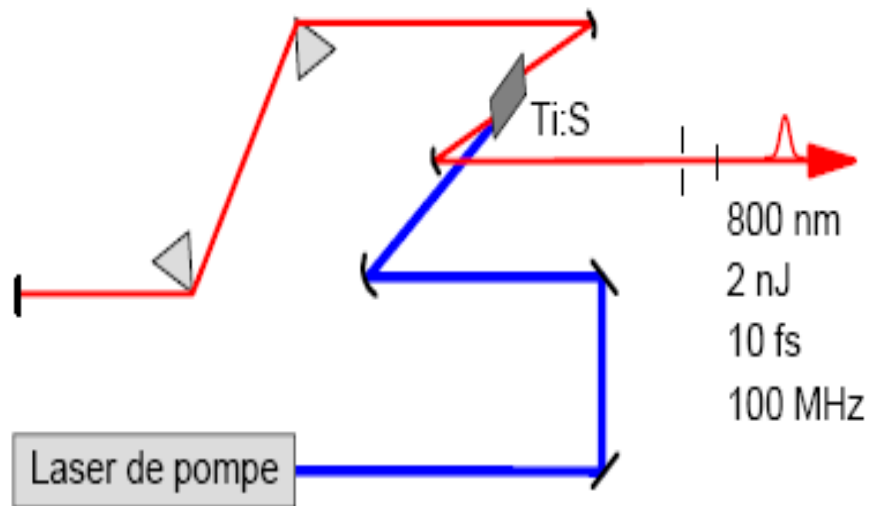
The single crystal is hard, chemically inert, and has high thermal conductivity and excellent electrical resistivity. These characteristics make sapphire a successful insulating substrate for microelectronic components. Furthermore it is an excellent material for fabrication of optical windows in applications where robustness and high optical transmission are needed.

References

- [1] L.D. Morpeth “Ti: sapphire fabrication via High Energy Ion Implantation” University of Melbourne December 2002
- [2] P.F.Moulton, Quant. Electron. Conf., Munich, Germany, June 1982.
- [3] E.J.Lerner, Laser Focus World 34, 143 (Oct 1998).
- [4] P.F.Moulton, *Tunable Solid-state Lasers* (Springer-Verlag, 1985).
- [5] P.Lacovara, L.Esterowitz, and M.Kokta, IEEE. Journal of Quantum Electronics 21, 1614 (1985).
- [6] S.K.Roy and R.L.Coble, J. Am. Ceram. Soc. 51, 1 (1968).
- [7] A.R.Moon and M.R.Phillips, J. Am. Ceram. Soc. **77**, 356 (1994).
- [8] *Optical Properties and applications* (Technical Bulletin, Union Carbide Crystal Products, 1988).
- [9] Fabien PLE « Etude de l'amplification parasite transverse de la fluorescence dans les cristaux de Ti:Sa de grandes dimensions » Université Paris XI Orsay
- [10] J.K.Kim “investigation of high nonlinearity glass fibers for potential applications in ultrafast nonlinear fiber devices” PhD faculty of the Virginia 2005.
- [11] G.P.Agrawal, “Nonlinear Fiber Optics”, Third Edition, Optics and Photonics, 2001.

CHAP II

ULTRASHORT LASER PULSE GENERATION AND COMPRESSION



Ultrashort laser pulses are considered to be those whose pulse duration is less than a few picoseconds (10^{-12} s) long. Recent research has led to techniques such as Kerr-lens mode locking to enable pulse duration down to around 5 femtoseconds (10^{-15} s) and chirped pulse amplification giving pulses peak powers of several terawatts. In very recent years research has driven towards the attosecond regime (10^{-18} s), allowing for the possibility to probe such phenomena as the motion of electrons, by utilizing the progress in ultrashort laser pulses. The best commercially available lasers operate mode-locked with titanium sapphire as the gain medium and the Ultrafast Laser is an excellent example.

2.1 Introduction [1]

A laser can be described as an optical source that emits a coherent beam of photons at an exact wavelength or frequency. In stark contrast, other common light sources emit incoherent light in all directions, normally over a wide range of wavelengths or frequencies. All lasers have some very important components in common. With reference to Figure.2.1, these are the laser's gain medium (1), an energy source to pump the laser medium (2), a highly reflective mirror (3) and a partially reflective mirror (4). The highly reflective mirror and the partially reflective mirror, or output coupler, are aligned so as to cause most of the light to oscillate between them through the gain medium. With each trip the light undergoes further amplification. The partially reflective mirror reflects most of the light incident on it but allows a small percentage to be transmitted through it, forming the laser output (5).

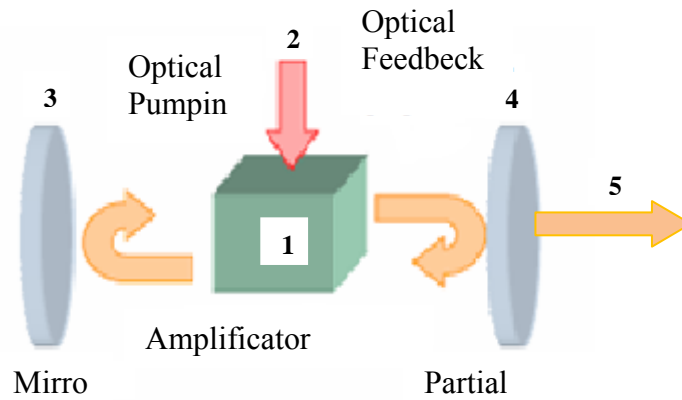


Figure.2.1: A schematic of a laser set-up.

In most materials light is absorbed, though in some the light is amplified. The only real difference is the state the atoms are in before they interact with light (see Figure 2.2). The energy for pumping the laser Figure.2.1 needs to be resonant with the system to raise atoms to an excited state and then to stimulate them into emitting photons. For the ruby laser a flash lamp was used, though typically today a continuous wave (CW) laser is used to supply light at the correct wavelength for absorption and emission in the gain medium. Einstein concluded that there are three interactions between matter and light, which are shown in Figure 2.2.

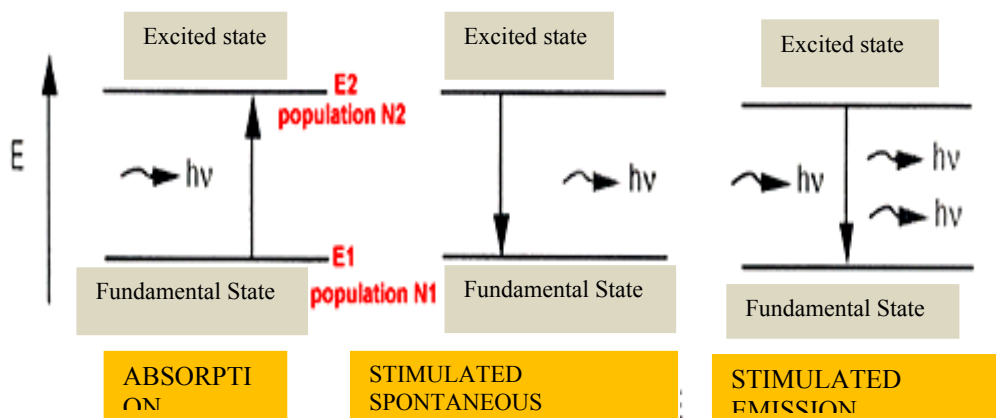


Figure.2.2: The interactions between light and matter.

2.1.1 Definitions:

2.1.1.1. Absorption – A photon, with energy $\hbar\omega$, from the radiation field transfers its energy to an electron as potential energy when it moves from E_1 to E_2 , raising the atom's energy and putting it in an excited state.

2.1.1.2. Spontaneous Emission – When an electron in an excited state E_2 drops to a lower state E_1 via decay there is a loss of potential energy in the atom. This is released as a photon and the photon's energy is equal to $E_2 - E_1 = \hbar\omega$. The released photon's phase, direction and polarization are all random.

2.1.1.3. Stimulated Emission – When an electromagnetic field is present around an atom, a photon with energy $\hbar\omega$ can stimulate the emission of a twin photon from an excited atom. This twin photon is emitted with identical energy, direction, phase and polarization as the inducing photon, thus amplifying the energy [1, 2, 3].

2.1.2 Longitudinal Modes

When it comes to the use of lasers as short pulse generators, the most important property of optical resonators is the existence of longitudinal modes. In other words, we now know how to apply a feedback to a gain medium. We need to explore the conditions under which this feedback can constructively interfere with the main signal. Fabry-Perot interferometers were originally developed as high resolution band-pass filters. An electromagnetic field can be established between two parallel mirrors only when a wave propagating in one direction adds constructively with the wave propagating in the reverse direction. The result of this superposition is a standing wave which is established if the distance L between the two mirrors is an integer multiple of the half-wavelength of light.

The existence of longitudinal modes is the most important characteristic of an optical resonator when using lasers as short pulse generators. Longitudinal modes, sometimes called axial modes, are known to have a time-frequency property. For laser oscillations to occur within a cavity, a wave must be able to self-replicate after two reflections so that the electric fields constructively

interfere and add up in phase. All other frequencies of light consequently destructively interfere. The discrete sets of frequencies that are formed directly from these standing waves are then called the longitudinal modes of the cavity. The condition for a standing wave, where λ is the wavelength of light and the length of the cavity is L , is

$$\frac{m\lambda}{2} = L \quad (2.1.1)$$

The value of the positive integer m is known as the mode order and it can be quite large. For example for a cavity of length $L = 0.5 \text{ m}$ and for $\lambda = 500 \text{ nm}$, m is about $2 \cdot 10^6$, meaning there are many possible values of m for just a small change in wavelength λ . Using $\nu = c/\lambda$, Eq.2.1.1 can be written as

$$\nu = mc/2L \quad (2.1.2)$$

The frequency separation $\Delta\nu$ between adjacent modes ($\Delta m = 1$) is also of importance and can be found using

$$\Delta\nu = c/2L \quad (2.1.3)$$

The round-trip time of flight, T , in the cavity is very easily calculated using Eq.2.1.4,

$$T = 2L/c \quad (2.1.4)$$

For a fairly typical laser, the cavity length is $L = 1.5 \text{ m}$ and so the period $T = 10 \text{ ns}$. This gives a characteristic frequency $\nu = 100 \text{ MHz}$. These numbers control the repetition rate of the mode-locked laser and the period of the pulse train.

Although there are a large number of longitudinal modes (Eq.2.1.1) in the cavity, spaced from adjacent modes by Eq.2.1.3, they can only oscillate if there is gain at their specific frequency. Figure.2.3 shows schematically how not all of the frequencies are amplified and therefore do not all contribute to the laser output spectrum. The amplifying medium in the laser only amplifies over certain frequencies. The gain medium, primarily determines the bandwidth over which the laser may operate. The bandwidth of a laser can be quoted in either frequency or wavelength as the two have an inverse relationship. Converting between nanometers and gigahertz depends on the central wavelength or frequency. To convert a small wavelength interval, $\Delta\lambda$, into a frequency interval, $\Delta\nu$, the following relation is needed

$$\Delta\nu = \Delta\lambda \cdot c/\lambda^2 \quad (2.1.5)$$

Analysis of Eq. 2.1.5 shows that one nanometer is worth more than one gigahertz if the central wavelength, λ , is shorter (note that c is the speed of light). It is generally accepted that Ti: Sapphire has a bandwidth of around 128 THz , which corresponds to around a 300 nm wavelength range and could potentially support approximately $250,000 \text{ modes}$ (for a 30 cm cavity). Compared to a medium such as helium: neon (He: Ne), which has a 1.5 GHz bandwidth (a 0.002 nm wavelength range) and could support just 3 longitudinal modes (again a 30 cm cavity), it's clear that Ti: Sapphire is the savior of the mode-locked laser.

Figure 2.3 also highlights the fact that it is both the bandwidth of the laser and the number of longitudinal modes allowed to oscillate, that are responsible for the laser's output spectrum [4].

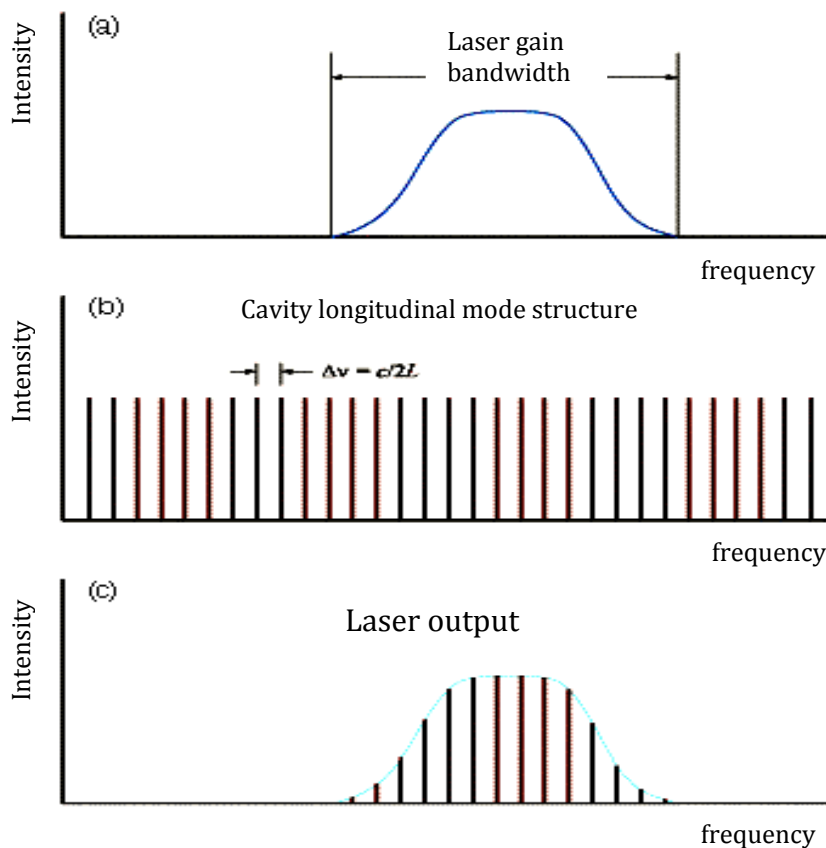


Figure.2.3: A schematic of the longitudinal mode structure in a laser. (a) The laser's gain medium will only amplify light over a certain range of frequencies. This refers to a laser's gain bandwidth. (b) The longitudinal modes are equally spaced by Eq.2.1.3. (c) Only the modes whose corresponding frequencies fall into the laser's gain bandwidth will be amplified [5].

2.1.2.1 Pulsed Operation

The longitudinal modes which are able to self-oscillate in the free multimode regime of the laser are those for which the unsaturated gain is greater than the cavity losses, as shown in Figure.2.3.c. The number of modes N can vary from just a few (in He-Ne lasers for example) to some 10^4 (in dye lasers and in Ti:sapphire lasers for example). Therefore a laser cannot deliver ultrashort pulses while functioning in its usual regime, in which the cavity plays the part of a frequency selector. However, it has been shown that when a laser operates in its most usual regime, it oscillates simultaneously over all the resonance frequencies of the cavity for which the unsaturated gain is greater than the cavity losses. These frequencies make up the set of longitudinal modes for the laser. While operating in the multimode regime, the output intensity of the laser is no longer necessarily constant with time.

2.1.3 Mode-locking techniques [6]

A multi-mode laser is said mode-locked if its modes have a well-defined and fixed phase relationship. If the phases are locked in such way that there is a constructive interference between the modes at an instant and a destructive interference at other times, the output will appear as a pulse. It is instructive to consider a simple example of mode-locking in which all oscillating modes have equal amplitude (Fig.2.4). The electromagnetic field due to $(2n + 1)$ equally spaced modes is given by:

$$E(t) = a_0 \sum_{k=0}^{N-1} \cos \left((w_j - w_k) \cdot t - (\phi_j - \phi_k) \right) \quad (2.1.6)$$

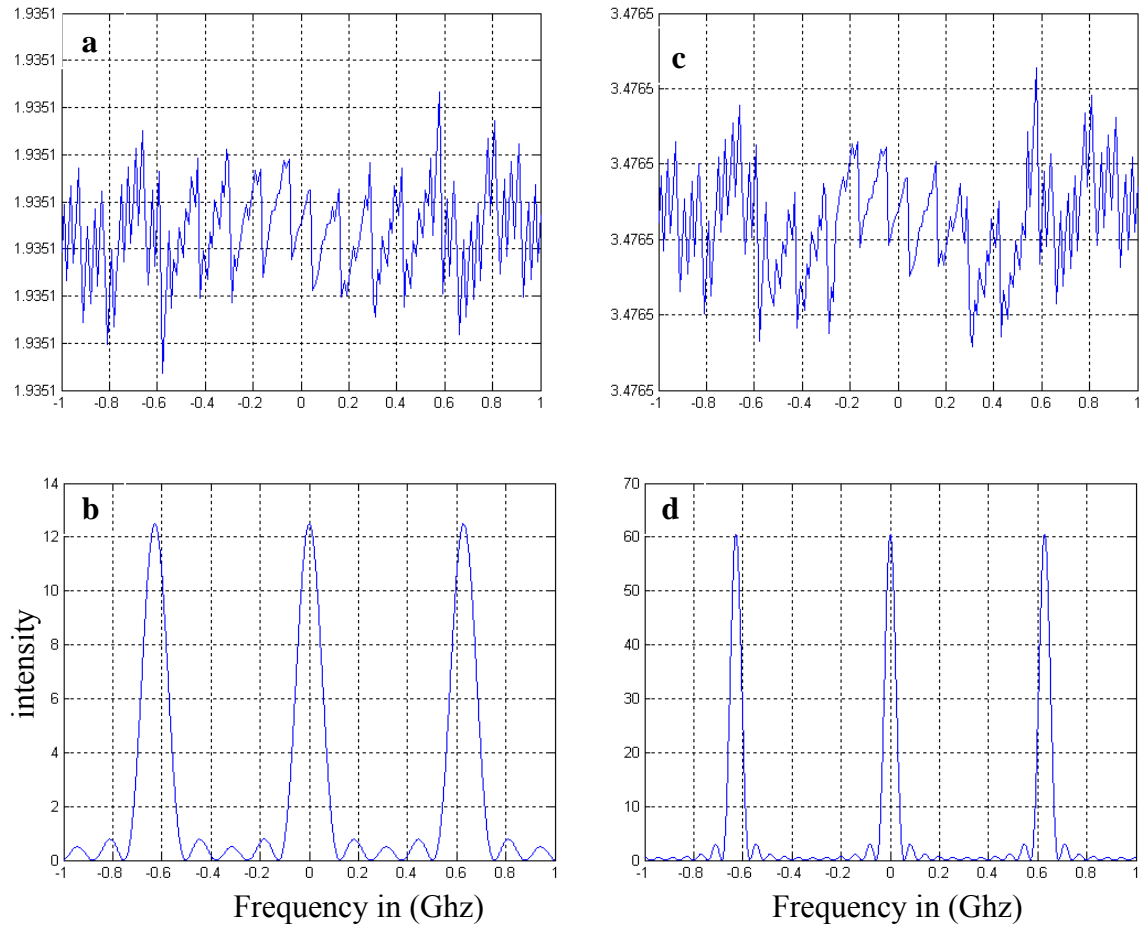


Figure.2.4: The influence of the phase relation between oscillating modes on the output intensity of the oscillation. (a) two modes with random phases, (b) two modes in phase, (c) five modes with random phases and (d) five modes in phase.

Figure 2.4 shows how the time distribution of a laser output depends upon the phase relations between the modes. Figure 2.4.a shows how the intensity varies for two oscillating modes with random phases and Figure 2.4.b is the resultant intensity of two modes in phase. Figure 2.4.c gives an idea of how five modes with random phase relations to one another give a random distribution of intensity maxima, but let these five modes oscillate with the same initial phase, Figure 2.4.d, is the resultant intensity of five modes in phase and a period repetition of a wave packet from the resultant constructive interference can be seen. In a general continuous wave multi-mode laser, the modes will oscillate independently from each other and will have random phases relative to one another.

Since the total electromagnetic field at any point inside the cavity is given by the sum of the fields of the oscillating modes, the output of such a laser will be noise-like, fluctuating in intensity due to interference between the modes. However it is possible to manipulate the phases of the modes to obtain a more useful output, using a technique known as mode-locking. When a laser operates naturally, it will oscillate simultaneously over all resonant frequencies of the cavity, as long as the unsaturated gain remains greater than the cavity losses. A mode-locked femtosecond laser requires a broadband gain medium, such as Ti: Sapphire, which can sustain over 100,000 longitudinal modes in a laser cavity where we have summed over all possible modes. $E(t)$ is the amplitude of the q th mode, w_q is the frequency of a central mode, Δw is the (angular) frequency spacing between modes, and φ_q is the phase of the q th mode. In the case of equal amplitudes (E_0) and locked phases ($\varphi_q - \varphi_{q-1} = \text{const}$) considered here, this sum becomes:

$$E(t) = E_0 e^{iw_0 t} \sum_{q=-n}^n e^{iqwt} \quad (2.1.7)$$

Then, it can be written as

$$E(t) = A(t) \cdot e^{iw_0 t} \quad \text{where } A(t) = E_0 \sum_{q=-n}^n e^{iqwt} \quad (2.1.8)$$

So we have got an amplitude-modulated wave oscillating at the central mode frequency (w_0). In fact the expression for $A(t)$ contains a geometrical progression. Consequently, we can convert it to another form and write down the intensity as a function of time in the following way:

$$I(t) \propto [A(t)]^2 = \frac{\sin^2[(2n+1)\Delta w.t/2]}{\sin^2(\Delta w.t/2)} \quad (2.1.9)$$

This function is a periodic one, with strong peaks (pulses) equally spaced by very weak subsidiary peaks (Figure 2.4.b, and 2.4.d). From the analysis, one can show several other important properties of this function. The pulse duration decreases and its amplitude increases, as the number of modes increases. The

period of this function (time spacing between pulses) is $T = 2\pi/\Delta\omega$. The pulse duration t can be approximately given as $\Delta t \approx 2\pi/(2n + 1)\Delta\omega = 1/\Delta\nu$, where $\Delta\nu$ is the full width of the generation band. From this simple example, it becomes clear that mode-locking results in a periodic intensity pulse, in contrast to the noisy, fluctuating output of the non-mode-locked case.

The process leading to mode-locking can be explained in either the time domain or the frequency domain. In the frequency domain, we can consider that all the involved modes under modulation develop individual sidebands. The sidebands of any mode lie close to its neighboring modes, provided that the frequency of modulation is close to the frequency spacing of the oscillating laser modes. In turn, the sidebands can couple to the neighboring modes near which they fall, leading to the phase-locking of an axial mode to its neighbors. Practically, the methods of achieving mode locking can be split into three main techniques: active mode-locking, passive mode-locking, and self-mode-locking:

2.1.3.1 Active Mode-Locking [7]

Active mode-locking is a technique for generating ultrashort pulses by modulating the cavity losses or modulating the round-trip phase change. This is done with either an acousto-optic or electro-optic modulator (see Figure 2.5 for its position in the cavity). Ultrashort pulses are generated if the modulation is synchronized with the cavity round-trips. Using an acousto-optic modulator is the most common method and when driven with an electrical signal, a sinusoidal amplitude modulation (AM) of each longitudinal mode is induced. If the modulation frequency is driven close to the intermode frequency separation, $\Delta\nu$, (Eq.2.1.3), then the two sidebands will be very close to the adjacent modes of the chosen mode. The sidebands and longitudinal modes will now compete against each other in the gain medium for maximum amplification.

However, the most efficient use of the energy in the gain medium is for the longitudinal modes to lock their phases onto the sidebands, which in turn causes a global phase-locking over the whole spectral distribution. Global phase-locking will yield a single oscillating pulse that contains all the energy of the cavity.

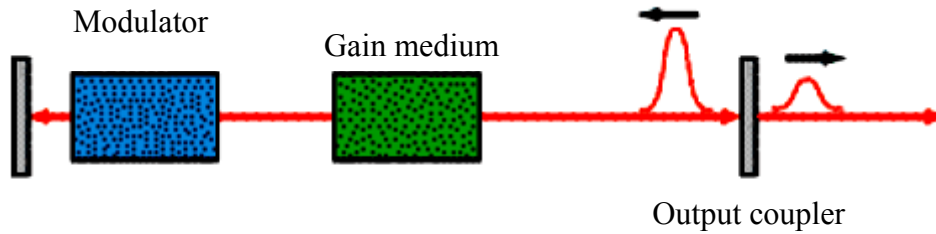


Figure. 2.5: The position of a modulator in an actively mode-locked laser set-up.

Let us insert an element inside the cavity which modulates its losses (figure 2.6). This element will induce a modulation of the amplitude of each longitudinal mode. If we assume the modulation to be sinusoidal, of angular frequency Ω , and to have a modulation depth α , the time dependency of modes n of frequency w_n can be written as

$$e_n(t) = E_n \cos(w_n t + \varphi_n) [1 - \alpha(1 - \cos(\Omega t + \varphi))] \quad (2.1.10)$$

This expression can also be written as follows, showing that in the frequency domain two sidebands show up at either side of mode $e_n(t)$:

$$e_n(t) = E_n(1 - \alpha) \cdot \cos(w_n t + \varphi_n) + E_n \frac{\alpha}{2} \cos[(w_n - \Omega)t + \varphi_n - \varphi] + E_n \frac{\alpha}{2} \cos[(w_n + \Omega)t + \varphi_n - \varphi]. \quad (2.1.11)$$

Now if the modulation frequency $\Omega/2\pi$ is close to the intermode frequency separation $c/2L$, the two sidebands will be very close to the two neighboring modes $n + 1$ and $n - 1$, as shown in figure 2.6 (a modulation frequency of the order of $mc/2L$, where m is an integer, can also be used to couple mode n to modes $n + m$ and $n - m$). The sidebands and the longitudinal modes themselves therefore complete inside the amplifying medium for maximum gain.

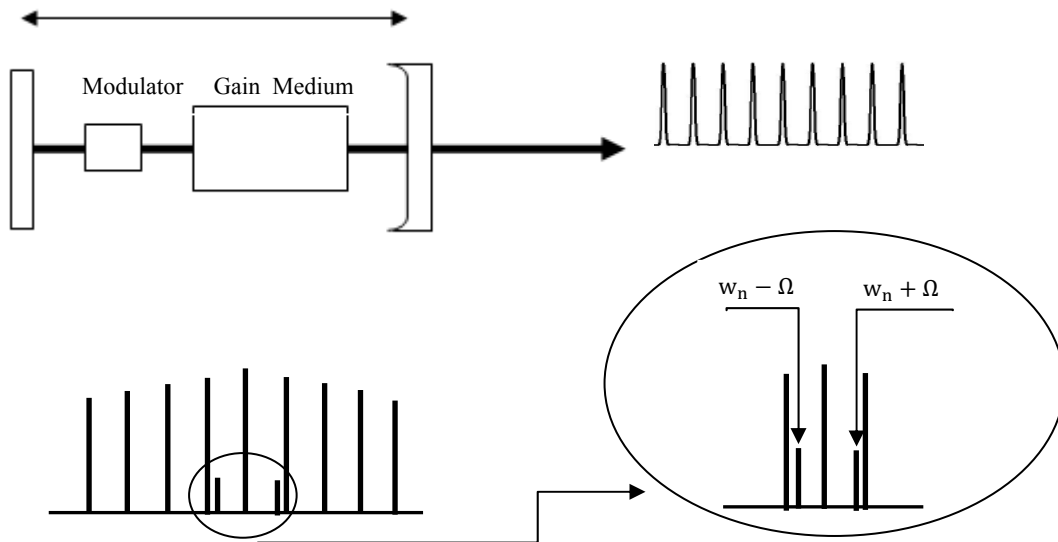


Figure.2.6: Illustration of an actively mode-locked laser cavity

The situation in which the medium is used most efficiently is that in which the longitudinal modes lock their phases onto the sidebands, causing a global phase-locking over the whole spectral distribution. This global phase-locking, in turn, is the condition under which the competition will give rise to the concentration of all the electromagnetic energy of the cavity into a single pulse traveling back and forth inside it [8].

2.1.3.2. Passive Mode-Locking [7]

Passive mode-locking works by placing a saturable absorber inside the laser cavity, which does not need an external modulating signal to operate. This method introduces a self amplitude modulation into the cavity and allows far shorter pulses than the active mode-locking method does, because a saturable absorber, when driven by already very short pulses, can modulate cavity losses far quicker than any electronic modulator. A saturable absorber is an optical device; usually a semiconductor saturable absorber mirror (SESAM), with an intensity-dependent transmission property, meaning it will allow transmission of high intensity light and will absorb low intensity light. Dyes can also be used but they are very wavelength-dependent and often exist in liquid form, and thus have to be refreshed regularly or be free flowing. Furthermore, the concentration of

these dyes has to be altered as the laser power changes. A SESAM normally consists of a Bragg mirror, which has alternating layers of two different optical materials with an optical thickness corresponding to one quarter of the wavelength of light for which the mirror is designed. The reflectivity then varies with the intensity of light incident upon it. Figure 2.7 shows the position of a saturable absorber in a laser set-up.

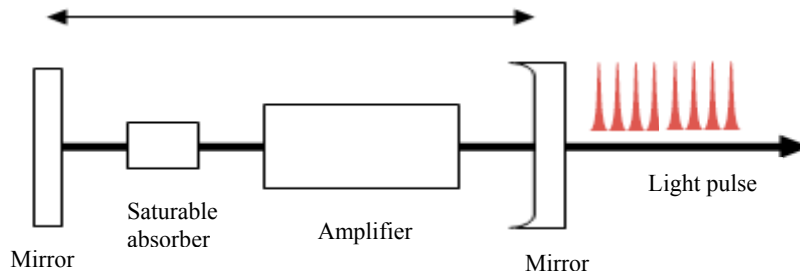


Figure.2.7 Saturable absorber set-up in a passively mode-locked laser.

Let us now follow the pulse along its round trip through the cavity. Let us start the point where the pulse, which will eventually take over, is already formed, but has not reached its final shape or its final duration. As the pulse travels through the saturable absorber, the pulse front is strongly absorbed (figure 2.8), but if the maximum of the pulse saturates the absorber medium and if as is the case in a dye laser or in a Ti: sapphire laser, the relaxation time of the medium is longer than the pulse duration, the tail of the pulse will benefit from the induced transparency of the medium and will travel through it without being attenuated.

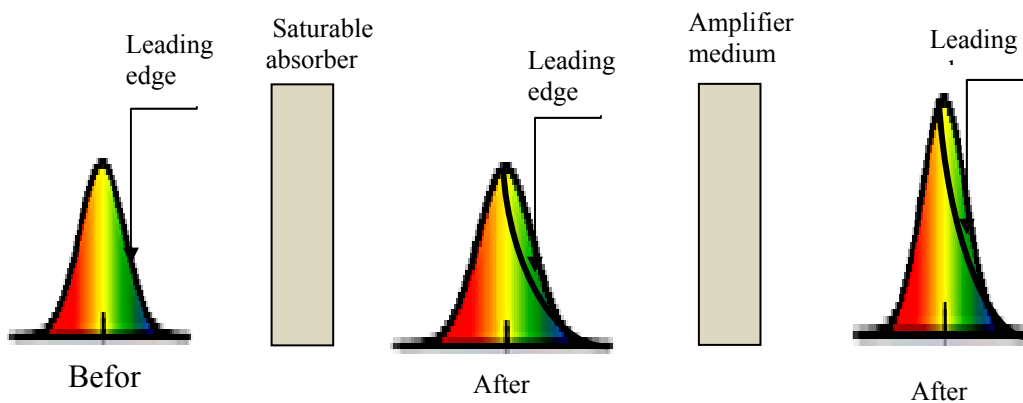


Figure.2.8 Illustration of a pulse shape modification after crossing a saturable absorber and an amplifying medium

When the pulse reaches the amplifying medium, the pulse front will come upon the unsaturated gain G_0 and will be strongly amplified while the tail of the pulse will feel a much weaker gain, which has just been saturated by the front of the pulse, and thus it will be much less amplified (figure2.8).

It is clear that after many back and forth trips, the resulting pulse will have narrowed and will have a very strong maximum, since the center of the initially broad pulse is not affected by the absorber but is amplified by the amplifying medium. This process is illustrated in figure 2.8. The fact that the saturation dynamics of the absorber are more rapid than those of the amplifying medium explains why only the center of the pulse is amplified, the wings, on the contrary, being attenuated. The pulse reaches its final shape when it becomes self-consistent in the cavity, that is, when the system reaches a steady state. For the pulse to be self-consistent, it must keep the same shape after a round trip through the cavity.

2.1.3.3. Kerr Lens Mode-Locking [9]

Ti: Sapphire was discovered as gain medium with the bandwidth that could support femtosecond pulses in 1986 and it was generally assumed that everything was known about mode-locked femtosecond lasers by the end of the 80's. However, 1990 saw two important discoveries. Ishida *et al* [10] produced stable 190 fs pulses using a passively mode-locked Ti: Sapphire laser with a saturable absorber. Then Sibbet *et al* [11] showed it was possible to produce 60 fs pulses from a Ti: Sapphire laser that appeared to have no saturable absorber at all. The phenomenon was soon understood and is now called Kerr lens mode-locking (KLM). The optical Kerr effect is a nonlinear interaction of light in a medium with an instantaneous response. The Kerr effect can be described as a modification of the refractive index in response to an electric field. Scottish

physicist John Kerr discovered the occurrence in 1875 and the effect can occur in glasses, crystals and gases, though certain materials display the effect stronger than others. The effect is directly proportional to the square of the electric field (where I is the intensity of light) and this leads to an intensity-dependent refractive index in the material of

$$n = n_0 + n_2 I \tag{2.1.12}$$

Equation 2.1.12 governs the optical Kerr effect where n is the overall refractive index, n_0 is the linear refractive index, n_2 is the second-order nonlinear refractive index and I is the intensity of the incident light. Figure 2.9.a is the intensity distribution of a regular Gaussian beam. Figure 2.9.b shows the change in the index of refraction for a positive n_2 ; the index of refraction experienced by the beam is larger at the center than at the sides.

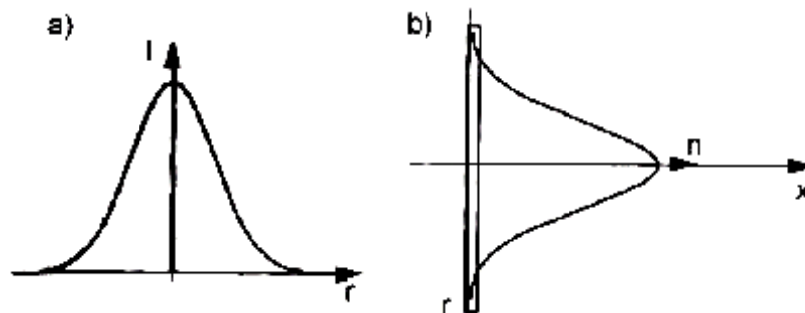


Figure.2.9: a) is the intensity distribution of a regular Gaussian beam and b) is the variation of the index of refraction for $n_2 > 0$, which follows the intensity distribution along the diameter [12].

The index of refraction of a material has implications on the light passing through the material. The velocity of light in a material is equal to the speed of light in vacuum divided by the index of refraction n . Therefore the larger the value of n is, the lower the velocity of light in the material becomes. A lens is a common refractive element that is thicker in the middle than at the edges, causing the light to slow down more in the middle than at the edges. Light is focused towards the center as it becomes bent inwards. In this case the lens has a constant index of

refraction . However, altering so that it is larger in the center than at the edges will also bend light towards the center and produce a lens. Studying Equation 2.1.12 and Figure 2.9 highlights the fact that light itself can alter the index of refraction. When the intensity of light is high enough, the electric field of light becomes strong enough to distort the atoms of the material and change its refractive index.

As the beam is more intense in the center than at the edges, the index of refraction becomes higher in the center than at the edges, which causes light to focus. The focusing from the Kerr lens limits, when the beam’s diameter is narrow enough, is large enough to balance out the Kerr effect (Figure 2.10). The effect is known as self-focusing.

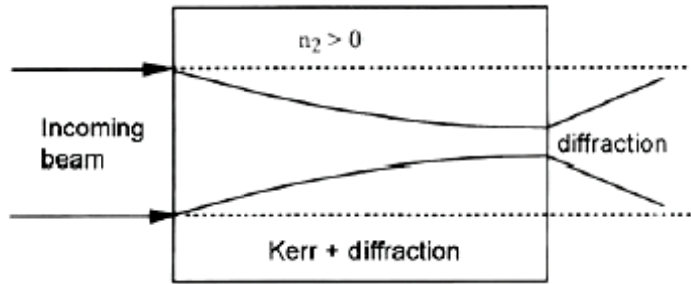


Figure.2.10 - Self-focusing of a laser beam in a medium with $n_2 > 0$. [12]

The Kerr lens is only formed when the intensity of light is extremely high, such as the instantaneous intensity of a mode-locked pulse. The weak intensity of a CW laser is not intense enough to induce an optical Kerr effect. This mechanism of only focusing the high intensity mode-locked pulses has been utilized for Kerr lens mode-locking.

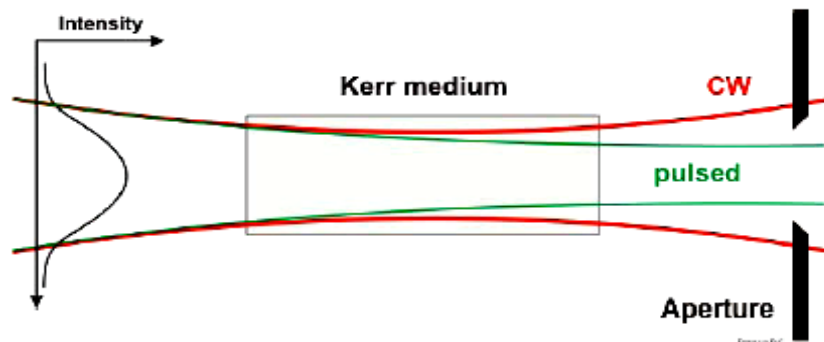


Figure 2.11- Kerr lens mode-locking [12]

The self-focusing from the Kerr lens means that the strong intensity maxima in a laser cavity are focused much more strongly than the weaker maxima, which end up with negligible focusing. The strong intensity maxima have now had their transverse structures reduced in size and so are less vulnerable to losses in the cavity, but the weaker intensities occupying a large volume experience enhanced losses. This leads to self mode-locking of the laser. Putting a slit or aperture into the system, as in Figure.2.11, increases the difference between the losses experienced by weaker intensity maxima and stronger intensity maxima by allowing most of the power of the stronger intensity maxima through, while heavily attenuating most of the weaker intensities.

2.1.4. Applications

2.1.4.1. Mode-Locked Rhodamine 6G Dye Lasers [7]

Commonly used ultrashort laser sources tend to be passively mode-locked, because they are more efficient and, hence, of more practical importance. Until recently, the most widely used ultrashort laser sources were of the type derived from one form or another of Rhodamine 6G (Rh6 G) dye laser with an intracavity saturable absorber such as DODCI, oscillating at 630 nm (Fork *et al.*, [1981]). These have recently largely been superseded by mode-locked solid-state Ti:sapphire lasers (Spence *et al.*, [1991]).

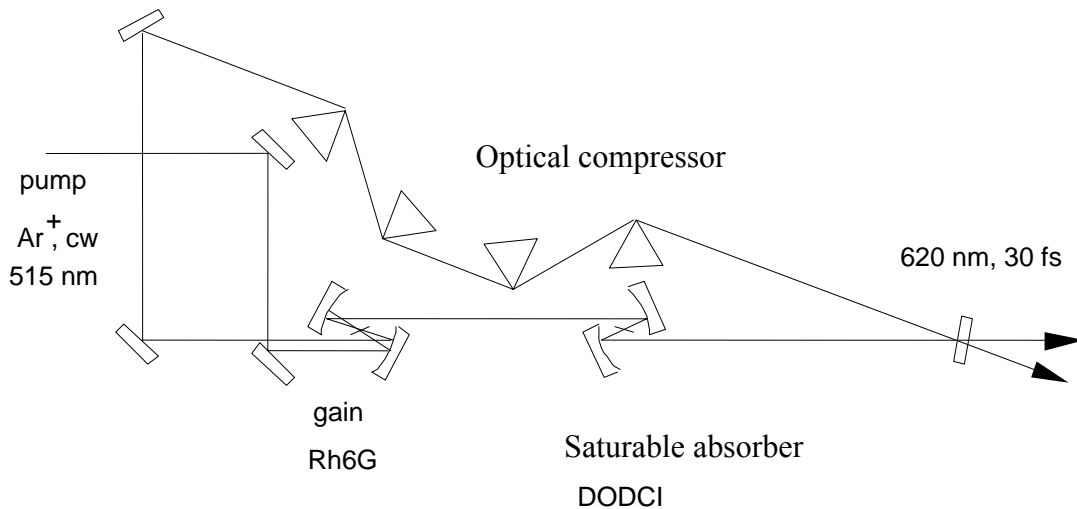


Figure.2.12: Sketch of a balanced colliding pulse mode-locked dye laser. The geometry of the cavity is that of a ring laser with Rhodamine 6G as a gain medium. These molecules are optically pumped by a CW argon ion laser delivering 5W in its 515nm green line. To ensure mode-locking, a second jet, dyed with DODCI(3.3'-diethyloxadicarbocyanine iodide), is placed at the focal point of a short focal length telescope. The maximum emission of Rhodamine 6G is close to 590nm. This wavelength is strongly absorbed by the DODCI molecules, for which the maximum absorption is close to 580nm in the ground state. Absorption of photons induces a conformation change of the DODCI molecules to a photoisomeric state, for which the absorption is red-shifted down to 620nm.

2.1.4.2 The Mode-locked Laser Oscillator [13]

In a Ti: S oscillator, the fundamental frequency is usually 80MHz, which lies in the radio frequency spectrum. Ti: S supports much higher multiples of this fundamental frequency that lie in the near infrared to visible light spectrum. Stimulated emission in Ti: S can span across a broad band of frequencies. This broad band corresponds to over one million different cavity modes. A laser usually operates at one single cavity mode, closest in frequency to the peak of the emission spectrum.

However, it is possible to force the laser (using filters etc.) to operate at other single frequencies in the emission spectrum. A laser oscillator is designed such that several modes across the emission spectrum are brought to laser at once.

The modes will then interfere to construct a pulse. This pulse will propagate between the end mirrors of the cavity, part of it exiting at each round trip, through a partially transmissive end mirror (output coupler). Each pass through the crystal amplifies away any energy loss since the last pass. Since the pulse is composed of several waves with discretely spaced frequencies, the frequency spectrum of a pulse will be a series of discretely spaced peaks. The peaks will be evenly spaced in frequency by the fundamental frequency, which is also the rate at which pulses emerge from the output coupler. The intensity of each peak is governed by the emission profile of the gain medium. This profile can be approximated as a Gaussian function.

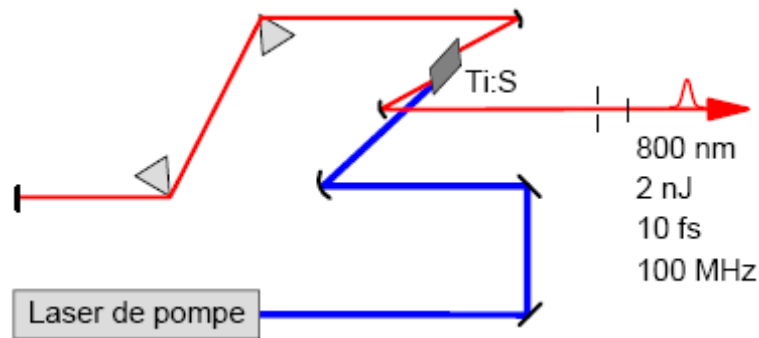


Figure.2.13: A Ti: sapphire oscillator. The compensation of dispersion speed of group is ensured by both prisms, producing a negative dispersion speed of group. The blocking of mode is ensured by Kerr effect. On the one hand, in the temporal field, the non-linear phase makes it possible to compensate for the negative quadratic component resulting from the dispersion of the cavity in linear mode, which makes it possible to have perfectly equidistant longitudinal modes. In addition, in the space field, self focusing by a Kerr lens makes it possible to decrease the losses when the various longitudinal modes are in phase, thus privileging the pulse mode [8].

This laser possesses a favorable combination of properties which are, up to now, the best among all known broadband laser materials. First, the active medium is solid-state, which means a long operational time and laser compactness. Second, sapphire has a high thermal conductivity, an exceptional

chemical inertness and a mechanical resistance. Third, a very broad spectrum is generated.

2.2 Ultrashort Lasers Pulses

Ultrashort pulses are generated using mode-locked lasers and are defined as having a pulse duration of a few tens of picoseconds at the very most. De Maria *et al* produced the first ultrashort pulses just six years after Maiman's first laser was demonstrated. In addition to ultrashort pulse duration, ultrashort pulses have a broad spectrum, high peak intensity and can form pulse trains at a high repetition rate. First it is important to acknowledge the relationship between spectral width and pulse duration when considering the generation of ultrashort pulses. The general time and frequency Fourier transforms of a pulse are,[14]

$$E(t) = \frac{1}{2\pi} \int_{-\infty}^{+\infty} E(\omega) e^{-i\omega t} d\omega \quad \text{and} \quad E(\omega) = \int_{-\infty}^{+\infty} E(t) e^{i\omega t} dt \quad (2.2.1)$$

The duration and spectral width of a pulse can then be calculated with standard statistical definitions,

$$\langle \Delta t^2 \rangle = \frac{\int_{-\infty}^{+\infty} t^2 |\varepsilon(t)|^2 dt}{\int_{-\infty}^{+\infty} |\varepsilon(t)|^2 dt}, \quad \langle \Delta \omega^2 \rangle = \frac{\int_{-\infty}^{+\infty} \omega^2 |E(\omega)|^2 d\omega}{\int_{-\infty}^{+\infty} |E(\omega)|^2 d\omega} \quad (2.2.2)$$

These quantities can then be related by the following inequality,

$$\Delta t \cdot \Delta \omega \geq \frac{1}{2} \quad (2.2.3)$$

Eq.2.2.3 is the product of pulse duration and spectral bandwidth and is known as the time-bandwidth product. In principle this means that in order to generate a short pulse of light with a specific duration Δt , a broad spectral bandwidth $\Delta \omega$ is required. For example, if a pulse is to last a picosecond (10^{-12} s) then the spectral bandwidth must be at least 0.441 THz ($\Delta \omega = 4.41 \cdot 10^{11}$ Hz). When equality to 1/2 is reached in Eq.2.2.3 the pulse is called a Fourier transform-limited pulse. The variation in phase of such a pulse is beautifully uniform and so has linear time dependence; the instantaneous frequency is time independent. This can define

the pulse duration, though the most commonly used definition is based on the full-width at half-maximum (FWHM) principle of optical power against time, because experimentally, it is easier to measure. Eq.2.2.3 then becomes

$$\Delta \tau \Delta \nu \geq K \quad (2.2.4)$$

$\Delta \nu$ is the frequency at full-width half-maximum and $\Delta \tau$ is the duration at half maximum. The value of K from Table.1 depends upon the symmetrical shape of the pulse

Shape	K
Gaussian function	0.441
Exponential function	0.140
Hyperbolic secant	0.315
Rectangular	0.892
Cardinal sine	0.336
Lorentzian function	0.142

Table 1: Various values for K depending on the pulse shape.

It follows directly from Eq.2.2.4 that the minimum achievable duration is limited by the spectrum of the pulse. In other words, in order to produce ultrashort pulses a very broad spectral bandwidth is needed. The shortest possible pulse, for a given spectrum, is known as the *transform-limited pulse duration*. It should be noted that Eq.2.2.4 is not an equality, i.e. the product can very well exceed K . If the product exceeds K the pulse is no longer transform-limited and all frequency components that constitute the pulse do not coincide in time, i.e. the pulse exhibits a frequency modulation and so is very often referred to as a *chirp* [15].

2.2.1 Mathematical Description of Laser Pulses

Ultrashort laser pulses are coherent bursts of electromagnetic radiation, confined in time and space. They are characterized by several parameters:

temporal coherence, spatial coherence (i.e. focusing ability) contrast, power, etc. Here the description is concentrated on their temporal aspects.

In order to completely describe a laser pulse, the temporal profile, the spectral profile and the phase of the pulse have to be known. However, time and frequency are related through a Fourier transform and it is therefore sufficient to know only two of these parameters since the third can always be calculated from the other two.

2.2.1.1 Time Domain Description

The electric field $E(t)$, is a real quantity and all measured quantities are real. However, the mathematical description is simplified if a complex representation is used:

$$\tilde{E}(t) = \tilde{A}(t) \cdot e^{-i\omega_0 t}. \quad (2.2.5)$$

where $\tilde{A}(t)$ is the complex envelope, usually chosen such that the real physical field is twice the real part of the complex field, and ω_0 is the carrier frequency, usually chosen at the center of the spectrum. In this way, the rapidly varying envelope is separated from the slowly varying envelope $\tilde{A}(t)$. $\tilde{E}(t)$ can be further decomposed into:

$$\tilde{E}(t) = |\tilde{E}(t)| \cdot e^{i\varphi_0} \cdot e^{-i\varphi(t)} = |\tilde{E}(t)| \cdot e^{i\varphi_0} \cdot e^{-i(\varphi(t) - \varphi_0)}. \quad (2.2.6)$$

$\varphi(t)$ is often referred to as the temporal phase of the pulse and φ_0 the absolute phase, which relates the position of the carrier wave to the temporal envelope of the pulse (see figure.2.14). In $\varphi(t)$, the strong linear term due to the carrier frequency, ωt , is omitted. The absolute phase is important mainly for pulses consisting of only a few cycles and has recently attracted a great deal of attention. The absolute phase has, for instance, been shown to be very important when generating high-order harmonics with few-cycle pulses.

The instantaneous frequency $w(t)$ is given by the first derivative of the temporal phase:

$$w(t) = \frac{d\varphi(t)}{dt} = \frac{d\varphi(t)}{dt} - \omega_0. \quad (2.2.7)$$

which means that a nonlinear temporal phase yields a time-dependent frequency modulation. The pulse is said to carry a chirp (illustrated in Figure 2.15) [15].

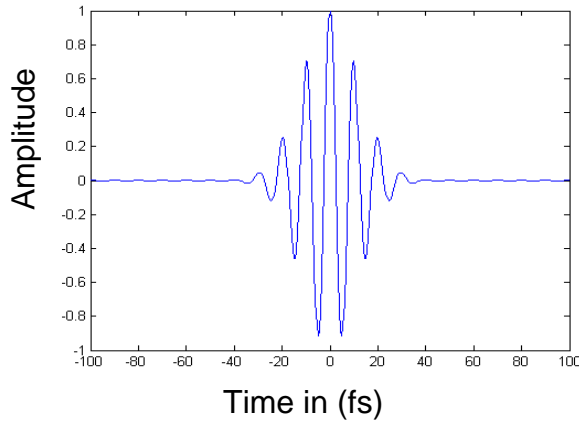


Figure 2.14: the electric field of an ultrashort laser pulse consisting of only a

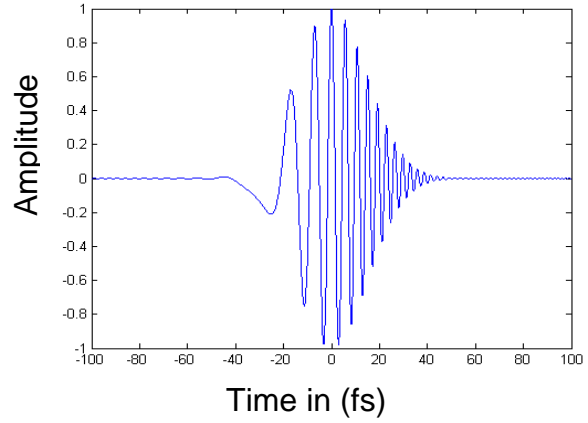


Figure 2.15: the electric field of an ultrashort laser pulse with a strong positive chirp. Note the frequency variation as a function of time. At the leading edge (to the left) the wavelength is longer than at the trailing edge.

2.2.1.2 Frequency Domain Description

It is usually more convenient to represent the pulse in the frequency domain rather than in the time domain. The frequency representation is obtained from the time domain by a complex Fourier transform,

$$E(\omega) = \frac{1}{\sqrt{2\pi}} \int_{-\infty}^{+\infty} E(t) \cdot e^{i\omega t} \cdot dt. \tag{2.2.8}$$

Just as in the time domain, $\tilde{E}(\omega)$ can be written as:

$$\tilde{E}(\omega) = |\tilde{E}(\omega)| e^{i\varphi(\omega)}. \tag{2.2.9}$$

where $\varphi(\omega)$ now denotes the spectral phase. An inverse transform leads back to the time domain,

$$\tilde{E}(t) = \frac{1}{\sqrt{2\pi}} \int_{-\infty}^{+\infty} \tilde{E}(\omega) \cdot e^{i\omega t} \cdot d\omega. \tag{2.2.10}$$

From Eq.2.2.10 it is clear that $\tilde{E}(t)$ can be seen as a superposition of monochromatic waves. The square of the spectral amplitude, $|\tilde{E}(\omega)|^2$, represents the power spectrum, or spectral power density, which is the pulse parameter that

is most easily accessible experimentally. It is commonly referred to as the spectrum of the pulse. The spectral phase can, in the same manner as the temporal phase, be decomposed into different parts. A common procedure is to employ Taylor expansion

$$\phi(\omega) = \phi_0 + \sum_{n=1}^{\infty} \frac{1}{n!} a_n (\omega - \omega_0)^n. \quad \text{with} \quad a_n = \left. \frac{d^n \phi}{d\omega^n} \right|_{\omega=\omega_0}. \quad (2.2.11)$$

It can be seen by inserting this Taylor expansion into Eq.2.2.10 that the first two terms will not change the temporal profile of the pulse. A linear phase variation does not change the shape of the pulse, but only introduces a temporal shift of the entire pulse. Therefore, usually only the nonlinear part of the spectral phase is of interest. Any nonlinear addition to the phase will redistribute the frequency components and alter the temporal shape of the pulse [16].

2.2.2 Propagation of a Light Pulse in Transparent Medium

What happens to a short optical pulse propagating in a transparent medium? Because of its large spectral width and because of group velocity dispersion in transparent media, it undergoes a phase-distortion inducing an increase of its duration. This happens with any optical element and needs to be properly corrected in the course of experiments.

The frequency Fourier transform of a Gaussian pulse has already been given as

$$E(\omega) = E_0 \sqrt{\frac{\pi}{\Gamma}} \exp\left[-\frac{(\omega - \omega_0)^2}{4\Gamma}\right] \quad (2.2.12)$$

After the pulse has propagated a distance z , its spectrum is modified to

$$E(z, \omega) = E_0(0, \omega) \exp[ik(\omega)z] = E_0(\omega) \exp[ik(\omega)z] \quad (2.2.13)$$

where $k(\omega) = kz = \frac{\omega}{v}z = \frac{\omega}{c}n(\omega)z$ where $k(\omega)$ is now a frequency dependent

propagation factor. In order to allow for a partial analytical calculation of the propagation effects, the propagation factor is rewritten using a Taylor expansion as a function of the angular frequency, assuming that $\Delta\omega \ll \omega_0$ (this condition is only weakly true for the shortest pulses). Applying the Taylor expansion

$$k(w) = k(w_0) + (w - w_0) \left. \frac{dk}{dw} \right|_{w_0} + \frac{1}{2} (w - w_0)^2 \left. \frac{d^2k}{dw^2} \right|_{w_0} + \dots + \frac{1}{n!} (w - w_0)^n \left. \frac{d^n k}{dw^n} \right|_{w_0} + \theta(w) \quad (2.2.14)$$

Where $\frac{dk}{dw} = \left(\frac{dk(w)}{dw} \right)_{w_0}$ and $\frac{d^2k}{dw^2} = \left(\frac{d^2k(w)}{dw^2} \right)_{w_0}$ (2.2.15)

to Eq.2.2.13, the pulse spectrum becomes

$$E(r, w) = E_0(0, w) \cdot \exp \left[-ik(w_0)z - ik^{(1)}z(w - w_0) - \left(\frac{1}{4\Gamma} + \frac{1}{2}k^{(2)} \right) (w - w_0)^2 \right] \quad (2.2.16)$$

The time evolution of the electric field in the pulse is then derived from the calculation of the inverse Fourier transform of Eq.2.2.16,

$$E(t, z) = TF^{-1} \{ E(w, z) \} \\ = \frac{1}{2} \int_{-\infty}^{+\infty} E(w, z = 0) \cdot \exp(j\phi(w)) \cdot \exp(jwt) d\hat{w} \quad (2.2.17)$$

So that $E(t, z) = \zeta_0 \sqrt{\frac{\Gamma(z)}{\pi}} \cdot \exp \left[\underbrace{-\Gamma(z) \left(t - \frac{z}{V_g(w_0)} \right)^2}_{\alpha} \right] \cdot \exp \left[\underbrace{jw_0 \left(t - \frac{z}{V_\phi(w_0)} \right)}_{\beta} \right]$ (2.2.18)

where $\frac{1}{\Gamma(z)} = \frac{1}{\Gamma} + 2 \cdot j \cdot k^{(2)} \cdot z$, $V_\phi(w_0) = \left[\frac{w}{k} \right]_{w=w_0}$, $V_g(w_0) = \left[\frac{dw}{dk} \right]_{w=w_0}$ (2.2.19)

In the first exponential of Eq.2.2.18, it is clear that, after propagation over a distance z , the pulse keeps a Gaussian envelope. This envelope is delayed by an amount z/V_g , V_g being the group velocity.

In the second term of Eq.2.2.18, one can observe that the phase of the central frequency w_0 is delayed by an amount $\frac{z}{V_\phi}$ after propagation over a distance z . The

phase velocity $V_\phi(w_0)$ measures the propagation speed of the plane wave components of the pulse in the medium. These plane waves do not carry any information, because of their infinite duration. The resultant intensity is

$$I(z, t) = I_0 \cdot \frac{1}{\sqrt{1 + 4(\Gamma k^{(2)} z)}} \cdot \exp \left[-2\Gamma \frac{\left(t - \frac{z}{V_g} \right)^2}{1 + 4(\Gamma_0 k^{(2)} z)^2} \right] \quad (2.2.20)$$

The Temporal Pulse width at point z is

$$\Delta\tau_z = \Delta\tau_0 \sqrt{1 + 4(\Gamma.k^{(2)}.z)^2} \tag{2.2.21}$$

In summary, the propagation of a short optical pulse through a transparent medium results in a delay of the pulse, a duration broadening and a frequency chirp.

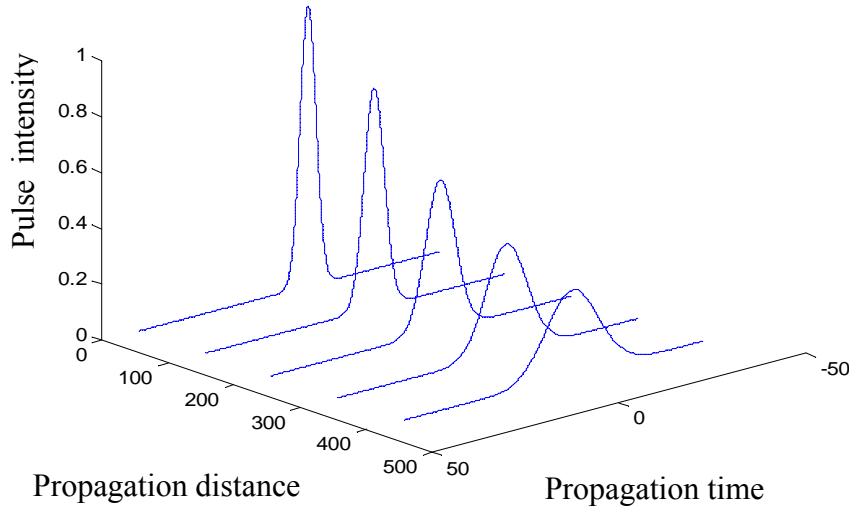


Figure.2.16: A numerical calculation of the intensity envelope of a pulse propagating along z , in a lossless, transparent medium. The pulse broadens with time but, from energy conservation, its time integrated intensity remains constant.

2.2.3 Dispersion Parameter of a Transparent Medium

The dispersion of an index of refraction is usually tabulated as a function of the wavelength of light in vacuum. We therefore need to recalculate the dispersion as a function of the wavelength.

From Eq.2.2.15 we obtain

$$k^{(2)} = -\frac{\lambda^2}{2\pi.c} D, \tag{2.2.22}$$

Where D is the dispersion parameter.

$$k^{(2)} = -\frac{\lambda^3}{2\pi.c^2} \frac{d^2n}{d\lambda^2}. \tag{2.2.23}$$

The sign of $k^{(2)}$ depends on the curvature of the index dispersion $\frac{d^2n}{d\lambda^2}$.

2.2.3.1. Temporal study of the widening of ultra-short pulses introduced by the elements of the cavity

Propagation of ultrashort optical pulses in a linear optical medium consisting of free space, dispersive media, diffractive optical elements [8,9], focusing elements and apertures has been extensively studied analytically, though only a few isolated attempts have been made on numerical simulation. In view of the recent advance in ultrashort pulse propagation, a strong need is felt for developing a numerical formalism capable of performing such a complete analysis of the issues involved in pulse propagation. Here we introduce a numerical simulation tool for the propagation of ultrashort pulses of arbitrary shape through linear homogeneous media based on wave optical field representation, which enables an easy evaluation for the merit functions of the pulsed field. This allows us to analyze the pulse in the time-frequency domain at any arbitrary plane. With this tool, we investigate the spectral and temporal evolution of ultrashort pulses at any arbitrary propagation distance. The propagation of the pulse is achieved in terms of its spectral equivalent.

Furthermore, we introduce certain sampling rules for the spectral phase so that the phase information is sampled properly when we move from one spectral component to another in the spectral equivalent of the pulse. As a consequence, the algorithm becomes computationally efficient since we only considered a small number of spectral components for simulation of pulse propagation [17, 18, 19].

The Fourier theorem is the most classical approach for describing the propagation of electromagnetic signals through dispersive media. In the case of signals characterized by a slow temporal varying envelope, the phase is usually approximated by the Taylor expansion in the neighborhood of the central

frequency of the input pulse. For shorter pulses, the concept of group velocity is irrelevant and the envelope distortion is a function of the higher order terms.

Ultrashort pulses, less than 10 fs, are now available. Their envelope harmonic content is so high that the Taylor expansion of the phase is now more possible. There is no other way than a numerical computation of the Fourier integral. However this method does not permit a straightforward physical understanding of the envelope propagation and principally does not picture the fact that this is the group velocity dispersion which generates the ultrashort pulse distortions. Such a situation claims for another type of decomposition involving both a time and frequency dependence of the components.

Numerous bidimensional representations of acoustic and electromagnetic signals have already been suggested. We propose here a method derived from the Gabor transformation in order to decompose the signal into an infinite number of elementary components (wavelets) of same duration (much more longer than that of the original signal), each of them being centered at a frequency Ω belonging to the Fourier spectrum of the pulse[20].

2.2.4. Time-Frequency Decomposition

2.2.4.1 Wavelet Theory

Geophysicist *Jean Morlet* proposed in 1983, a revolutionary process, the analysis and the synthesis by the wavelet, which makes it possible to analyze signals effectively or combine very different phenomena of scales. The wavelets are very particular elementary functions. They are the shortest and most elementary vibrations that one can consider. One can say that the wavelet carries out a zooming on any interesting phenomenon of the signal, in the vicinity of the point considered [21].

2.2.4.2 Wavelet Techniques

Starting with a signal $e(t)$, in plane $z = 0$, we define a wavelet centered at Ω by $\theta(\Omega) = E(w) \cdot \exp\left[-\frac{(w-\Omega)^2}{4\gamma}\right]$, with $E(w) = \frac{E_0}{2\pi} \sqrt{\frac{\pi}{\Gamma}} \exp\left[-\frac{(w-w_0)^2}{4\Gamma}\right]$, (2.2.24)

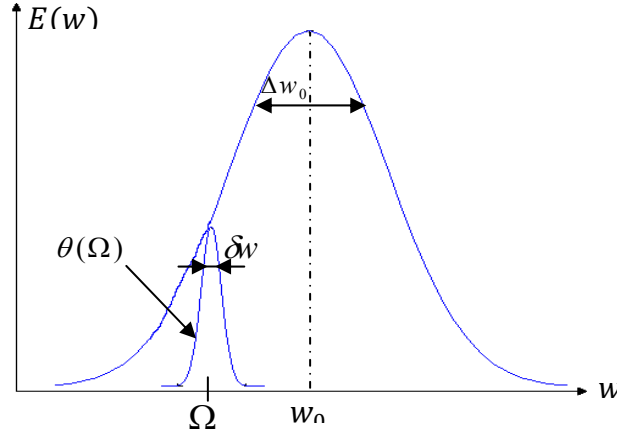


Figure.2.17: A Gaussian envelope decomposed in a number of wavelets

We calculate the electric field associated with the wavelet $\theta(\Omega, z = 0)$.

$$\theta(t, z = 0) = TF\{\theta(\Omega, z = 0)\} \tag{2.2.25}$$

$$\theta(t, z = 0) = E_0 \sqrt{\frac{\gamma}{\gamma+\Gamma}} \cdot \exp\left[-\frac{(w_0-\Omega)^2}{4(\gamma+\Gamma)}\right] \cdot \exp\left[-\frac{\gamma\Gamma}{\gamma+\Gamma} t^2\right] \cdot \exp\left[j\frac{\gamma w_0 + \Gamma\Omega}{\gamma+\Gamma} t\right]. \tag{2.2.26}$$

The maximum amplitude of the wavelet $\theta(t, x = 0)$ varies with Ω , center frequency of analysis on a Gaussian of parameter $\gamma + \Gamma$ [22].

In time, the pulse is also Gaussian, of parameter $\frac{\gamma\Gamma}{\gamma+\Gamma}$.

The signal propagates in the positive z direction in a linear dispersive and transparent medium, which fills the half space $z > 0$ and whose refractive index is $n(w)$. After propagation, the wavelet $\theta(\Omega, z)$ may be written as

$$\theta(\Omega, z) = \frac{E_0}{2\sqrt{\pi}\gamma} E(w) \cdot \exp\left[-\frac{(w-\Omega)^2}{4\gamma}\right] \cdot \exp[j\phi(w)]. \tag{2.2.27}$$

We can say that $\tau_{wavelet}$ is large enough to ensure a good application of the function $\theta(t, z = 0)$ over a spectral range lying in the neighbourhood of Ω in Figure 2.17. Under these circumstances, we have

$$\begin{aligned} \phi(w) = & \phi(\Omega) + (w - \Omega) \left. \frac{d\phi}{dw} \right|_{w=\Omega} + \frac{1}{2!} (w - \Omega)^2 \left. \frac{d^2\phi}{dw^2} \right|_{w=\Omega} + \dots + \frac{1}{n!} (w - \\ & \Omega)^n \left. \frac{d^n\phi}{dw^n} \right|_{w=\Omega} + \theta(w). \end{aligned} \quad (2.2.28)$$

Neglecting the higher terms in Eq.2.2.28:

$$\phi(w) = \phi(\Omega) + (w - \Omega) \left. \frac{d\phi}{dw} \right|_{w=\Omega} + \frac{1}{2!} (w - \Omega)^2 \left. \frac{d^2\phi}{dw^2} \right|_{w=\Omega} + \theta(w). \quad (2.2.29)$$

$$\begin{aligned} \theta(\Omega, z) = & \frac{E_0}{2\sqrt{\pi}\gamma} \sqrt{\frac{\pi}{\Gamma}} \exp\left[-\frac{(w-w_0)^2}{4\Gamma}\right] \cdot \exp\left[-\frac{(w-\Omega)^2}{4\gamma}\right] \\ & \cdot \exp\left[j\phi^{(0)} + j(w - \Omega)\phi^{(1)} + \frac{1}{2}j(w - \Omega)^2 \cdot \phi^{(2)}\right]. \end{aligned} \quad (2.2.30)$$

We calculate the temporal electric field associated with the wavelet $\theta(\Omega, z)$.

$$\theta(t, z) = \frac{1}{2\pi} \int_{-\infty}^{+\infty} \theta(\Omega, z) \cdot \exp(j\omega t) d\omega \quad (2.2.31)$$

$$\begin{aligned} \theta(t, z) = & \frac{1}{2\pi} \frac{E_0}{2\sqrt{\pi}\gamma} \sqrt{\frac{\pi}{\Gamma}} e^{\left[-\frac{(\Omega-w_0)^2}{4\Gamma}\right]} e^{j\phi^{(0)}} \cdot e^{-\left[\frac{1}{4\Gamma} + \frac{1}{4\gamma} - \frac{1}{2}j\phi^{(2)}\right]\Omega^2} \cdot e^{\left[\frac{(\Omega-w_0)}{2\Gamma} - j\phi^{(1)}\right]\Omega} \times \\ & \int_{-\infty}^{+\infty} e^{-\left[\frac{1}{4\Gamma} + \frac{1}{4\gamma} - \frac{1}{2}j\phi^{(2)}\right]w^2} \cdot e^{\left[\frac{1}{4\Gamma} + \frac{1}{4\gamma} - \frac{1}{2}j\phi^{(2)}\right]2\Omega w} \cdot e^{\left[-\frac{(\Omega-w_0)^2}{2\Gamma} - j\phi^{(1)}\right]} \cdot e^{j\omega t} d\omega. \end{aligned} \quad (2.2.32)$$

The amplitude of the incident Ω wavelet is given, from Eq.2.2.33, by

$$\begin{aligned} \theta(t, z) = & \frac{E_0}{2\sqrt{\pi}\gamma} \sqrt{\frac{\Gamma(z)}{\Gamma}} \cdot \exp(j\phi^{(0)}) \exp\left(-\Gamma(z) \left[t + \frac{z}{v_g(\Omega)}\right]^2\right) \times \\ & \exp\left(-\frac{(\Omega-w_0)^2}{4\Gamma} \left[1 - \frac{\Gamma(z)}{\Gamma}\right]\right) \cdot \exp\left[j\left(1 - \frac{\Gamma(z)}{\Gamma}\right)\Omega + \frac{\Gamma(z)}{\Gamma}w_0\right] \left(t + \frac{z}{v_g(\Omega)}\right). \end{aligned} \quad (2.2.33)$$

This wavelet is characterized by a Gaussian envelope (see Appendix B). This decomposition is valid only for the values of $\Delta\omega$ much larger than $\delta\omega$ ($\Delta\omega \gg \delta\omega$).

The delay of group of the wavelet $\left[t + \frac{z}{v_g(\omega)} \right]$ is characterized by a Gaussian envelope which is the temporal width.

The delay of group of the wavelet is inversely proportional to the velocity of group. Its envelope propagates without deformation [20].

2.2.4.3 Simulations and Comparison with silica fiber

Initial pulse:	$\Delta\tau_0 = 10 \text{ fs}$
Wavelength:	$\lambda = 800 \text{ nm}$
Pulse of the wavelet:	$\Delta\tau_{\text{wavelet}} = 1000 \text{ fs}$
Propagation length:	$x = 1 \text{ m and } 5 \text{ m}$

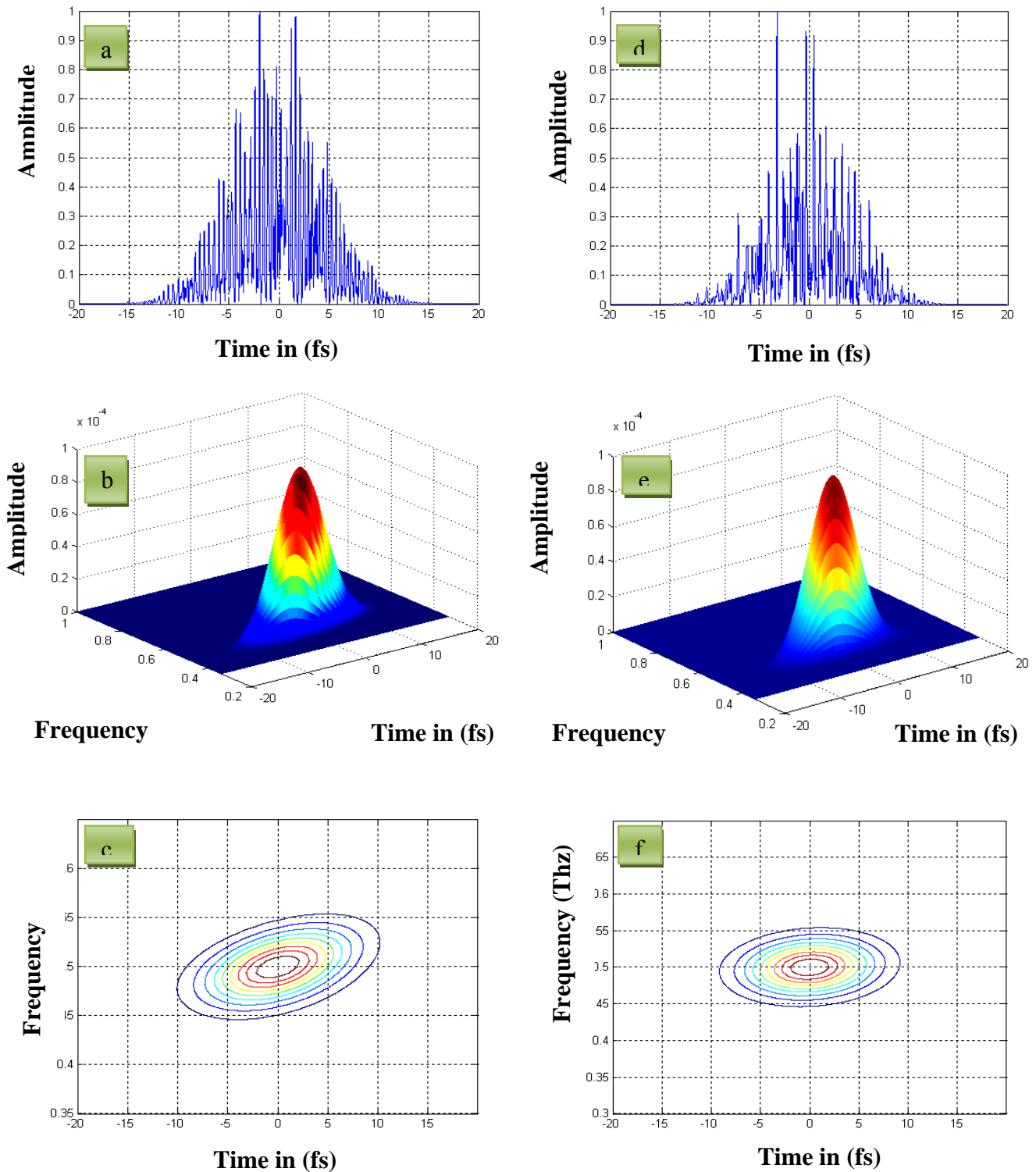


Figure 2.18: (a) Pulse after propagating 5 cm in silica fiber, (b) Wavelet after propagating 5 cm in silica fiber, (c) Contour of the wavelet after propagating 5 cm in silica fiber, (d) Pulse after propagating 1 m in Titanium-Sapphire, (e) wavelet after propagating 1m in Titane-Sapphire, (f) Contour of the wavelet after propagating 1 m in Titanium-Sapphire.

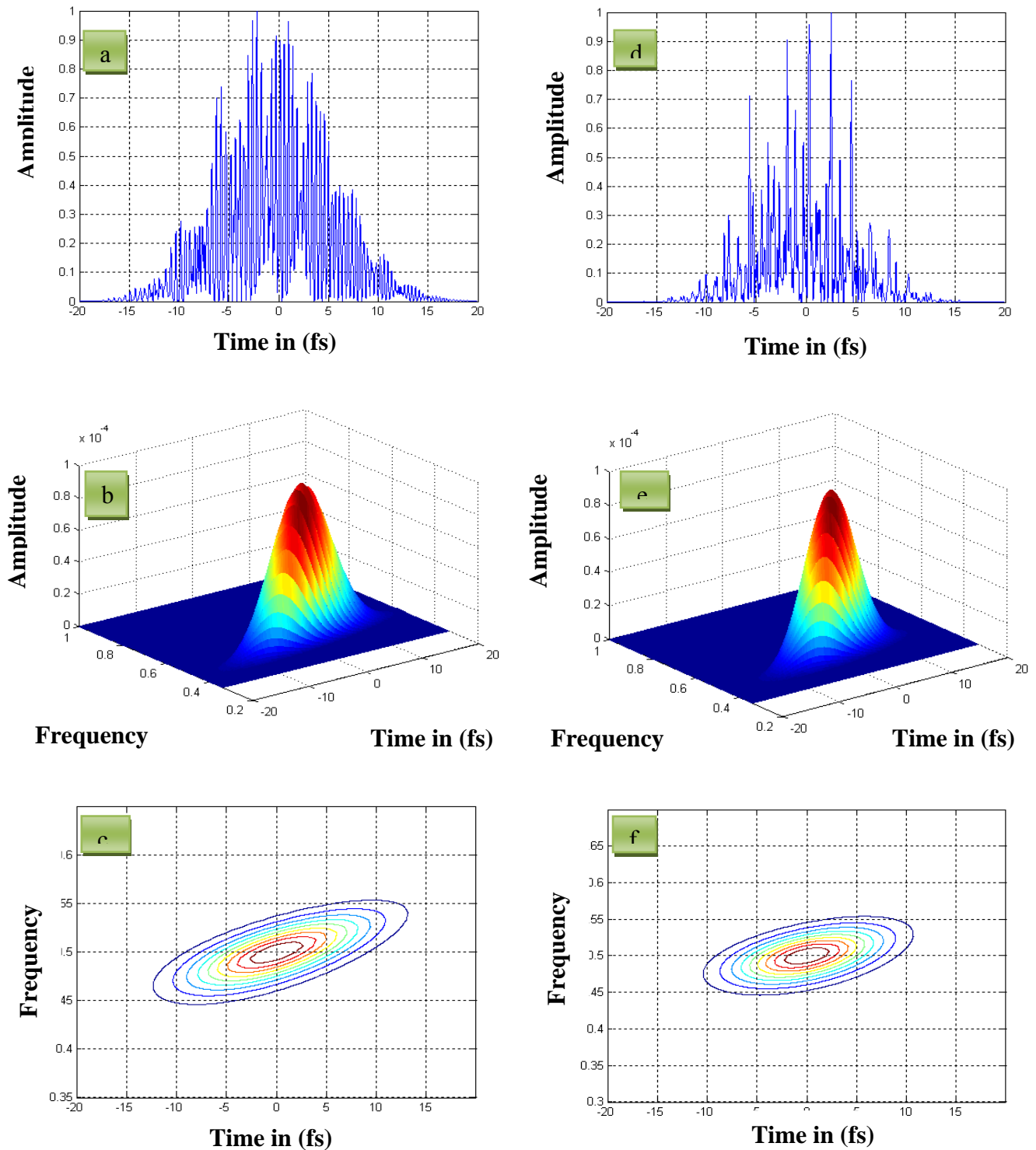


Figure 2.19: (a) Pulse after propagating 10 cm in silica fiber, (b) Wavelet after propagating 10 cm in silica fiber, (c) Contour of the wavelet after propagating 10 cm in silica fiber, (d) Pulse after propagating 5 m in Titanium-Sapphire, (e) Wavelet after propagating 5 m in Titanium-Sapphire, (f) Contour of the wavelet after propagating 5 m in Titanium-Sapphire [21-23].

In this part, we made a detailed study of comparison of the propagation of ultrashort laser pulses in Titanium-Sapphire and in silica fiber. We have demonstrated here the possible decomposition of an ultrashort pulse into an infinite number of longer Fourier-transform limited wavelets which propagate without any deformation through a dispersive medium. After propagation through the medium, the pulse may be visualized in a three dimensional representation by the locus of the wavelet maxima. This representation permits the evaluation of the broadening suffered by the pulse. For a transparent medium, the propagation of the Ω wavelet is described by the convolution of the incident Ω wavelet with a $\theta(\Omega)$ distribution centered at the group delay, relative to Ω [21, 23].

Although this technique represents a big improvement in our ability to describe such pulses, they require additional effort, both in the apparatus and in the extraction of the pulse intensity and phase from the experimental trace. Our results show that Titanium-Sapphire is a better candidate for a novel generation of optical fibers for the transmission and propagation of an ultrashort laser pulse.

2.3 Cavity Alignment

2.3.1. Group Velocity Dispersion [1]

An ultrashort pulse of light will lengthen after it has passed through glass, as the index of refraction, which dictates the speed of light in the material, depends on the nonlinearly on the wavelength of light. The wavelength of an ultrashort pulse of light is formed from the distribution of wavelengths on either side of the center wavelength, with the width of this distribution inversely proportional to the pulse duration. At a given wavelength, the refractive index determines the velocity of a single mode, known as the phase velocity. Figure 2.20 is a plot of the refractive index, $n(\lambda)$, versus the wavelength, λ , and it sees $n(\lambda)$ decrease monotonically as λ increases, with a gradual upward curvature for most materials that are transparent in the optical spectrum. This is called dispersion. A material producing a downward curvature is said to have an anomalous dispersion.

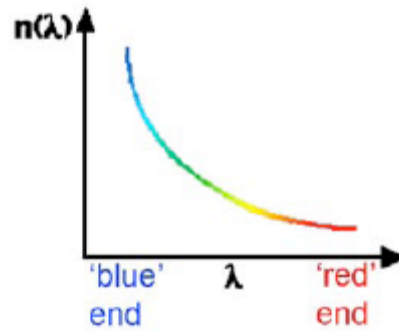


Figure. 2.20: Group velocity dispersion curve

The slope of the curve, $\frac{dn(\lambda)}{d\lambda}$ is the group velocity, which defines the velocity of the wave packet with a central wavelength λ . The second derivative of the slope, $\frac{d^2n(\lambda)}{d\lambda^2}$, yields the group velocity dispersion (GVD), which is defined as the rate at which the frequency components of the wave packet change their relative phases. Group velocity dispersion is responsible for a dispersive broadening of the pulses.

2.3.2. Self Phase Modulation [1]

The optical Kerr effect is responsible for the nonlinear effect of Self Phase Modulation (SPM). Each of the different frequency components of the pulse experiences a different phase shift, generating new frequencies and broadening the frequency spectrum of the pulse, symmetrically. The leading edge of the pulse is shifted to lower frequencies (down chirp) while the trailing edge is shifted to higher frequencies (up chirp). The center of the pulse experiences an approximate linear chirp.

Self phase modulation itself is not a dispersive effect, but it causes a pulse to no longer be transform-limited when crossing a transparent material, which means the pulse is then subject to dispersion, like that in Figure 2.21. Dispersion causes the 'redder' parts of the pulse to have a higher velocity than the 'bluer' parts, forcing the front of the pulse to move quicker than the back, temporally broadening the pulse. In anomalous dispersion the opposite is true and the pulse is temporally compressed. The self phase modulation becomes stronger as the pulse becomes more intense, in turn causing more broadening.

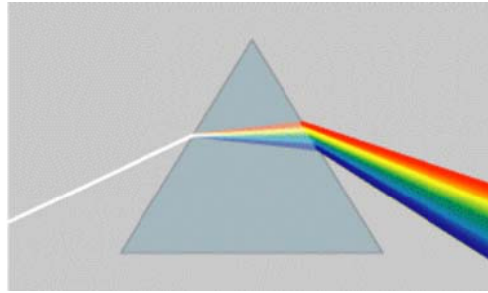


Figure 2.21: Dispersion of light through a prism

2.3.3 Prismatic Group Delay Dispersion Compensator [1]

There are many dispersive elements within a laser cavity. An oscillating pulse will receive a slight chirp from each of these dispersive elements every round-trip. The cumulative effect from a lack of compensation for both GVD and SPM effects would see a temporal broadening for the pulse. The oscillator uses a pair of prisms that the light passes through twice for complete compensation against the positively chirped dispersion an ultrashort pulse experiences on a round-trip. The choice of a material, orientation and distance between the prisms is such that they introduce a net negative GVD, cancelling out the positive GVD from the rest of the system.

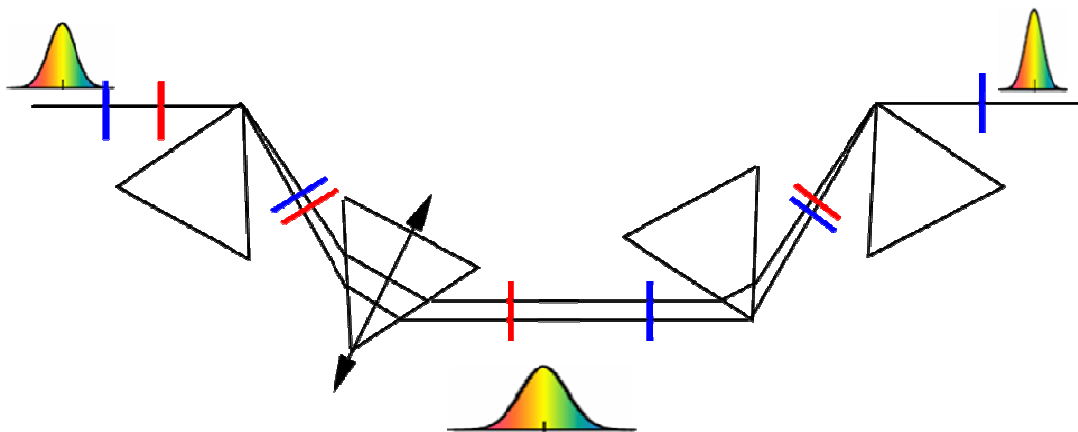


Figure 2.22. Pulse compressor, with a negative GDD. Longer wavelengths traverse more glass. The use of two prisms and a mirror simplifies the device somewhat, but it remains difficult to vary its GDD over a wide range and to tune it.

Group Delay Dispersion (GDD) is a ubiquitous, and often irritating, phenomenon in ultrafast laser labs. When ultrashort pulses propagate through dispersive media, their frequency components emerge at different times due to GDD, causing the resulting pulse to be chirped and stretched and reducing the pulse's peak power. This effect can be compensated by using a *pulse compressor*, which can introduce negative GDD. The most common method for introducing negative GDD is through angular dispersion. Martinez et al. showed that angular dispersion, regardless of its sign, yields negative GDD. Therefore, simply propagating the pulse through a prism or diffracting it off a grating (but we will, for simplicity, discuss only prism devices here) yields negative GDD, whose magnitude depends on the propagation distance. But the output pulse has inconvenient angular and spatial dispersion. Adding a second identical prism, anti-parallel to the first one, eliminates the angular dispersion from the output beam. Eliminating the spatial dispersion requires propagation through an additional identical pair of prisms (see Fig.2.22). As a result, the *four-prism pulse compressor* can compensate for the material dispersion and also reconstruct the beam. Indeed, with the geometry shown in Figure 2.22 for two prisms, we can obtain the GDD by:

$$\varphi_P'' = \frac{\lambda^3}{\pi c^2} l \left\{ \left[\frac{dn^2}{d\lambda^2} + \left(2 - \frac{1}{n^3} \right) \left(\frac{dn}{d\lambda} \right)^2 \right] \sin\beta - 2 \left(\frac{dn}{d\lambda} \right)^2 \cos\beta \right\} \quad (2.3.1)$$

As a comparison, we recall the expression of the dispersion introduced by a length l of a transparent medium

$$\varphi_m'' = - \frac{\lambda^3}{2\pi c^2} \frac{dn^2}{d\lambda^2} l \quad (2.3.2)$$

Looking at these different expressions of n , one can see that if usual materials (including Ti: Sa) present a positive dispersion, it can be compensated by prisms with a sufficient spacing between them.

2.3.4 Time Compression with a Pair of Gratings [1]

In order to correct for group velocity dispersion distortions, several optical devices have been designed that have overall negative group velocity dispersion. As an example we consider a pair of transmission gratings R_1 and R_2 . These gratings have a groove spacing d , and their separation is l (Fig.2.23).

A light ray, with wavelength λ , impinges on gratings R_1 with an angle of incidence γ and is scattered with an angle θ . The gratings are set in such a way that their wavelength dispersions are reversed, which implies that the exiting ray at point B is parallel to the incident ray. P_1 and P_2 are wave planes at the entrance A and exit B of the system. P_2 crosses the emerging ray at point C. Between points A and B the light travels a distance $b = l/\cos\theta$. The diffraction due to a grating can be written as

$$d(\sin\gamma + \sin\theta) = \lambda \quad (2.3.3)$$

In order to calculate the dispersion from Eq.2.3.2, the group delay experienced by the light must first be evaluated. In this specific case, where propagation takes place only in air, the group delay is simply equal to the travel time of light along ABC,

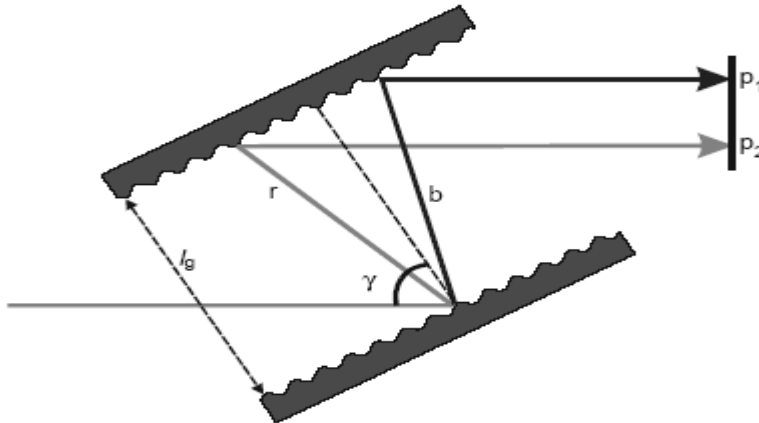


Figure 2.23 Grating pairs used in the control of dispersion. r and b indicate the relative paths of arbitrary long- and short-wavelength rays. γ is the (Brewster) angle of incidence at the prism face. Light is reflected in the plane (p_1 - p_2) in order to remove the spatial dispersion shown.

$$D = \frac{1}{cd^2} \left[1 - \left(\frac{\lambda}{d} - \sin\gamma \right)^2 \right]^{-1}, \quad (2.3.4)$$

$$k'' = -\frac{\lambda^3}{2\pi c^2 d^2} \left[1 - \left(\frac{\lambda}{d} - \sin\gamma \right)^2 \right]^{-1}, \quad (2.3.5)$$

This expression demonstrates the possibility of selecting a set of parameters in such a way as to design a pair of gratings producing positive or negative active group velocity dispersion. Therefore, one can build optical devices that compensate a positive group velocity dispersion suffered by optical pulses traveling through a transparent material.

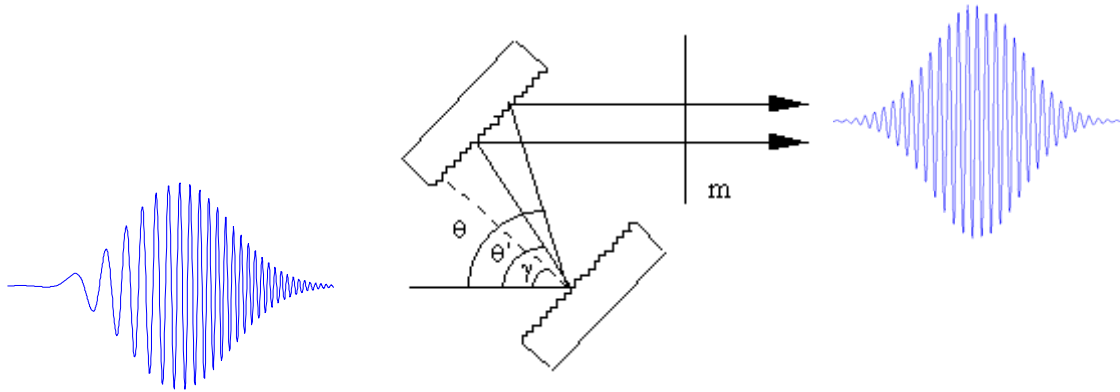


Figure.2.24: Grating optical compressor. Two gratings are set in subtractive diffraction geometry. The red components of a light pulse have a longer optical path than the blue ones. The various components of a positively dispersed pulse can therefore be reset in phase.

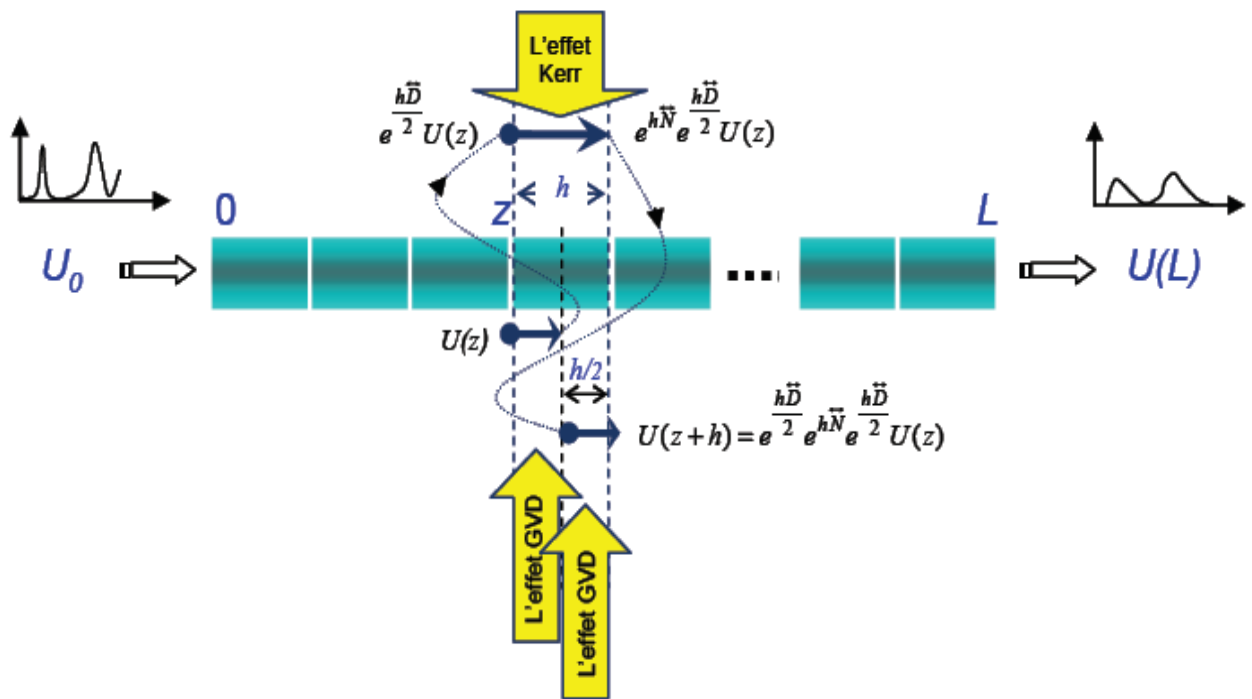
Optical compressors have played a key role in the development of various fields in which short optical pulses have been used as a primary tool. Figure 2.24 shows a typical arrangement for a reflective pulse compressor.

References

- [1] Rullière, C.; *Femtosecond Laser Pulses: Principles and Experiments*, Springer, 2005,
- [2] Wilson, J.; Hawkes, J.F.B.; *Lasers: Principles and Experiments*, Prentice Hall, 1987,
- [3] <http://en.wikipedia.org/wiki/Lasers>
- [4] <http://en.wikipedia.org/wiki/Modelocking>
- [5] <http://en.wikipedia.org/wiki/Image:Modelock-1.png>
- [6] Rudolph, D.; *Ultrashort Laser Pulse Phenomena*, Academic Press, 1995, p. 209
- [7] Claude Rullière (ed) "Femtosecond Light Pulses: Principles and Experiment" Springer 1998
- [8] http://www.rp-photonics.com/img/actively_ml_laser.png
- [9] Moulton, P.F.; Spectroscopic and laser characteristics of Ti:Al₂O₃, *J. Opt. Soc. Am. B* 3,1986
- [10] Ishida, Y.; Sarukura, N.; Nakano, H; Conference: Ultrafast Phenomena VII, OSA, California, 1990
- [11] Keller, U.; et al.; Femtosecond Pulses From A Continuously Self-Starting Passively Mode-Locked Ti:Sapphire Laser, *Optics Letters*, 16, 13, 1991, p. 1024
- [12] Ell, R.; et al.; Generation of 5-fs pulses and octave-spanning spectra directly from a Ti:sapphire laser, *Opt. Lett.*, 26, 6, 2001
- [13] Christoph A. Roedig « Development of an Ultra-Short 2.0 Micron Seed Pulse»The Ohio State University June 2006.
- [14] CHRITOV (I.P.), Propagation of femtosecond light pulses, *Opt. Commun.* 53, 364-366 (1985).
- [15] Ziolkowski.R.W., Judkins.J.B., Propagation characteristics of ultrawide bandwidth pulsed Gaussian beams, *J.Opt. Soc. Am. A* 11, 2021-2030 (1992).
- [16] Sheppard.C.J.R., Xianosong.G, Free-space propagation of femtosecond lighthpulses, *Opt. Commun.* 133, 1-6 (1997).
- [18] Agrawal.G.P, Spectrum-induced changes in diffraction of pulsed beams, *Opt. Commun.* 157, 52-56 (1998).
- [19] Porras.M.A., Propagation of single-cycle pulse light beams in dispersive media, *Phys. Rev. A* 60, 5069-5073 (199).
- [20] Fuchss.U, Zeitner.U.D and Tunnermenn.A, Ultrashort pulse propagation in complex optical systems, *Opt. Express* 13, 3852-3861 (2005).
- [21] M.khelladi, O.Sedikki, F.T.bendimerad, " Time-frequency Decomposition of an Ultrashort Pulse" *J, radioengineering*, ISSN 1210-2512, Vol 17,N°1, April 2008.
- [22] Meyer.Y, Jaffort.S., Rioul.O, wavelet analysis, edition Française de scientifique American (1987).
- [23] M.khelladi, O.Sedikki, F.T.bendimerad, " Time-frequency Decomposition of an Ultrashort Laser Pulse Propagatin in chalcogenide waveguide", International Conference on Materials Discovery and DataBases Materials Informatics and DFT, Oran, Algeria, 11-13 October 2008

CHAP III

ULTRASHORT LASER PULSE MODELING



For an understanding of the nonlinear phenomena in optical fibers, it is necessary to consider the theory of electromagnetic wave propagation in dispersive nonlinear media. The objective of this chapter is to obtain a basic equation that governs propagation of optical pulses in single-mode fibers. Section 3.1 introduces Maxwell's equations and important concepts such as the linear and nonlinear parts of the induced polarization and the frequency-dependent dielectric constant. The concept of fiber modes is introduced in Section 3.2 where the single-mode condition is also discussed. Section 3.3 considers the theory of pulse propagation in nonlinear dispersive media in the slowly varying envelope approximation with the assumption that the spectral width of the pulse is much smaller than the frequency of the incident radiation. The numerical methods used to solve the resulting propagation equation are discussed in Section 3.4.

3.1 Maxwell's Equations

Optical communication systems use the phenomenon of total internal reflection for guiding optical pulses in optical fibers. The propagation of light through such a dielectric waveguide can be described using Maxwell's equations for electromagnetic waves. The propagation of electromagnetic fields in any medium whose electric and magnetic field vectors are given by E and H and their corresponding flux densities are given by D and B , respectively, is governed by the following four Maxwell's equations [1]:

$$\nabla \times \mathbf{E} = -\frac{\partial \mathbf{B}}{\partial t}, \quad (3.1)$$

$$\nabla \times \mathbf{H} = \mathbf{J} + \frac{\partial \mathbf{D}}{\partial t}, \quad (3.2)$$

$$\nabla \cdot \mathbf{D} = \rho, \quad (3.3)$$

$$\nabla \cdot \mathbf{B} = 0, \quad (3.4)$$

where \mathbf{E} and \mathbf{H} are electric and magnetic field vectors, respectively, and \mathbf{D} and \mathbf{B} are corresponding electric and magnetic flux densities. The current density vector \mathbf{J} and the charge density ρ represent the sources for the electromagnetic field. In the absence of free charges in a medium such as optical fibers, $\mathbf{J} = 0$ and $\rho = 0$. The flux densities \mathbf{D} and \mathbf{B} arise in response to the electric and magnetic fields \mathbf{E} and \mathbf{H} propagating inside the medium and are related to them through the constitutive relations given by [1]

$$\mathbf{D} = \varepsilon_0 \mathbf{E} + \mathbf{P}, \quad (3.5)$$

$$\mathbf{B} = \mu_0 \mathbf{H} + \mathbf{M}, \quad (3.6)$$

where ε_0 is the vacuum permittivity, μ_0 is the vacuum permeability, and \mathbf{P} and \mathbf{M} are the induced electric and magnetic polarizations. For a nonmagnetic medium such as optical fibers, $\mathbf{M} = 0$.

Maxwell's equations can be used to obtain the wave equation that describes light propagation in optical fibers. By taking the curl of Eq.3.1 and using Eqs. (3.2), (3.5), and (3.6), one can eliminate \mathbf{B} and \mathbf{D} in favor of \mathbf{E} and \mathbf{P} and obtain

$$\nabla \times \nabla \times \mathbf{E} = -\frac{1}{c^2} \frac{\partial^2 \mathbf{E}}{\partial t^2} - \mu_0 \frac{\partial^2 \mathbf{P}}{\partial t^2}, \quad (3.7)$$

where c is the speed of light in vacuum and the relation $\mu_0 \varepsilon_0 = 1/c^2$ was used. To complete the description, a relation between the induced polarization \mathbf{P} and the electric field \mathbf{E} is needed. In general, the evaluation of \mathbf{P} requires a quantum-mechanical approach. Although such an approach is often necessary when the optical frequency is near a medium resonance, a phenomenological relation of the form (1.7) can be used to relate \mathbf{P} and \mathbf{E} far from medium resonances. This is the case for optical fibers in the wavelength range $0.5 - 2\mu\text{m}$ that is of interest for the study of nonlinear effects. If we include only the third-order nonlinear effects governed by $\chi^{(3)}$, the induced polarization consists of two parts such that

$$\mathbf{P}(r, t) = \mathbf{P}_L(r, t) + \mathbf{P}_{NL}(r, t), \quad (3.8)$$

where the linear part \mathbf{P}_L and the nonlinear part P_{NL} are related to the electric field by the general relations [2-4]

$$\mathbf{P}_L(r, t) = \varepsilon_0 \int_{-\infty}^{+\infty} \chi^{(1)}(t - t') \cdot E(r, t') dt' \quad (3.9)$$

$$\begin{aligned} \mathbf{P}_{NL}(r, t) = \varepsilon_0 \iiint_{-\infty}^{+\infty} \chi^{(3)}(t - t_1, t - t_2, t - t_3) : \\ \times E(r, t_1)E(r, t_2)E(r, t_3) dt_1 dt_2 dt_3. \end{aligned} \quad (3.10)$$

These relations are valid in the electric-dipole approximation and assume that the medium response is local. Eqs.(3.7)–(3.10) provide a general formalism for studying the third-order nonlinear effects in optical fibers. Because of their complexity, it is necessary to make several simplifying approximations.

In a major simplification, the nonlinear polarization P_{NL} in Eq.(3.8) is treated as a small perturbation to the total induced polarization. The first step therefore consists of solving Eq.(3.7) with $P_{NL} = 0$. Because Eq.(3.7) is then linear in E , it is useful to write in the frequency domain as

$$\nabla \times \nabla \times \check{E}(r, \omega) - \varepsilon(\omega) \frac{\omega^2}{c^2} \check{E}(r, \omega) = 0, \quad (3.11)$$

where $\check{E}(r, \omega)$ is the Fourier transform of $E(r, t)$ defined as

$$\check{E}(r, \omega) = \int_{-\infty}^{+\infty} E(r, t) \cdot \exp(i\omega t) dt. \quad (3.12)$$

The frequency-dependent dielectric constant appearing in Eq.(3.11) is defined as

$$\varepsilon(\omega) = 1 + \tilde{\chi}^{(1)}(\omega), \quad (3.13)$$

where $\tilde{\chi}^{(1)}(\omega)$ is the Fourier transform of $\chi^{(1)}(t)$. As $\tilde{\chi}^{(1)}(\omega)$ is in general complex, so is $\varepsilon(\omega)$. Its real and imaginary parts can be related to the refractive index $n(\omega)$ and the absorption coefficient $\alpha(\omega)$ by using the definition

$$\varepsilon = \left(n + \frac{i\alpha c}{2\omega} \right)^2. \quad (3.14)$$

From Eqs. (3.13) and (3.14), n and α are related to $\chi^{(1)}$ by the relations

$$n(\omega) = 1 + \frac{1}{2} \text{Re}[\tilde{\chi}^{(1)}(\omega)], \quad (3.15)$$

$$\alpha(\omega) = \frac{\omega}{nc} \text{Im}[\tilde{\chi}^{(1)}(\omega)], \quad (3.16)$$

where R_e and I_m stand for the real and imaginary parts, respectively. Two further simplifications can be made before solving Eq.(3.11). First, because

of low optical losses in fibers in the wavelength region of interest, the imaginary part of $\varepsilon(\omega)$ is small in comparison to the real part.

Thus, we can replace $\varepsilon(\omega)$ by $n^2(\omega)$ in the following discussion of fiber modes and include fiber loss later in a perturbative manner. Second, as $n(\omega)$ is often independent of the spatial coordinates in both the core and the cladding of step-index fibers, one can use

$$\nabla \times \nabla \times E \equiv \nabla(\nabla \cdot E) - \nabla^2 E = \nabla^2 E, \quad (3.17)$$

where the relation $\nabla \cdot D = \varepsilon \nabla \cdot E = 0$ was used from Equation.3.3. With these simplifications, Equation.3.11 takes the form

$$\nabla^2 \check{E} - n^2(\omega) \frac{\omega^2}{c^2} \check{E} = 0. \quad (3.18)$$

This equation is solved in the next section on fiber modes.

3.2 Fiber Modes

At any frequency ω , optical fibers can support a finite number of guided modes whose spatial distribution $\check{E}(r, \omega)$ is a solution of the wave equation (3.18) and satisfies all appropriate boundary conditions. In addition, the fiber can support a continuum of unguided radiation modes. Although the inclusion of radiation modes is crucial in problems involving transfer of power between bounded and radiation modes [5], they do not play an important role in the discussion of nonlinear effects. As fiber modes are covered in many textbooks [5-7], they are discussed only briefly in this section.

3.2.1 Eigenvalue Equation

Because of the cylindrical symmetry of fibers, it is useful to express the wave Eq.3.18 in cylindrical coordinates ρ, ϕ and z :

$$\frac{\partial^2 \check{E}}{\partial \rho^2} + \frac{1}{\rho} \frac{\partial \check{E}}{\partial \rho} + \frac{1}{\rho^2} \frac{\partial^2 \check{E}}{\partial \phi^2} + \frac{\partial^2 \check{E}}{\partial z^2} + n^2 k_0^2 \check{E} = 0, \quad (3.19)$$

where $k_0 = \frac{\omega}{c} = \frac{2\pi}{\lambda}$ and \check{E} is the Fourier transform of the electric field E , i.e.,

$$E(r, t) = \frac{1}{2\pi} \int_{-\infty}^{+\infty} \check{E}(r, \omega) \cdot \exp(-i\omega t) d\omega. \quad (3.20)$$

Similar relations exist for the magnetic field $H(r, t)$. As E and H satisfy Maxwell's equations (3.1)-(3.4), only two components out of six are independent.

It is customary to choose \tilde{E}_z and \tilde{H}_z as the independent components and express $\tilde{E}_\rho, \tilde{E}_\phi, \tilde{H}_\rho,$ and \tilde{H}_ϕ in terms \tilde{E}_z and \tilde{H}_z . Both \tilde{E}_z and \tilde{H}_z satisfy Eq.3.19. The wave equation for \tilde{E}_z is easily solved by using the method of separation of variables, resulting in the following general form:

$$\tilde{E}_z(r, w) = A(w)F(\rho) \exp(\pm im\phi) \exp(i\beta z), \quad (3.21)$$

where A is a normalization constant, β is the propagation constant, m is an integer, and $F(\rho)$ is the solution of

$$\frac{d^2F}{d\rho^2} + \frac{1}{\rho} \frac{dF}{d\rho} + \left(n^2 k_0^2 - \beta^2 - \frac{m^2}{\rho^2} \right) F = 0, \quad (3.22)$$

where the refractive index $n = n_1$ for $\rho \leq a$ for a fiber of core radius a but takes the value n_2 outside the core ($\rho > a$). Eq.3.22 is the well-known differential equation for Bessel functions. Its general solution inside the core can be written as

$$F(\rho) = C_1 J_m(k\rho) + C_2 N_m(k\rho), \quad (3.23)$$

where J_m is the Bessel function, N_m is the Neumann function, and

$$k = (n_1^2 k_0^2 - \beta^2)^{1/2} \quad (3.24)$$

The constants C_1 and C_2 are determined using the boundary conditions. As $N_m(k\rho)$ has a singularity at $\rho = 0$, $C_2 = 0$ for a physically meaningful solution. The constant C_1 can be absorbed in A appearing in Eq. (3.21). Thus,

$$F(\rho) = J_m(k\rho), \quad \rho \leq a \quad (3.25)$$

In the cladding region $\rho \geq a$ the solution $F(\rho)$ should be such that it decays exponentially for large ρ . The modified Bessel function k_m represents such a solution. Therefore,

$$F(\rho) = k_m(\gamma\rho), \quad \rho \geq a \quad (3.26)$$

where

$$\gamma = (\beta^2 - n_2^2 k_0^2)^{1/2} \quad (3.27)$$

The same procedure can be followed to obtain the magnetic field component \tilde{H}_z . The boundary condition that the tangential components of \tilde{E} and \tilde{H} be continuous across the core-cladding interface requires that $\tilde{E}_z, \tilde{H}_z, \tilde{E}_\phi$ and \tilde{H}_ϕ be the same when $\rho = a$ is approached from inside or outside the core. The equality of these field components at $\rho = a$ leads to an eigenvalue equation whose solutions

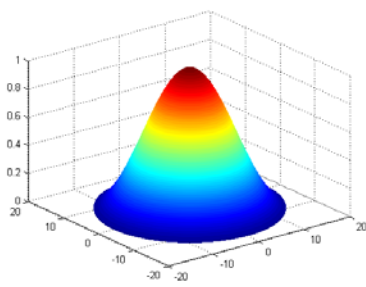
determine the propagation constant β for the fiber modes. Since the whole procedure is well known [5]–[7], we write the eigenvalue equation directly:

$$\left[\frac{J'_m(ka)}{kJ_m(ka)} + \frac{k'_m(\gamma a)}{\gamma k_m(\gamma a)} \right] \left[\frac{J'_m(ka)}{kJ_m(ka)} + \frac{n_2^2 k'_m(\gamma a)}{n_1^2 \gamma k_m(\gamma a)} \right] = \left(\frac{m\beta k_0(n_1^2 - n_2^2)}{an_1 k^2 \gamma^2} \right)^2 \quad (3.28)$$

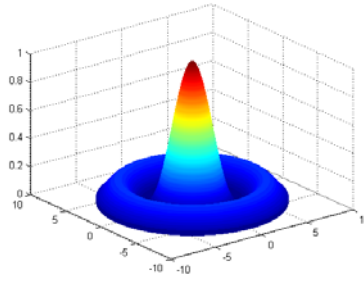
where a prime denotes differentiation with respect to the argument and we used the important relation

$$k^2 + \gamma^2 = (n_1^2 - n_2^2)k_0^2 \quad (3.29)$$

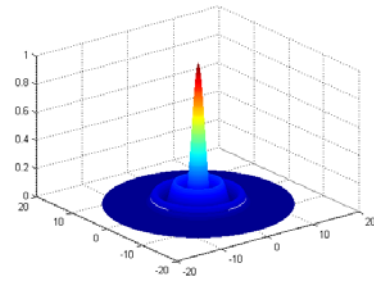
The eigenvalue Eq.3.28 in general has several solutions for β for each integer value of m . It is customary to express these solutions by β_{mn} , where both m and n take integer values. Each eigenvalue β_{mn} corresponds to one specific mode supported by the fiber. The corresponding modal field distribution is obtained from Eq.3.21. It turns out [5-7] that there are two types of fiber modes, designated as HE_{mn} and EH_{mn} . For $m = 0$, these modes are analogous to the transverse-electric (TE) and transverse-magnetic (TM) modes of a planar waveguide because the axial component of the electric field, or the magnetic field, vanishes. However, for $m > 0$, fiber modes become hybrid, i.e., all six components of the electromagnetic field are nonzero.



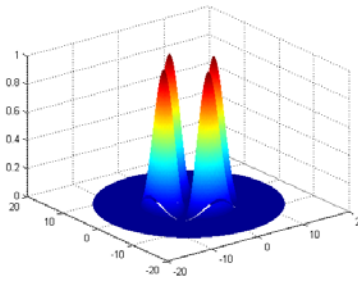
LP0



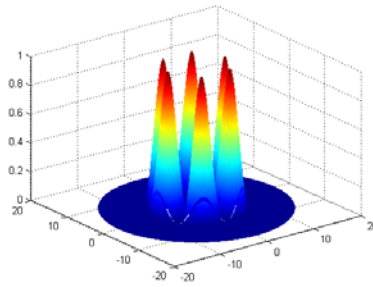
LP0



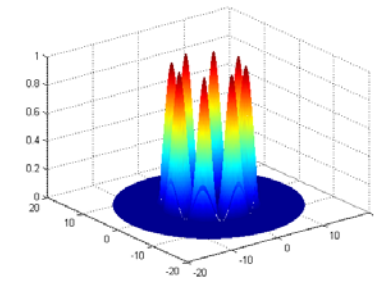
LP0



LP2



LP3



LP4

3.2.2 Single-Mode Condition

The number of modes supported by a specific fiber at a given wavelength depends on its design parameters, namely the core radius a and the core-cladding index difference $(n_1 - n_2)$. An important parameter for each mode is its cut-off frequency. This frequency is determined by the condition $\gamma = 0$. The value of k when $\gamma = 0$ for a given mode determines the cut-off frequency from Eq. (3.29). It is useful to define a normalized frequency V by the relation

$$V = k_c \cdot a = k_0 \cdot a(n_1^2 - n_2^2)^{1/2}, \quad (3.30)$$

where k_c is obtained from Eq.(3.29) by setting $\gamma = 0$.

The eigenvalue equation (3.28) can be used to determine the values of V at which different modes reach cut-off. The procedure is complicated, but has been described in many texts [5-7]. Since we are interested mainly in single-mode fibers, we limit the discussion to the cut-off condition that allows the fiber to support only one mode. A single-mode fiber supports only the HE_{11} mode, also referred to as the fundamental mode.

3.2.3 Characteristics of the Fundamental Mode

The field distribution $E(r, t)$ corresponding to the HE_{11} mode has three nonzero components E_ρ, E_ϕ , and E_z or in Cartesian coordinates E_x, E_y and E_z . Among these, either E_x or E_y dominates. Thus, to a good degree of approximation, the fundamental fiber mode is linearly polarized in either x or y direction depending on whether E_x or E_y dominates. In this respect, even a single-mode fiber is not truly single mode because it can support two modes of orthogonal polarizations. The notation LP_{mn} is sometimes used to denote the linearly polarized modes, which are approximate solutions of Eq.3.19. The fundamental mode HE_{11} corresponds to LP_{01} in this notation [6].

The two orthogonally polarized modes of a single-mode fiber are degenerate (i.e., they have the same propagation constant) under ideal conditions. In practice, irregularities such as random variations in the core shape and size along the fiber length break this degeneracy slightly, mix the two

polarization components randomly, and scramble the polarization of the incident light as it propagates down the fiber. Assuming that the incident light is polarized along a principal axis (chosen to coincide with the x axis), the electric field for the fundamental fiber mode HE_{11} is approximately given by

$$\tilde{E}(r, w) = \hat{x}\{A(w)F(x, y)\exp[i\beta(w)z]\}, \quad (3.31)$$

where $A(w)$ is a normalization constant. The transverse distribution inside the core is found to be

$$F(x, y) = J_0(k\rho), \quad \rho \leq a \quad (3.32)$$

where $\rho = (x^2 + y^2)^{1/2}$ is the radial distance. Outside the fiber core, the field decays exponentially as [5]

$$F(x, y) = \left(\frac{a}{\rho}\right)^{\frac{1}{2}} J_0(ka)\exp[-\gamma(\rho - a)], \quad \rho \geq a \quad (3.33)$$

where $K_m(\gamma\rho)$ in Eq.3.26 was approximated by the leading term in its asymptotic expansion and a constant factor was added to ensure the equality of $F(x, y)$ at $\rho = a$. The propagation constant $\beta(w)$ in Eq.3.31 is obtained by solving the eigenvalue Eq.3.28. Its frequency dependence results not only from the frequency dependence of n_1 and n_2 but also from the frequency dependence of k . The evaluation of $\beta(w)$ generally requires a numerical solution of Eq.3.28 although approximate analytic expressions can be obtained in specific cases [5]. The effective mode index is related to β by $n_{eff} = \beta/k_0$. As the use of modal distribution $F(x, y)$ given by Eqs.3.32 and Eq.3.33 is cumbersome in practice, the fundamental fiber mode is often approximated by a Gaussian distribution of the form

$$F(x, y) \approx \exp\left[-\frac{(x^2+y^2)}{r^2}\right], \quad (3.34)$$

where the width parameter r is determined by fitting the exact distribution to a Gaussian form or by following a variational procedure.

3.3 Pulse-Propagation Equation

The study of most nonlinear effects in optical fibers involves the use of short pulses with widths ranging from $\sim 10\text{ns}$ to 10fs . When such optical pulses propagate inside a fiber, both dispersive and nonlinear effects influence their shape and spectrum. In this section we derive a basic equation that governs propagation of optical pulses in nonlinear dispersive fibers. The starting point is the wave Eq.3.7. By using Eqs. (3.8) and (3.17), it can be written in the form

$$\nabla^2 E - \frac{1}{c^2} \frac{\partial^2 E}{\partial t^2} = \mu_0 \frac{\partial^2 P_L}{\partial t^2} + \mu_0 \frac{\partial^2 P_{NL}}{\partial t^2}, \quad (3.35)$$

where the linear and nonlinear parts of the induced polarization are related to the electric field $E(r, t)$ through Eqs.(3.9) and (3.10), respectively.

3.3.1 Nonlinear Pulse Propagation

It is necessary to make several simplifying assumptions before solving Eq. 3.35. First, P_{NL} is treated as a small perturbation to P_L . This is justified because nonlinear changes in the refractive index are $< 10^{-6}$ in practice. Second, the optical field is assumed to be quasi-monochromatic, i.e., the pulse spectrum, centered at w_0 , is assumed to have a spectral width Δw such that $\Delta w/w_0 \ll 1$. Since $w_0 \sim 10^{15} \text{S}^{-1}$, the last assumption is valid for pulses as short as 0.1ps . In the slowly varying envelope approximation adopted here, it is useful to separate the rapidly varying part of the electric field by writing it in the form

$$E(r, t) = \frac{1}{2} \hat{x} [E(r, t) \exp(-iw_0 t) + c.c.] \quad (3.36)$$

where \hat{x} is the polarization unit vector, and $E(r, t)$ is a slowly varying function of time (relative to the optical period). The polarization components P_L and P_{NL} can also be expressed in a similar way by writing

$$P_L(r, t) = \frac{1}{2} \hat{x} [P_L(r, t) \exp(-iw_0 t) + c.c.] \quad (3.37)$$

$$P_{NL}(r, t) = \frac{1}{2} \hat{x} [P_{NL}(r, t) \exp(-iw_0 t) + c.c.] \quad (3.38)$$

The linear component P_L can be obtained by substituting Eq.3.37 in Eq.3.9 and is given by

$$\begin{aligned}
P_L(r, t) &= \varepsilon_0 \int_{-\infty}^{+\infty} \chi_{xx}^{(1)}(t - t') \cdot E(r, t') \exp[iw_0(t - t')] dt' \\
&= \frac{\varepsilon_0}{2\pi} \int_{-\infty}^{+\infty} \tilde{\chi}_{xx}^{(1)}(w) \tilde{E}(r, w - w_0) \exp[-i(w - w_0)t] dw, \quad (3.39)
\end{aligned}$$

where $\tilde{E}(r, w)$ is the Fourier transform of $E(r, t)$ and is defined similarly to Eq.3.12. The nonlinear component $P_{NL}(r, t)$ is obtained by substituting Eq.3.38 in Eq.3.10. Considerable simplification occurs if the nonlinear response is assumed to be instantaneous so that the time dependence of $\chi^{(3)}$ in Eq.3.10 is given by the product of three delta functions of the form $\delta(t - t_1)$. Eq.3.10 then reduces to

$$P_{NL}(r, t) = \varepsilon_0 \chi^{(3)} : E(r, t)E(r, t)E(r, t). \quad (3.40)$$

The assumption of instantaneous nonlinear response amounts to neglecting the contribution of molecular vibrations to $\chi^{(3)}$ (the Raman effect).

When Eq.3.36 is substituted in Eq.3.40, $P_{NL}(r, t)$ is found to have a term oscillating at w_0 and another term oscillating at the third-harmonic frequency $3w_0$. The latter term requires phase matching and is generally negligible in optical fibers. By making use of Eq.3.38, $P_{NL}(r, t)$ is given by

$$P_{NL}(r, t) \approx \varepsilon_0 \varepsilon_{NL} E(r, t), \quad (3.41)$$

where the nonlinear contribution to the dielectric constant is defined as

$$\varepsilon_{NL} = \frac{3}{4} \chi_{xxxx}^{(3)} |E(r, t)|^2 \quad (3.42)$$

To obtain the wave equation for the slowly varying amplitude $E(r, t)$, it is more convenient to work in the Fourier domain. This is generally not possible as Eq.3.35 is nonlinear because of the intensity dependence of ε_{NL} . In one approach, ε_{NL} is treated as a constant during the derivation of the propagation equation. The approach is justified in view of the slowly varying envelope approximation and the perturbative nature of P_{NL} .

The nonlinear Schrodinger equation that governs propagation of optical pulses inside single fiber is given by.

$$\frac{\partial A}{\partial z} + \beta_1 \frac{\partial A}{\partial t} + \frac{i\beta_2}{2} \frac{\partial^2 A}{\partial t^2} + \frac{\alpha}{2} A = i\gamma |A|^2 A, \quad (3.43)$$

where the nonlinear parameter γ is defined as

$$\gamma = \frac{n_2 w_0}{c A_{eff}}, \quad n_2 = \frac{3}{8n} \text{Re}(\chi_{xxxx}^{(3)}) \quad (3.44)$$

In obtaining Eq.(3.43) the pulse amplitude A is assumed to be normalized such that $|A|^2$ represents the optical power. The quantity $\gamma|A|^2$ is then measured in units of m^{-1} if n_2 is expressed in units of m^2/W . The parameter A_{eff} is known as the effective core area and is defined as

$$A_{eff} = \frac{\left(\iint_{-\infty}^{+\infty} |F(x,y)|^2 dx dy \right)^2}{\iint_{-\infty}^{+\infty} |F(x,y)|^4 dx dy}. \quad (3.45)$$

Its evaluation requires the use of modal distribution $F(x, y)$ for the fundamental fiber mode. Clearly A_{eff} depends on fiber parameters such as the core radius and the core-cladding index difference. If $F(x, y)$ is approximated by a Gaussian distribution as in Eq. (3.34), $A_{eff} = \pi r^2$.

Equation (3.43) describes propagation of picosecond optical pulses in single-mode fibers. It is often referred to as the nonlinear Schrödinger (NLS) equation because it can be reduced to that form under certain conditions. It includes the effects of fiber losses through α , of chromatic dispersion through β_1 and β_2 , and of fiber nonlinearity through γ . Briefly, the pulse envelope moves at the group velocity $v_g \equiv 1/\beta_1$ while the effects of group-velocity dispersion (GVD) are governed by β_2 .

3.3.2 Higher-Order Nonlinear Effects

Although the propagation Eq.3.43 has been successful in explaining a large number of nonlinear effects, it may need modification depending on the experimental conditions. For example, Eq.3.43 does not include the effects of stimulated inelastic scattering such as SRS and SBS. If the peak power of the incident pulse is above a threshold level, both SRS and SBS can transfer energy from the pulse to a new pulse, which may propagate in the same or the opposite direction. The two pulses interact with each other through the Raman or Brillouin gain and XPM. A similar situation occurs when two or more pulses at different wavelengths (separated by more than individual spectral widths) are incident on

the fiber. Simultaneous propagation of multiple pulses is governed by a set of equations similar to Eq.3.43, modified suitably to include the contributions of XPM and the Raman or Brillouin gain.

Eq.3.43 should also be modified for ultrashort optical pulses whose width is close to or $< 1ps$ [9,10]. The spectral width of such pulses becomes large enough that several approximations made in the derivation of Eq.3.43 become questionable. The most important limitation turns out to be the neglect of the Raman effect. For pulses with a wide spectrum ($> 0.1 THz$), the Raman gain can amplify the low-frequency components of a pulse by transferring energy from the high-frequency components of the same pulse. This phenomenon is called intrapulse Raman scattering. As a result of it, the pulse spectrum shifts toward the low-frequency (red) side as the pulse propagates inside the fiber, a phenomenon referred to as the self-frequency shift [8]. The physical origin of this effect is related to the delayed nature of the Raman (vibrational) response [13]. Mathematically, Eq.3.40 cannot be used in the derivation of Eq.3.43; one must use the general form of the nonlinear polarization given in Eq.3.10.

The starting point is again the wave Eq.3.35. Eq.3.10 describes a wide variety of third-order nonlinear effects, and not all of them are relevant to our discussion. For example, nonlinear phenomena such as third harmonic generation and four-wave mixing are unlikely to occur unless an appropriate phase-matching condition is satisfied [18,19]. For pulses shorter than $5 ps$ but wide enough to contain many optical cycles ($\text{widths} \gg 10 fs$), we can obtain:

$$\frac{\partial A}{\partial z} + \frac{\alpha}{2}A + \frac{i\beta_2}{2}\frac{\partial^2 A}{\partial t^2} - \frac{\beta_3}{6}\frac{\partial^3 A}{\partial t^3} = i\gamma \left(|A|^2 A + \frac{i}{\omega_0} \frac{\partial}{\partial T} (|A|^2 A) - T_{RA} \frac{\partial |A|^2}{\partial T} \right), \quad (3.46)$$

It is easy to identify the origin of the last three higher-order terms in Eq.3.46. The term proportional to β_3 results from including the cubic term in the expansion of the propagation constant. This term governs the effects of third-order dispersion and becomes important for ultrashort pulses because of their wide bandwidth. The term proportional to ω_0^{-1} results from including the first derivative of P_{NL} . It

is responsible for self-steepening and shock formation [13-14]. The last term, proportional to T_R in Eq.3.46, has its origin in the delayed Raman response, and is responsible for the self-frequency shift induced by intrapulse Raman scattering. For pulses of width $T_0 > 5 \text{ ps}$, the parameters $(\omega_0 T_0)^{-1}$ and T_R/T_0 become so small ($< 0,001$) that the last two terms in Equation.3.46 can be neglected. As the contribution of the third-order dispersion term is also quite small for such pulses (as long as the carrier wavelength is not too close to the zero-dispersion wavelength), one can use the simplified equation [11-12]

$$i \frac{\partial A}{\partial z} + i \frac{\alpha}{2} A - \frac{\beta_2}{2} \frac{\partial^2 A}{\partial T^2} - \gamma |A|^2 A = 0. \quad (3.47)$$

In the special case of $\alpha = 0$, Eq.3.47 is referred to as the NLS equation because it resembles the Schrodinger equation with a nonlinear potential term (variable z playing the role of time). To extend the analogy further, Eq.3.46 is called the generalized (or extended) NLS equation. The NLS equation is a fundamental equation of nonlinear science and has been studied extensively in the context of solitons [15-17]. Eq.3.47 is the simplest nonlinear equation for studying third order nonlinear effects in optical fibers.

3.4 Numerical Method

3.4.1 Introduction

A numerical approach is therefore often necessary for an understanding of the nonlinear effects in optical fibers. A large number of numerical methods can be used for this purpose [18]. The one method that has been used extensively to solve the pulse-propagation problem in nonlinear dispersive media is the split-step Fourier method [19-20].

3.4.2 Split-Step Fourier Method

The relative speed of this method compared with most finite-difference schemes can be attributed in part to the use of the finite-Fourier-transform (FFT)

algorithm [21, 22]. This section describes various numerical techniques used to study the pulse-propagation problem in optical fibers with emphasis on the split-step Fourier method and its modifications (see Appendix B).

To understand the philosophy behind the split-step Fourier method, it is useful to write Eq. (3.46) formally in the form

$$\frac{\partial A}{\partial z} = (\tilde{D} + \tilde{N})A, \quad (3.48)$$

where \hat{D} is a differential operator that accounts for dispersion and absorption in a linear medium and \hat{N} is a nonlinear operator that governs the effect of fiber nonlinearities on pulse propagation. These operators are given by

$$\hat{D} = -\frac{i\beta_2}{2} \frac{\partial^2}{\partial T^2} + \frac{\beta_3}{6} \frac{\partial^3}{\partial T^3} - \frac{\alpha}{2}, \quad (3.49)$$

$$\hat{N} = i\gamma \left(|A|^2 + \frac{i}{w_0 A} \frac{\partial}{\partial T} (|A|^2 A) - T_R \frac{\partial |A|^2}{\partial T} \right), \quad (3.50)$$

In general, dispersion and nonlinearity act together along the length of the fiber. The split-step Fourier method obtains an approximate solution by assuming that in propagating the optical field over a small distance h , the dispersive and nonlinear effects can be pretended to act independently [23,24]. More specifically, propagation from z to $z + h$ is carried out in two steps (see Appendix B).

3.5 Chapter Summary

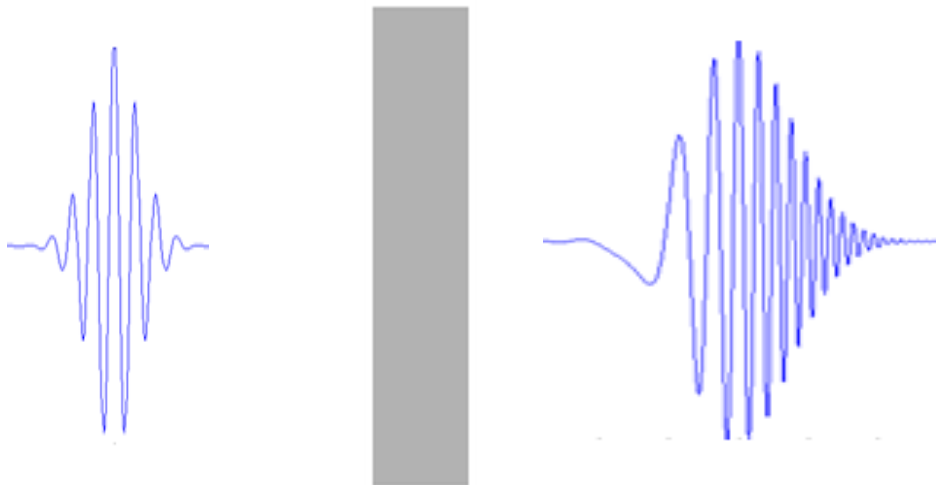
Pulse propagation in optical fibers is governed by the NLS equation. In this chapter we have derived the NLS equation that governs the propagation of optical pulses in optical fibers from the Maxwell's equations. We gave the analytical solutions to this equation for two specific cases and discussed the properties of these solutions. We also presented a numerical method that can be used to study the propagation of pulse through titanium sapphire.

References

- [1] P. Diament, *Wave Transmission and Fiber Optics* (Macmillan, New York, 1990), Chap. 3.
- [2] Y. R. Shen, *Principles of Nonlinear Optics* (Wiley, New York, 1984), Chap. 1.
- [3] M. Schubert and B. Wilhelmi, *Nonlinear Optics and Quantum Electronics* (Wiley, New York, 1986), Chap. 1.
- [4] P. N. Butcher and D. N. Cotter, *The Elements of Nonlinear Optics* (Cambridge University Press, Cambridge, UK, 1990), Chap. 2.
- [5] D. Marcuse, *Theory of Dielectric Optical Waveguides* (Academic Press, San Diego, CA, 1991), Chap. 2.
- [6] A. W. Snyder and J. D. Love, *Optical Waveguide Theory* (Chapman and Hall, London, 1983), Chaps. 12–15.
- [7] J. A. Buck, *Fundamentals of Optical Fibers* (Wiley, New York, 1995), Chap. 3.
- [8] D. Marcuse, *J. Opt. Soc. Am.* 68, 103 (1978).
- [9] F. M. Mitschke and L. F. Mollenauer, *Opt. Lett.* 11, 659 (1986). [13] J. P. Gordon, *Opt. Lett.* 11, 662 (1986).
- [10] Y. Kodama and A. Hasegawa, *IEEE J. Quantum Electron.* 23, 510 (1987).
- [11] P. V. Mamyshev and S. V. Chernikov, *Opt. Lett.* 15, 1076 (1990).
- [12] S. V. Chernikov and P. V. Mamyshev, *J. Opt. Soc. Am. B* 8, 1633 (1991).
- [13] S. Chi and S. Wang, *Opt. Quantum Electron.* 28, 1351 (1996).
- [14] T. Brabec and F. Krausz, *Phys. Rev. Lett.* 78, 3282 (1997).
- [15] A. K. Atieh, P. Myslinski, J. Chrostowski, and P. Galko, *J. Lightwave Technol.* 17, 216 (1999).
- [16] V. E. Zakharov and A. B. Shabat, *Sov. Phys. JETP* 34, 62 (1972).
- [17] A. Hasegawa and F. Tappert, *Appl. Phys. Lett.* 23, 142 (1973).
- [18] G. D. Peng, Z. Xiong, and P. L. Chu, *Opt. Fiber Technol.* 5, 242 (1999).
- [19] R. H. Hardin and F. D. Tappert, *SIAM Rev. Chronicle* 15, 423 (1973).
- [20] R. A. Fisher and W. K. Bischel, *Appl. Phys. Lett.* 23, 661 (1973); *J. Appl. Phys.* 46, 4921 (1975).
- [21] T. R. Taha and M. J. Ablowitz, *J. Comput. Phys.* 55, 203 (1984).
- [22] J. W. Cooley and J. W. Tukey, *Math. Comput.* 19, 297 (1965).
- [23] J. A. Fleck, J. R. Morris, and M. D. Feit, *Appl. Phys.* 10, 129 (1976).
- [24] M. Lax, J. H. Batteh, and G. P. Agrawal, *J. Appl. Phys.* 52, 109 (1981).

CHAP IV

GROUP VELOCITY DISPERSION EFFECT



The preceding chapter discussed how the combined effects of group-velocity dispersion (GVD) and self-phase modulation (SPM) on optical pulses propagating inside a fiber can be studied by solving a pulse-propagation equation. Before considering the general case, it is instructive to study the effects of GVD alone. This chapter considers the pulse-propagation problem by treating fibers as a linear optical medium. In Section 4.1 we discuss the conditions under which the GVD effects dominate over the nonlinear effects by introducing two length scales associated with GVD and SPM. Dispersion-induced broadening of optical pulses is considered in Section 4.2 for several specific pulse shapes, including Gaussian and 'sech' pulses. The effects of initial frequency chirping are also discussed in this section. Section 4.3 is devoted to the effects of third-order dispersion on pulse broadening.

4.1 Different Propagation Regimes

In Section 3.3 we obtained the nonlinear Schrödinger (NLS) equation that governs propagation of optical pulses inside single-mode fibers. For pulse widths > 5 ps, one can use Eq.3.47 given by

$$i \frac{\partial A}{\partial z} = -i \frac{\alpha}{2} A + \frac{\beta_2}{2} \frac{\partial^2 A}{\partial T^2} + \gamma |A|^2 A. \quad (4.1)$$

where A is the slowly varying amplitude of the pulse envelope and T is measured in a frame of reference moving with the pulse at the group velocity $v_g = (T = t - z/v_g)$. The three terms on the right-hand side of Eq.4.1 govern, respectively, the effects of fiber losses, dispersion, and nonlinearity on pulses propagating inside optical fibers. Depending on the initial width T_0 and the peak power P_0 of the incident pulse, either dispersive or nonlinear effects may dominate along the fiber. It is useful to introduce two length scales, known as the dispersion length L_D and the nonlinear length L_{NL} [1-3]. Depending on the relative magnitudes of L_D, L_{NL} and the fiber length L , pulses can evolve quite differently.

Let us introduce a time scale normalized to the input pulse width T_0 as

$$\tau = \frac{T}{T_0} = \frac{t-z/v_g}{T_0} \quad (4.2)$$

At the same time, we introduce a normalized amplitude U as

$$A(z, \tau) = \sqrt{P_0} \exp(-\alpha z/2) U(z, \tau), \quad (4.3)$$

where P_0 is the peak power of the incident pulse. The exponential factor in Eq.4.3 accounts for fiber losses. By using Eqs.(4.1)–(4.3), $U(z, \tau)$ is found to satisfy the equation

$$i \frac{\partial U}{\partial z} = \frac{\text{sgn}(\beta_2)}{2L_D} \frac{\partial^2 U}{\partial \tau^2} - \frac{\exp(-\alpha z)}{L_{NL}} |U|^2 U, \quad (4.4)$$

where $\text{sgn}(\beta_2) = \pm 1$ depending on the sign of the GVD parameter β_2 and

$$L_D = \frac{T_0^2}{|\beta_2|}, \quad L_{NL} = \frac{1}{\gamma P_0}. \quad (4.5)$$

The dispersion length L_D and the nonlinear length L_{NL} provide the length scales over which dispersive or nonlinear effects become important for pulse evolution. Depending on the relative magnitudes of L , L_D , and L_{NL} , the propagation behavior can be classified in the following four categories.

When fiber length L is such that $L \ll L_{NL}$ and $L \ll L_D$, neither dispersive nor nonlinear effects play a significant role during pulse propagation. This can be seen by noting that both terms on the right-hand side of Eq.4.4 can be neglected in that case. (It is assumed that the pulse has a smooth temporal profile so that $\frac{\partial^2 U}{\partial \tau^2} \sim 1$). As a result, $U(z, \tau) = U(0, \tau)$, i.e., the pulse maintains its shape during propagation. The fiber plays a passive role in this regime and acts as a mere transporter of optical pulses (except for reducing the pulse energy because of fiber losses). This regime is useful for optical communication systems.

When the fiber length L is such that $L \ll L_{NL}$ but $L \sim L_D$, the last term in Eq. 4.4 is negligible compared to the other two. The pulse evolution is then governed by GVD, and the nonlinear effects play a relatively minor role. The effect of GVD on propagation of optical pulses is discussed in this chapter. The dispersion-dominant regime is applicable whenever the fiber and pulse parameters are such that

$$\frac{L_D}{L_{NL}} = \frac{\gamma P_0 T_0^2}{|\beta_2|} \ll 1. \quad (4.6)$$

When the fiber length L is such that $L \ll L_D$ but $L \sim L_{NL}$, the dispersion term in Eq.4.4 is negligible compared to the nonlinear term (as long as the pulse has a smooth temporal profile such that $\frac{\partial^2 U}{\partial \tau^2} \sim 1$). In that case, pulse evolution in the fiber is governed by SPM that leads to spectral broadening of the pulse. This phenomenon is considered in Chapter V. The nonlinearity-dominant regime is applicable whenever

$$\frac{L_D}{L_{NL}} = \frac{\gamma P_0 T_0^2}{|\beta_2|} \gg 1. \quad (4.7)$$

This condition is readily satisfied for relatively wide pulses ($T_0 > 100$ ps) with a peak power $P_0 \sim 1$ W. Note that SPM can lead to pulse shaping in the presence of weak GVD effects. If the pulse develops a sharp leading or trailing edge, the dispersion term may become important even when Eq.4.7 is initially satisfied.

When the fiber length L is longer or comparable to both L_D and L_{NL} , dispersion and nonlinearity act together as the pulse propagates along the fiber. The interplay of the GVD and SPM effects can lead to a qualitatively different behavior compared with that expected from GVD or SPM alone. In the anomalous-dispersion regime ($\beta_2 < 0$), the fiber can support solitons. In the normal-dispersion regime ($\beta_2 > 0$), the GVD and SPM effects can be used for pulse compression. Eq.4.4 is extremely helpful in understanding pulse evolution in optical fibers when both dispersive and nonlinear effects should be taken into account. However, this chapter is devoted to the linear regime, and the following discussion is applicable to pulses whose parameters satisfy Eq.4.6.

4.2 Dispersion-Induced Pulse Broadening

The effect of GVD on optical pulses propagating in a linear dispersive medium [4–8] is studied by setting $\gamma = 0$ in Eq.4.1. If we define the normalized amplitude $U(z, T)$ according to Eq.4.3, $U(z, T)$ satisfies the following linear partial differential equation:

$$i \frac{\partial U}{\partial z} = \frac{\beta_2}{2} \frac{\partial^2 U}{\partial T^2}. \quad (4.8)$$

This equation is similar to the paraxial wave equation that governs diffraction of CW light and becomes identical to it when diffraction occurs in only one transverse direction and β_2 is replaced by $-\lambda/2\pi$, where λ is the wavelength of light. For this reason, the dispersion-induced temporal effects have a close analogy with the diffraction-induced spatial effects [2].

Eq.4.8 is readily solved by using the Fourier-transform method. $\tilde{U}(z, \omega)$ is the Fourier transform of $U(z, T)$ such that

$$U(z, T) = \frac{1}{2\pi} \int_{-\infty}^{\infty} \tilde{U}(z, \omega) \exp(-i\omega T) d\omega, \quad (4.9)$$

then it satisfies an ordinary differential equation

$$i \frac{\partial \tilde{U}}{\partial z} = -\frac{1}{2} \beta_2 \omega^2 \tilde{U}, \quad (4.10)$$

whose solution is given by

$$\tilde{U}(z, \omega) = \tilde{U}(0, \omega) \exp\left(\frac{i}{2} \beta_2 \omega^2 z\right). \quad (4.11)$$

Eq.4.11 shows that GVD changes the phase of each spectral component of the pulse by an amount that depends on both the frequency and the propagated distance. Even though such phase changes do not affect the pulse spectrum, they can modify the pulse shape. By substituting Eq.4.11 in Eq.4.9, the general solution of Eq.4.8 is given by

$$U(z, T) = \frac{1}{2\pi} \int_{-\infty}^{\infty} \tilde{U}(0, \omega) \exp\left(\frac{i}{2} \beta_2 \omega^2 z - i\omega T\right) d\omega, \quad (4.12)$$

where $\tilde{U}(0, \omega)$ is the Fourier transform of the incident field at $z = 0$ and is obtained using

$$\tilde{U}(0, \omega) = \int_{-\infty}^{\infty} U(0, T) \exp(i\omega T) dT, \quad (4.13)$$

Eq.4.12 and 4.13 can be used for input pulses of arbitrary shapes.

4.2.1 Gaussian Pulses

As a simple example, consider the case of a Gaussian pulse for which the incident field is of the form [8]

$$U(0, T) = \exp\left(-\frac{T^2}{2T_0^2}\right), \quad (4.14)$$

where T_0 is the half-width. In practice, it is customary to use the full width at half maximum (FWHM) in place of T_0 . For a Gaussian pulse, the two are related as

$$T_{FWHM} = 2(\ln 2)^{1/2}T_0 \approx 1.665T_0 \quad (4.15)$$

By using Eqs. (4.12)–(4.14) and carrying out the integration, the amplitude at any point z along the fiber is given by

$$U(z, T) = \frac{T_0}{(T_0^2 - i\beta_2 z)^{1/2}} \exp\left(-\frac{T^2}{2(T_0^2 - i\beta_2 z)}\right). \quad (4.16)$$

Thus, a Gaussian pulse maintains its shape on propagation but its width T_1 increases with z as

$$T_1(z) = T_0[1 + (z/L_D)^2]^{1/2} \quad (4.17)$$

where the dispersion length $L_D = \frac{T_0^2}{|\beta_2|}$. Eq.4.17 shows how GVD broadens a Gaussian pulse. The extent of broadening is governed by the dispersion length L_D . For a given fiber length, short pulses broaden more because of a smaller dispersion length.

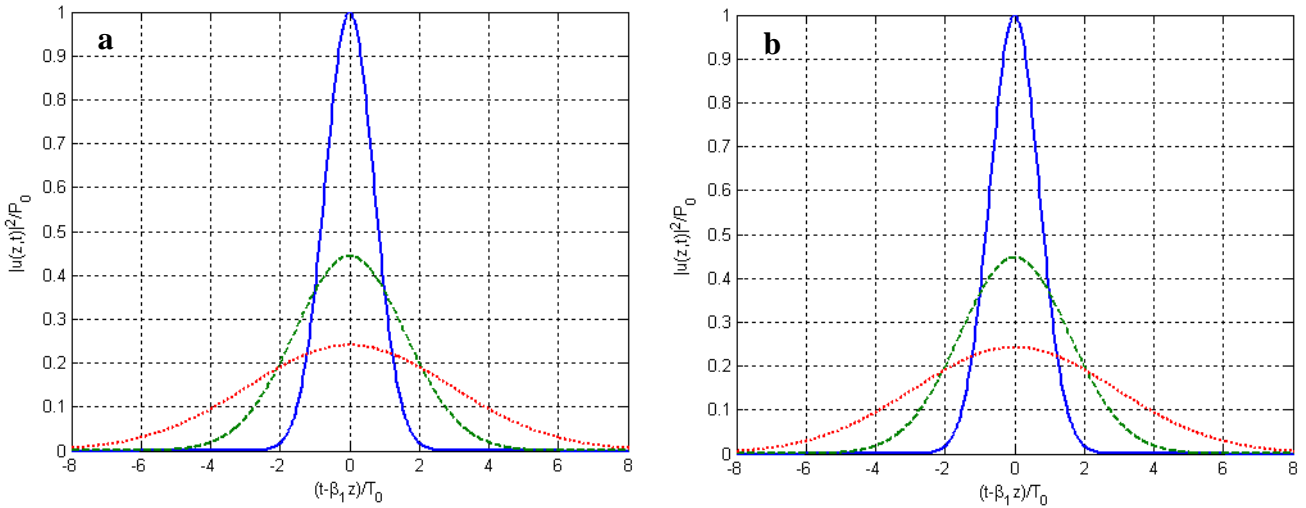


Figure.4.1: (a)Dispersion-induced broadening of a Gaussian pulse inside titane sapphire at $z = 2L_D$ and $z = 4L_D$. The solid curve shows the incident pulse at $z = 0$, for a) Titanium- Sapphire and (b) silica fiber (after [9]).

Fig.4.1 shows the extent of dispersion-induced broadening for Gaussian pulses by plotting $|U(z, T)|^2$ at $z = 0, 2L_D$ and $4L_D$, for titane sapphire and silica fiber. A comparison of Eqs. (4.14) and (4.16) shows that although the incident pulse is unchirped (with no phase modulation), the transmitted pulse becomes chirped. This can be seen clearly by writing $U(z, T)$ in the form

$$U(z, T) = |U(z, T)| \exp[i\phi(z, T)], \quad (4.18)$$

where

$$\phi(z, T) = -\frac{\text{sgn}(\beta_2)(z/L_D) T^2}{1+(z/L_D)^2 T_0^2} + \frac{1}{2} \tan^{-1} \left(\frac{z}{L_D} \right). \quad (4.19)$$

The time dependence of the phase $\phi(z, T)$ implies that the instantaneous frequency differs across the pulse from the central frequency ω_0 . The difference $\delta\omega$ is just the time derivative $-\partial\phi/\partial T$ [the minus sign is due to the choice of $\exp(-i\omega t)$ in Eq. 3.36] and is given by

$$\delta\omega(T) = -\frac{\partial\phi}{\partial T} = \frac{\text{sgn}(\beta_2)(2z/L_D) T}{1+(z/L_D)^2 T_0^2} \quad (4.20)$$

Eq.4.20 shows that the frequency changes linearly across the pulse, i.e., a fiber imposes linear a frequency chirp on the pulse. The chirp $\delta\omega$ depends on the sign of β_2 . In the normal-dispersion regime ($\beta_2 > 0$), $\delta\omega$ is negative at the leading edge ($T < 0$) and increases linearly across the pulse; the opposite occurs in the anomalous-dispersion regime ($\beta_2 < 0$).

Dispersion-induced pulse broadening can be understood by recalling from Section 1.3 that different frequency components of a pulse travel at slightly different speeds along the fiber because of GVD. More specifically, red components travel faster than blue components in the normal-dispersion regime ($\beta_2 > 0$), while the opposite occurs in the anomalous-dispersion regime ($\beta_2 < 0$). The pulse can maintain its width only if all spectral components arrive together. Any time delay in the arrival of the different spectral components leads to pulse broadening.

4.2.2 Chirped Gaussian Pulses

For an initially unchirped Gaussian pulse, Eq.4.17 shows that dispersion-induced broadening of the pulse does not depend on the sign of the GVD parameter β_2 . Thus, for a given value of the dispersion length L_D , the pulse broadens by the same amount in the normal - and anomalous - dispersion regimes of the fiber. This behavior changes if the Gaussian pulse has an initial frequency chirp [9]. In the case of linearly chirped Gaussian pulses, the incident field can be written as [compare with Eq.4.14]

$$U(0, T) = \exp\left(-\frac{(1+iC)T^2}{2T_0^2}\right), \quad (4.21)$$

where C is a chirp parameter. By using Eq.(4.18) one finds that the instantaneous frequency increases linearly from the leading to the trailing edge (up-chirp) for $C > 0$ while the opposite occurs (down-chirp) for $C < 0$. It is common to refer to the chirp as positive or negative depending on whether C is positive or negative.

The numerical value of C can be estimated from the spectral width of the Gaussian pulse. By substituting Eq. (4.21) in Eq.4.13, $\tilde{U}(0, \omega)$ is given by

$$\tilde{U}(0, \omega) = \left(\frac{2\pi T_0^2}{1+iC}\right)^{1/2} \exp\left(-\frac{\omega^2 T_0^2}{2(1+iC)}\right). \quad (4.22)$$

The spectral half-width (at 1/e-intensity point) from Eq. (4.22) is given by

$$\Delta\omega = (1 + C^2)^{1/2} / T_0 \quad (4.23)$$

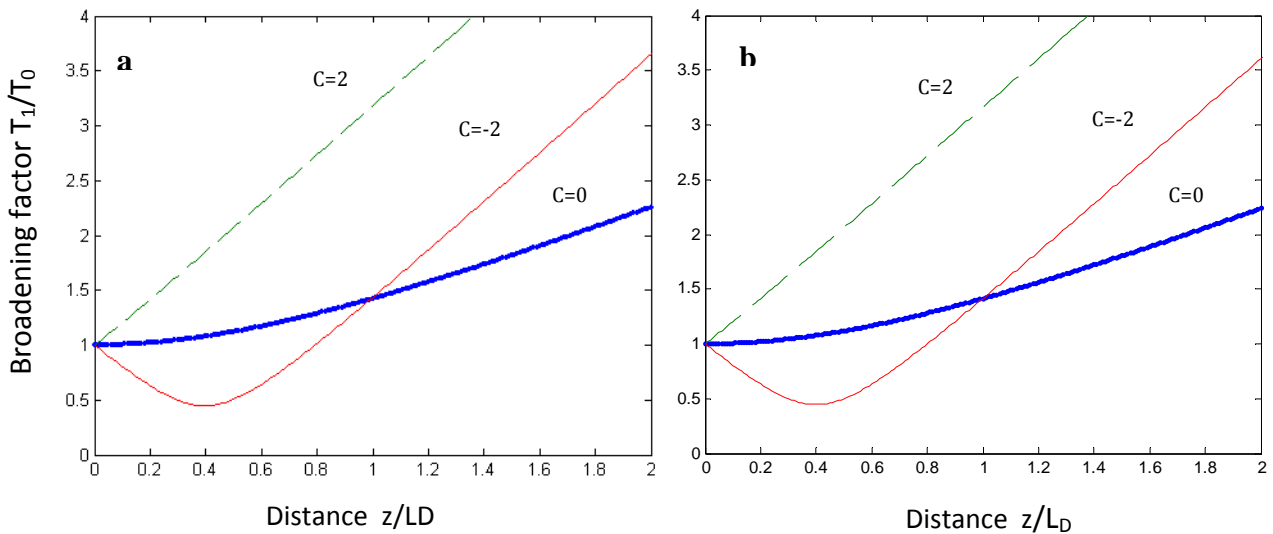


Figure.4.2 Broadening factor for a chirped Gaussian pulse as a function of distance. Dashed curve corresponds to the case of an unchirped Gaussian pulse. For $\beta_2 < 0$, the same curves are obtained if the sign of C is reversed (a) for titanium sapphire, and (b) for silica fiber (after [9]).

In the absence of frequency chirp ($C = 0$), the spectral width is transform-limited and satisfies the relation $\Delta\omega \cdot T_0 = 1$. The spectral width is enhanced by a factor of $(1 + C^2)^{1/2}$ in the presence of linear chirp. Eq.4.23 can be used to estimate $|C|$ from measurements of $\Delta\omega$ and T_0 .

To obtain the transmitted field, $\tilde{U}(0, \omega)$ from Eq.4.22 is substituted in Eq. 4.12. The integration can be carried out analytically with the result

$$U(z, T) = \frac{T_0}{[T_0^2 - i\beta_2 z(1+iC)]^{1/2}} \exp\left(-\frac{(1+iC)T^2}{2[T_0^2 - i\beta_2 z(1+iC)]}\right). \quad (4.24)$$

Thus, even a chirped Gaussian pulse maintains its Gaussian shape on propagation. The width T_1 after propagating a distance z is related to the initial width T_0 by the relation [9]

$$\frac{T_1}{T_0} = \left[\left(1 + \frac{C\beta_2 z}{T_0^2}\right)^2 + \left(\frac{\beta_2 z}{T_0^2}\right)^2 \right]^{1/2} \quad (4.25)$$

This equation shows that broadening depends on the relative signs of the GVD parameter β_2 and the chirp parameter C . Whereas a Gaussian pulse broadens monotonically with z if $\beta_2 C > 0$, it goes through an initial narrowing stage when $\beta_2 C < 0$. Figure 4.2 shows this behavior by plotting the broadening factor T_1/T_0 as a function of z/L_D for $C = 2$.

When the pulse is initially chirped and the condition $\beta_2 C < 0$ is satisfied, the dispersion-induced chirp is in opposite direction to that of the initial chirp. As a result the net chirp is reduced, leading to pulse narrowing. The minimum pulse-width occurs at a point at which the two chirps cancel each other. With a further increase in the propagation distance, the dispersion-induced chirp starts to dominate over the initial chirp, and the pulse begins to broaden.

4.2.3 Hyperbolic-Secant Pulses

Although pulses emitted from many lasers can be approximated by a Gaussian shape, it is necessary to consider other pulse shapes. Of particular interest is the hyperbolic-secant pulse shape that occurs naturally in the context of optical solitons and pulses emitted from some mode-locked lasers. The optical field associated with such pulses often takes the form

$$U(0, T) = \operatorname{sech}\left(\frac{T}{T_0}\right) \exp\left(-\frac{iCT^2}{2T_0^2}\right), \quad (4.26)$$

where the chirp parameter C controls the initial chirp similarly to that of Eq.4.21. The transmitted field $U(z, T)$ is obtained by using Eqs. (4.12), (4.13), and (4.26).

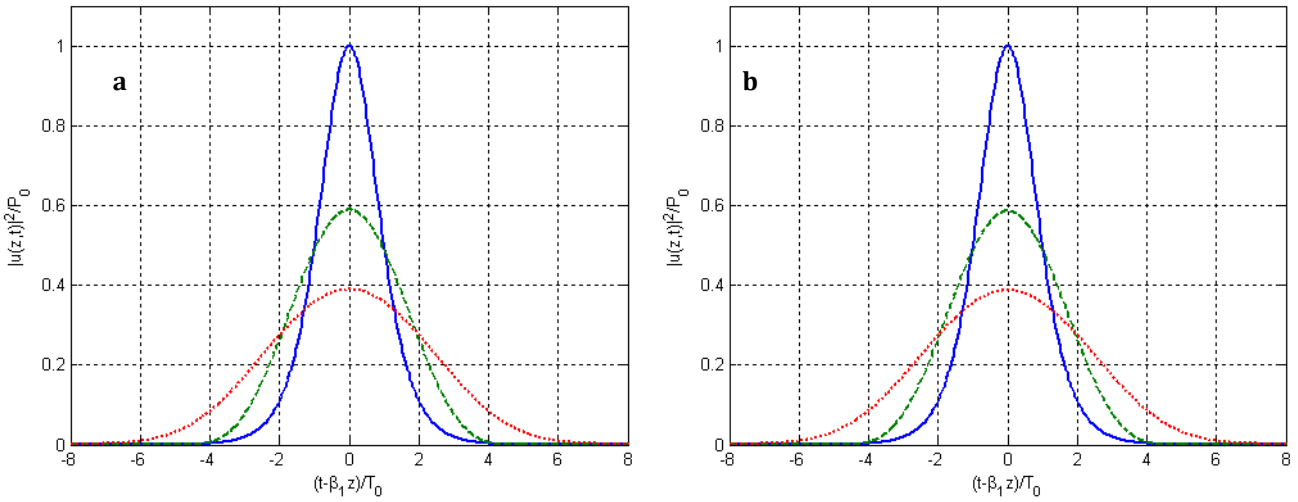


Figure.4.3 : Pulse shapes at $z = 2L_D$ and $z = 4L_D$ of a pulse whose shape at $z = 0$ (solid curve) is described by a “sech” profile for (a) titanium sapphire and, (b) for silica fiber (after [9]). Compare with Fig. 4.1 where the case of a Gaussian pulse is shown.

Unfortunately, it is not easy to evaluate the integral in Eq.4.12 in a closed form for non-Gaussian pulse shapes. Fig.4.3 shows the transmitted pulse shapes calculated numerically at $z = 2L_D$ and $z = 4L_D$ for the case of unchirped pulses ($C = 0$). A comparison of Figs. 4.1 and 4.3 shows that the qualitative features of dispersion-induced broadening are nearly identical for the Gaussian and “sech” pulses. Note that T_0 appearing in Eq.4.26 is not the FWHM but is related to it by

$$T_{FWHM} = 2\ln(1 + \sqrt{2})T_0 \approx 1.763T_0 \quad (4.27)$$

This relation should be used if the comparison is made on the basis of FWHM. The same relation for a Gaussian pulse is given in Eq. 4.15.

4.2.4 Super-Gaussian Pulses

So far we have considered pulse shapes with relatively broad leading and trailing edges. As one may expect, dispersion-induced broadening is sensitive to pulse-edge steepness. In general, a pulse with steeper leading and trailing edges broadens more rapidly with propagation simply because such a pulse has a wider spectrum to start with. Pulses emitted by directly modulated semiconductor lasers fall in this category and cannot generally be approximated by a Gaussian pulse.

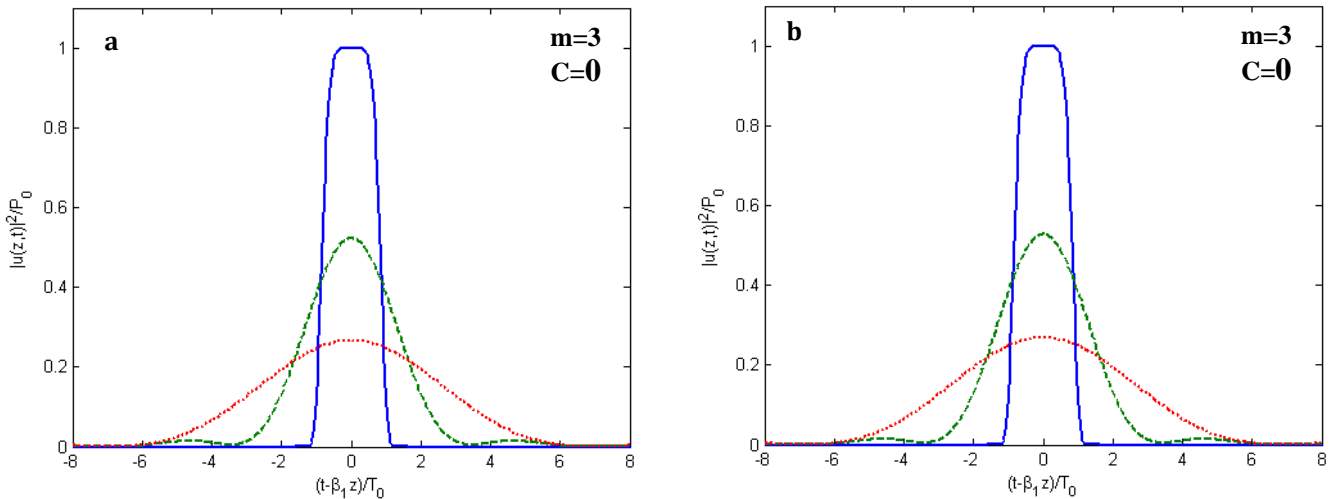


Figure.4.4: Pulse shapes at $z = L_D$ and $z = 2L_D$ of a pulse whose shape at $z = 0$ (solid curve) is described by a super-Gaussian profile for titanium-sapphire (a), and (b) for silica fiber (after [9]). Compare with Fig. 3.1 where the case of a Gaussian pulse is shown.

A super-Gaussian shape can be used to model the effects of steep leading and trailing edges on dispersion-induced pulse broadening. For a super-Gaussian pulse, Eq.4.21 is generalized to take the form [10]

$$U(0, T) = \exp \left[-\frac{(1+iC)}{2} \left(\frac{T}{T_0} \right)^{2m} \right], \quad (4.28)$$

where the parameter m controls the degree of edge sharpness. For $m = 1$ we recover the case of chirped Gaussian pulses. For larger values of m , the pulse becomes square shaped with sharper leading and trailing edges.

Fig.4.4 shows the pulse shapes at $z = 0$, L_D , and $2L_D$ in the case of an unchirped super-Gaussian pulse ($C = 0$) with $m = 3$. It should be compared with Fig.4.1 where the case of a Gaussian pulse ($m = 1$) is shown. The differences between the two can be attributed to the steeper leading and trailing edges associated with a super-Gaussian pulse.

Whereas the Gaussian pulse maintains its shape during propagation, the super-Gaussian pulse not only broadens at a faster rate but also distorts in shape. Enhanced broadening of a super-Gaussian pulse can be understood by noting that its spectrum is wider than that of a Gaussian pulse because of steeper leading and trailing edges. As the GVD-induced delay of each frequency component is directly related to its separation from the central frequency ω_0 , a wider spectrum results in a faster rate of pulse broadening.

4.3 Third-Order Dispersion

The dispersion-induced pulse broadening discussed in Section 4.2 is due to the lowest-order GVD term proportional to β_2 in Eq.1.2. Although the contribution of this term dominates in most cases of practical interest, it is sometimes necessary to include the third-order term proportional to β_3 in this expansion. For ultrashort pulses (width $T_0 < 1$ ps), it is necessary to include the β_3 term even when $\beta_2 \neq 0$ because the expansion parameter $\Delta\omega/\omega_0$ is no longer small enough to justify the truncation of the expansion in Eq.1.2 after the β_2 term.

This section considers the dispersive effects by including both β_2 and β_3 terms while still neglecting the nonlinear effects. The appropriate propagation equation for the amplitude $A(z, T)$ is obtained from Eq.3.46 after setting $\gamma = 0$.

Using Eq.4.3, $U(z, T)$ satisfies the following equation:

$$i \frac{\partial U}{\partial z} = \frac{\beta_2}{2} \frac{\partial^2 U}{\partial T^2} + i \frac{\beta_3}{6} \frac{\partial^3 U}{\partial T^3}. \quad (4.29)$$

This equation can also be solved by using the Fourier technique of Section 4.2. In place of Eq.4.12 the transmitted field is obtained from

$$U(z, T) = \frac{1}{2\pi} \int_{-\infty}^{\infty} \tilde{U}(0, \omega) \exp\left(\frac{i}{2}\beta_2 \omega^2 z + \frac{i}{6}\beta_3 \omega^3 z - i\omega T\right) d\omega, \quad (4.30)$$

where the Fourier transform $\tilde{U}(0, \omega)$ of the incident field is given by Eq.4.13. Eq.4.30 can be used to study the effect of higher-order dispersion if the incident field $U(0, T)$ is specified. In particular, one can consider Gaussian, super-Gaussian, or hyperbolic-secant pulses in a manner analogous to Section 4.2. An analytic solution in terms of the Airy functions can be obtained for Gaussian pulses [13].

4.3.1 Changes in Pulse Shape

As one may expect, pulse evolution along the fiber depends on the relative magnitudes of β_2 and β_3 , which in turn depend on the deviation of the optical wavelength λ_0 . In order to compare the relative importance of the β_2 and β_3 terms in Eq.(4.29), it is useful to introduce a dispersion length associated with the third-order dispersion (TOD) term as

$$L'_D = T_0^3 / |\beta_3|. \quad (4.31)$$

The TOD effects play a significant role only if $L'_D \leq L_D$ or $T_0 |\beta_2 / \beta_3| \leq 1$. The situation changes completely for ultrashort pulses with widths in the femtosecond range. For example, the effect of TOD can be studied experimentally by propagating 100 fs pulses across a few-meter-long fiber [11,12].

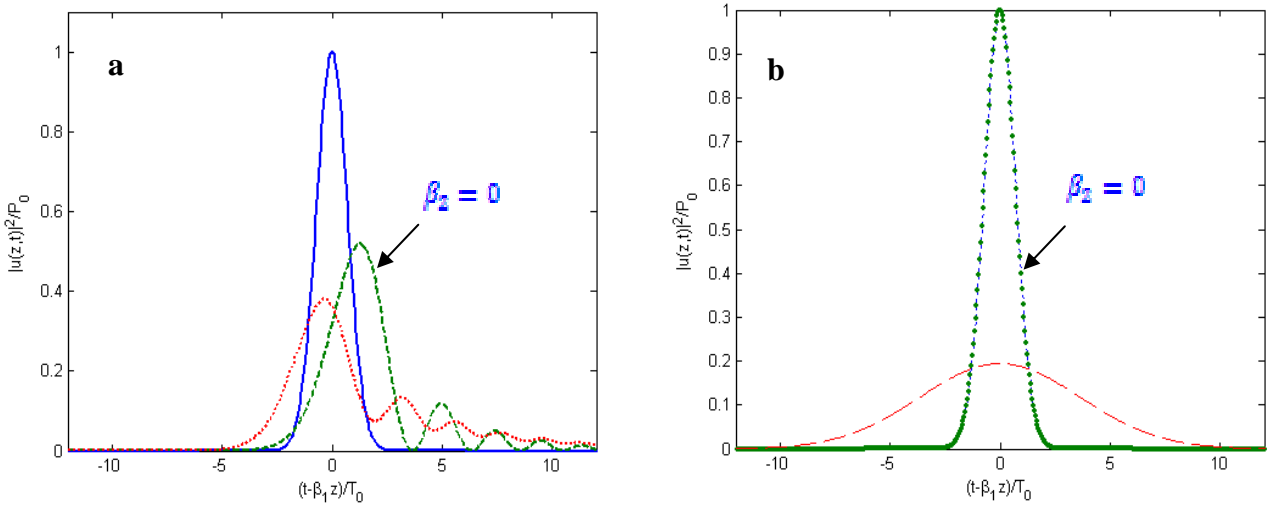


Figure.4.5 Pulse shapes at $z = 5L'_D$ of an initially Gaussian pulse at $z = 0$ (dotted curve) in the presence of higher-order dispersion. Dashed curve shows the effect of finite $\beta_2 = 0$ (a) in the case of titanium sapphire, and (b) in the case of silica fiber (after [9]).

Fig.4.5 shows the pulse shapes at $z = 5L'_D$ for an initially unchirped Gaussian pulse [$C = 0$ in Eq.4.21] for $\beta_2 = 0$ (solid curve) and for a value of $\beta_3 \neq 0$ (dashed curve). Whereas a Gaussian pulse remains Gaussian when only the β_2 term in Eq.4.29 contributes to GVD (Fig.4.1), the TOD distorts the pulse such that it becomes asymmetric with an oscillatory structure near one of its edges. In the case of positive β_3 shown in Fig. 4.5, oscillations appear near the trailing edge of the pulse. When β_3 is negative, it is the leading edge of the pulse that develops oscillations. When $\beta_2 = 0$, oscillations are deep, with intensity dropping to zero between successive oscillations. However, these oscillations damp significantly even for relatively small values of β_2 . For the case $L_D = L'_D$ shown in Fig. 4.5, oscillations have nearly disappeared, and the pulse has a long tail on the trailing side. For larger values of β_2 such that $L_D \ll L'_D$, the pulse shape becomes nearly Gaussian as the TOD plays a relatively minor role [13].

However, the titane sapphire have $\beta_3 = 0.00147$ it is very low value and does not contribute to the phenomenon of oscillations.

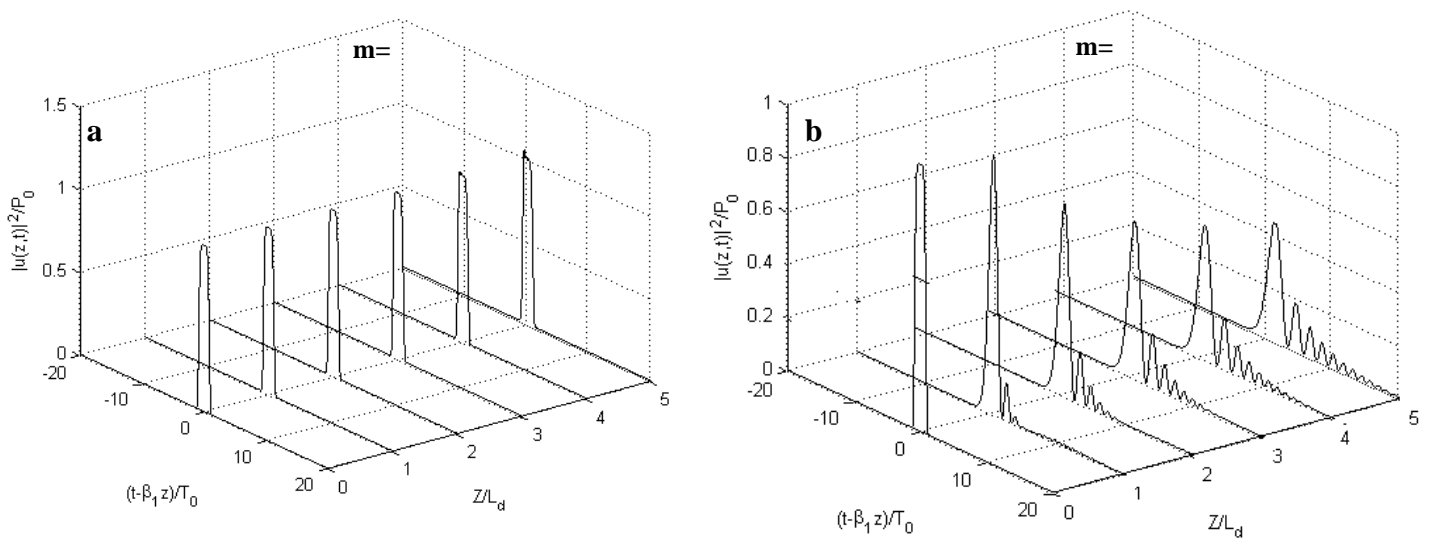


Figure.4.6: Evolution of a super-Gaussian pulse with $m = 3$ along the fiber length for the case of $\beta_2 \neq 0$ and $\beta_3 > 0$. Higher-order dispersion is responsible for the oscillatory structure near the trailing edge of the pulse (a) for titanium sapphire, and (b) for silica fiber (after [9]).

Eq.4.30 can be used to study pulse evolution for other pulse shapes (with or without chirp). By way of an example, Fig.4.6 shows evolution of an unchirped super-Gaussian pulse with $C = 0$ and $m = 3$ in Eq.4.28. It is clear that pulse shapes can vary widely depending on the initial conditions. In practice, one is often interested in the extent of dispersion-induced broadening rather than details of pulse shapes.

4.4 Dispersion Compensation

Even though operation at the zero-dispersion wavelength is most desirable from the standpoint of pulse broadening, other considerations may preclude such a design. For example, at most one channel can be located at the zero dispersion wavelength in a wavelength-division-multiplexed (WDM) system. The technique of dispersion management provides a solution to this dilemma.

It consists of combining fibers with different characteristics such that the average GVD of the entire fiber link is quite low while the GVD of each fiber section is chosen to be large enough to make the four-wave-mixing effects negligible.

Amplifiers compensate for accumulated fiber losses in each section. Between each pair of amplifiers, just two kinds of fibers, with opposite signs of β_2 , are combined to reduce the average dispersion to a small value. When the average GVD is set to zero, dispersion is totally compensated.

Such a dispersion-compensation technique takes advantage of the linear nature of Eq.(4.8). The basic idea can be understood from Eq.4.12 representing the general solution of Eq.4.8. For a dispersion map consisting of two fiber segments, Eq. 4.12 becomes

$$U(L_m, t) = \frac{1}{2\pi} \int_{-\infty}^{\infty} \tilde{U}(0, w) \exp \left[\frac{i}{2} w^2 (\beta_{21} L_1 + \beta_{22} L_2) - i w t \right] dw, \quad (4.32)$$

where $L_m = L_1 + L_2$ is the dispersion-map period, and β_{2j} is the GVD parameter of the fiber segment of length L_j ($j = 1, 2$). By using $D_j = -(2\pi c/\lambda^2)\beta_{2j}$, the condition for dispersion compensation can be written as

$$D_1 L_1 + D_2 L_2 = 0. \quad (4.33)$$

As $A(L_m, t) = A(0, t)$ when Eq.4.33 is satisfied, the pulse recovers its initial width after each map period even though the pulse width can change significantly within each period.

4.4.1 Compensation of Third-Order Dispersion

When the bit rate of a single channel exceeds 100 Gb/s, one must use ultrashort pulses (width ~ 1 ps) in each bit slot. For such short optical pulses, the pulse spectrum becomes broad enough that it is difficult to compensate GVD over the entire bandwidth of the pulse (because of the frequency dependence of β_2). The simplest solution to this problem is provided by fibers, or other devices, designed such that both β_2 and β_3 are compensated simultaneously. The necessary conditions for designing such fibers can be obtained from Eq.4.30.

For a fiber link containing two different fibers of lengths L_1 and L_2 , the conditions for broadband dispersion compensation are given by

$$\beta_{21}L_1 + \beta_{22}L_2 = 0 \quad \text{and} \quad \beta_{31}L_1 + \beta_{32}L_2 = 0 \quad (4.34)$$

where β_{2j} and β_{3j} are the GVD and TOD parameters for fibers of length $L_j (j = 1,2)$. It is generally difficult to satisfy both conditions simultaneously over a wide wavelength range [17,18].

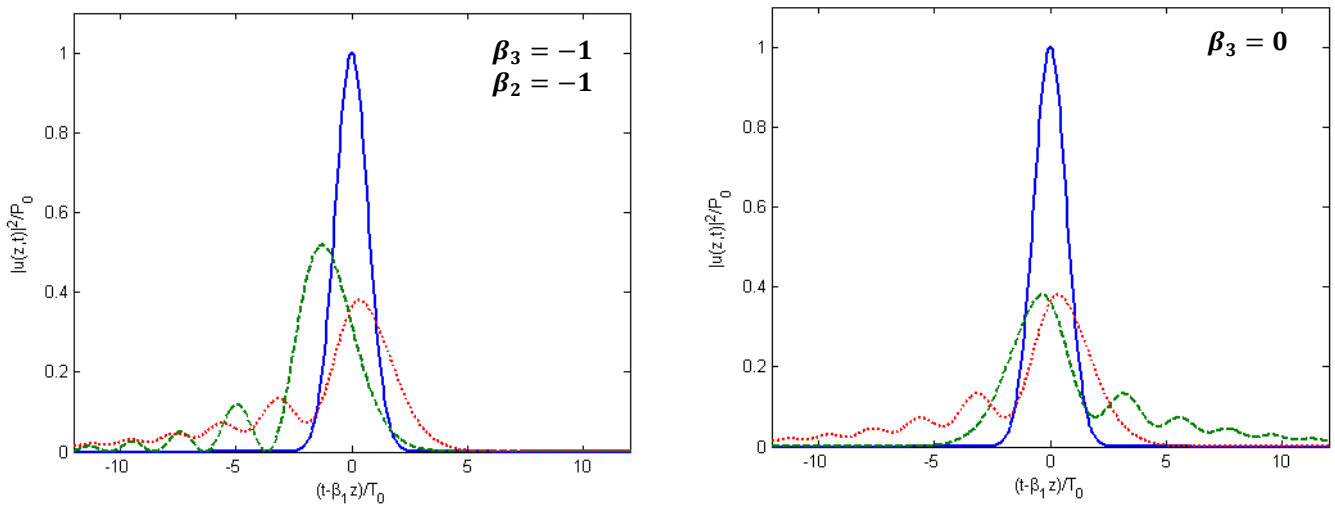


Figure4.7: (a) compensation of the β_3, β_2 at $z = 2$.

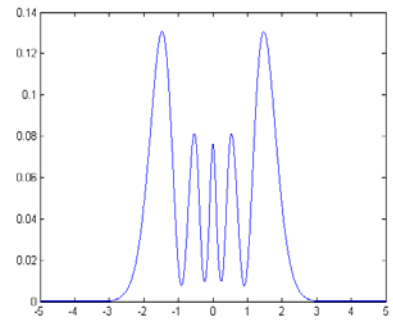
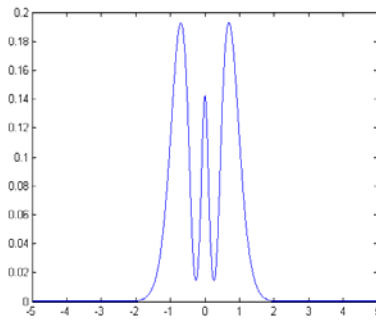
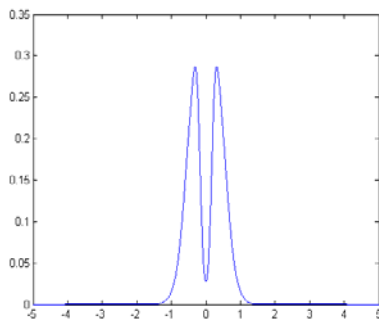
When both β_2 and β_3 are nearly compensated, propagation of femtosecond optical pulses is limited by the fourth-order dispersive effects governed by the parameter β_4 .

References

- [1] I. N. Sisakyan and A. B. Shvartsburg, *Sov. J. Quantum Electron.* 14, 1146 (1984).
- [2] S. A. Akhmanov, V. A. Vysloukh, and A. S. Chirkin, *Optics of Femtosecond Laser Pulses* (New York, 1992),
- [3] G. P. Agrawal, in *Supercontinuum Laser Source*, R. R. Alfano, ed. (Springer-Verlag, Heidelberg, 1989),
- [4] C. G. B. Garrett and D. E. McCumber, *Phys. Rev. A* 1, 305 (1970).
- [5] H. G. Unger, *Arch. Electron. Uebertragungstechn.* 31, 518 (1977).
- [6] M. Miyagi and S. Nishida, *Appl. Opt.* 18, 678 (1979).
- [7] D. Gloge, *Electron. Lett.* 15, 686 (1979).
- [8] D. Marcuse, *Appl. Opt.* 19, 1653 (1980).
- [9] G. P. Agrawal and M. J. Potasek, *Opt. Lett.* 11, 318 (1986).
- [10] D. Anderson and M. Lisak, *Opt. Lett.* 11, 569 (1986).
- [11] D. M. Bloom, L. F. Mollenauer, C. Lin, D. W. Taylor, and A. M. DelGaudio, *Opt. Lett.* 4, 297 (1979).
- [12] C. Lin, A. Tomita, A. R. Tynes, P. F. Glodis, and D. L. Philen, *Electron. Lett.* 18, 882 (1982).
- [13] D. Marcuse, *Appl. Opt.* 20, 3573 (1981).
- [14] D. S. Lerner and V. A. Bhagavatula, *Electron. Lett.* 21, 1171 (1985).
- [15] A. M. Vengsarkar and W. A. Reed, *Opt. Lett.* 18, 924 (1993).
- [16] C. D. Poole, J. M. Wiesenfeld, A. R. McCormick, and K. T. Nelson, *Opt. Lett.* 17, 985 (1992).
- [17] C. C. Chang, H. P. Sardesai, and A. M. Weiner, *Opt. Lett.* 23, 283 (1998).
- [18] T. Imai, T. Komukai, and M. Nakazawa, *Electron. Lett.* 34, 2422 (1998).

CHAP V

SELF PHASE MODULATION EFFECT



An interesting manifestation of the intensity dependence of the refractive index in nonlinear optical media occurs through self-phase modulation (SPM), a phenomenon that leads to spectral broadening of optical pulses [1-3]. SPM is the temporal analog of self-focusing. Indeed, it was first observed in 1967 in the context of transient self-focusing of optical pulses propagating in a CS₂-filled cell [1]. By 1970, SPM had been observed in solids and glasses by using picosecond pulses. The earliest observation of SPM in optical fibers was made with a fiber whose core was filled with CS₂ [5]. This chapter considers SPM as a simple example of the nonlinear optical effects that can occur in optical fibers. Section 5.1 is devoted to the case of pure SPM by neglecting the GVD effects. The effects of GVD on SPM are discussed in Section 5.2 with particular emphasis on the SPM-induced frequency chirp. Section 5.3 extends the results to include the higher-order nonlinear effects such as self-steepening.

5.1 SPM-Induced Spectral Broadening

A general description of SPM in optical fibers requires numerical solutions of the pulse-propagation Eq.3.46 obtained in Section 3.3. The simpler Eq.3.46 can be used for pulse widths $T_0 > 5$ ps. A further simplification occurs if the effect of GVD on SPM is negligible so that the β_2 term in Eq.3.47 can be set to zero. The conditions under which GVD can be ignored were discussed in Section 4.1 by introducing the length scales L_D and L_{NL} [see Eq.4.5]. In general, the pulse width and the peak power should be such that $L_D \gg L > L_{NL}$ for a fiber of length L . Eq. 4.7 shows that the GVD effects are negligible for relatively wide pulses ($T_0 > 100$ ps) with a large peak power ($P_0 > 1$ W).

5.1.1 Nonlinear Phase Shift

In terms of the normalized amplitude $U(z, T)$ defined as in Eq.4.3, the pulse-propagation Eq.4.4, in the limit $\beta_2 = 0$, becomes

$$\frac{\partial U}{\partial z} = \frac{ie^{-\alpha z}}{L_{NL}} |U|^2 U, \quad (5.1)$$

where α accounts for fiber losses. The nonlinear length is defined as

$$L_{NL} = (\gamma P_0)^{-1}, \quad (5.2)$$

where P_0 is the peak power and γ is related to the nonlinear-index coefficient n_2 as in Eq.3.44. Eq.5.1 can be solved substituting $U = V \exp(i\phi_{NL})$ and equating the real and imaginary parts so that

$$\frac{\partial V}{\partial z} = 0; \quad \frac{\partial \phi_{NL}}{\partial z} = \frac{e^{-\alpha z}}{L_{NL}} V^2. \quad (5.3)$$

As the amplitude V does not change along the fiber length L , the phase equation can be integrated analytically to obtain the general solution

$$U(L, T) = U(0, T) \exp[i\phi_{NL}(L, T)], \quad (5.4)$$

where $U(0, T)$ is the field amplitude at $z = 0$ and

$$\phi_{NL}(L, T) = |U(0, T)|^2 (L_{eff}/L_{NL}), \quad (5.5)$$

with the effective length L_{eff} defined as

$$L_{eff} = [1 - \exp(-\alpha L)]/\alpha. \quad (5.6)$$

Eq.5.4 shows that SPM gives rise to an intensity-dependent phase shift but the pulse shape remains unaffected. The nonlinear phase shift ϕ_{NL} in Eq.5.5 increases with fiber length L . The quantity L_{eff} plays the role of an effective length that is smaller than L because of fiber losses. In the absence of fiber losses, $\alpha = 0$, and $L_{eff} = L$, the maximum phase shift ϕ_{max} occurs at the pulse center located at $T = 0$. With U normalized such that $|U(0, 0)| = 1$, it is given by

$$\phi_{max} = \frac{L_{eff}}{L_{NL}} = \gamma P_0 L_{eff}. \quad (5.7)$$

The physical meaning of the nonlinear length L_{NL} is clear from Eq.5.7. It is the effective propagation distance at which $\phi_{max} = 1$. The SPM-induced spectral broadening is a consequence of the time dependence of ϕ_{NL} .

This can be understood by noting that a temporally varying phase implies that the instantaneous optical frequency differs across the pulse from its central value ω_0 . The difference $\delta\omega$ is given by

$$\delta\omega(T) = -\frac{\partial\phi_{NL}}{\partial T} = -\left(\frac{L_{eff}}{L_{NL}}\right)\frac{\partial}{\partial T}|U(0, T)|^2, \quad (5.8)$$

where the minus sign is due to the choice of the factor $\exp(-i\omega_0 t)$ in Eq.3.36. The time dependence of $\delta\omega$ is referred to as the frequency chirping. The chirp induced by SPM increases in magnitude with the propagated distance. In other words, new frequency components are continuously generated as the pulse propagates down the fiber. These SPM-generated frequency components broaden the spectrum over its initial width at $z = 0$.

The extent of spectral broadening depends on the pulse shape. Consider, for example, the case of a super-Gaussian pulse with the incident field $U(0, T)$ given by Eq. 4.28. The SPM-induced chirp $\delta\omega(T)$ for such a pulse is

$$\delta\omega(T) = \frac{2m}{T_0} \frac{L_{eff}}{L_{NL}} \left(\frac{T}{T_0}\right)^{2m-1} \exp\left[-\left(\frac{T}{T_0}\right)^{2m}\right], \quad (5.9)$$

where $m = 1$ for a Gaussian pulse. For larger values of m , the incident pulse becomes nearly rectangular with increasingly steeper leading and trailing edges. Fig.5.1 shows the variation of the nonlinear phase shift ϕ_{NL} and the induced frequency chirp $\delta\omega$ across the pulse at $L_{eff} = L_{NL}$ in the cases of a Gaussian pulse ($m = 1$) and a super-Gaussian pulse ($m = 3$). As ϕ_{NL} is directly proportional to $|U(0, T)|^2$ in Eq.5.5, its temporal variation is identical to that of the pulse intensity. The temporal variation of the induced chirp $\delta\omega$ has several interesting features. First, $\delta\omega$ is negative near the leading edge (red shift) and becomes positive near the trailing edge (blue shift) of the pulse. Second, the chirp is linear and positive (up-chirp) over a large central region of the Gaussian pulse. Third, the chirp is considerably larger for pulses with steeper leading and trailing edges. Fourth, super-Gaussian pulses behave differently than Gaussian pulses because the chirp occurs only near pulse edges and does not vary in a linear fashion.

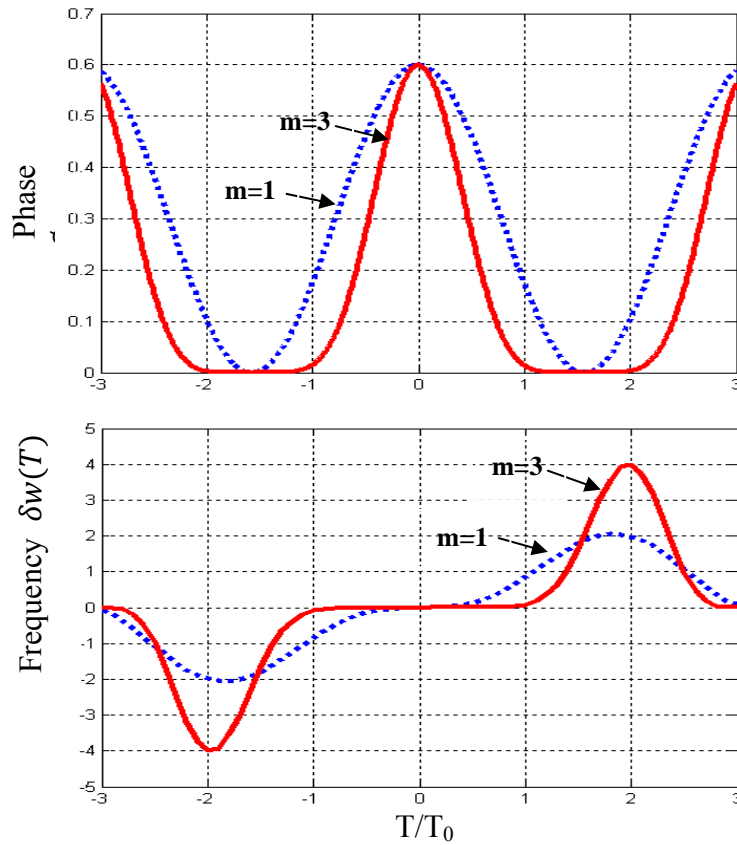


Figure 5.1: Temporal variation of SPM-induced phase shift ϕ_{NL} and frequency chirp δw for Gaussian (dashed curve) and super-Gaussian (solid curve) pulses.

5.1.2 Changes in Pulse Spectra

An estimate of the magnitude of SPM-induced spectral broadening can be obtained from the peak value of δw in Fig.5.1. More quantitatively, we can calculate the peak value by maximizing $\delta w(T)$ from Eq.5.9. Eq.5.9 shows that the broadening factor of a super-Gaussian pulse is also approximately given by ϕ_{max} . With $\phi_{max} \sim 100$, possible for intense pulses or long fibers, SPM can broaden the spectrum considerably. In the case of intense ultrashort pulses, the broadened spectrum can extend over 100 THz or more, especially when SPM is accompanied by other nonlinear processes such as stimulated Raman scattering and four-wave mixing. Such an extreme spectral broadening is referred to as *supercontinuum generation* [4].

The actual shape of the pulse spectrum $S(w)$ is obtained by taking the Fourier transform of Eq.5.4. Using $S(w) = |\tilde{U}(L, w)|^2$, we obtain

$$S(w) = \left| \int_{-\infty}^{\infty} U(0, T) \exp[i\phi_{NL}(L, T) + i(w - w_0)T] dT \right|^2. \quad (5.10)$$

In general, the spectrum depends not only on the pulse shape but also on the initial chirp imposed on the pulse. Figure 5.2 shows the spectra of an unchirped Gaussian pulse for several values of the maximum phase shift ϕ_{max} . For a given fiber length, ϕ_{max} increases linearly with peak power P_0 according to Eq. (5.7).

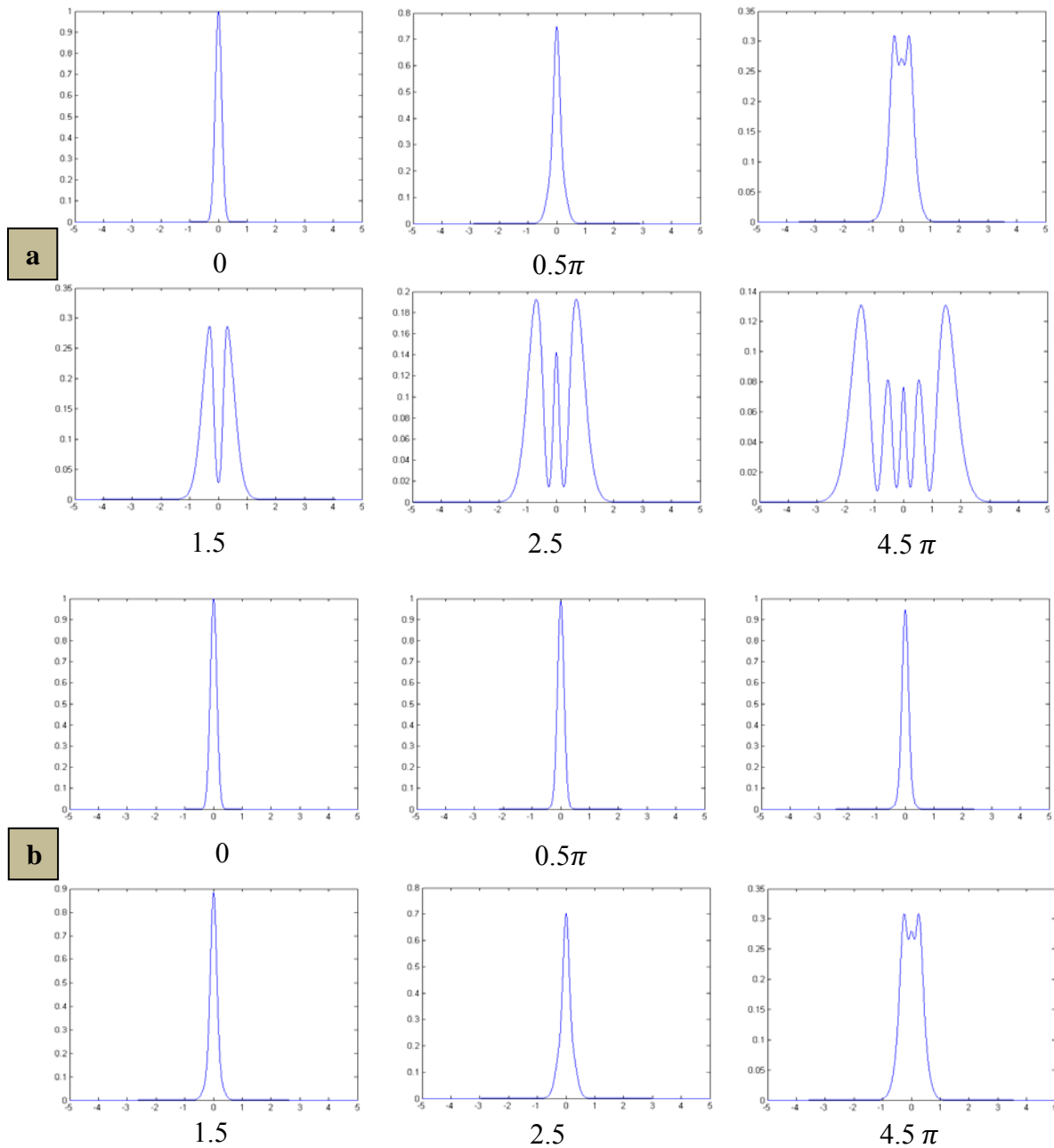


Figure 5.2: SPM-broadened spectra for an unchirped Gaussian pulse. Spectra are labeled by the maximum nonlinear phase shift ϕ_{max} . (After Ref. [9]) for a) silica fiber , and b) titanium sapphire.

The most notable feature of Fig.5.2 is that SPM-induced spectral broadening is accompanied by an oscillatory structure covering the entire frequency range. In general, the spectrum consists of many peaks, and the outermost peaks are the most intense. The number of peaks depends on ϕ_{max} and increases linearly with it. The origin of the oscillatory structure can be understood by referring to Figure.5.1, where the time dependence of the SPM-induced frequency chirp is shown. In general, the same chirp occurs at two values of T , showing that the pulse has the same instantaneous frequency at two distinct points. Qualitatively speaking, these two points represent two waves of the same frequency but different phases that can interfere constructively or destructively depending on their relative phase difference. The multippeak structure in the pulse spectrum is a result of such interference [1]. Mathematically, the Fourier integral in Eq.5.10 gets dominant contributions at the two values of T at which the chirp is the same. These contributions, being complex quantities, may add up in phase or out of phase.

5.1.3 Effect of Pulse Shape and Initial Chirp

As mentioned before, the shape of the SPM-broadened spectrum depends on the pulse shape and on the initial chirp if the input pulse is chirped [11]. Fig. 5.3 compares the pulse spectra for Gaussian ($m = 1$) and super-Gaussian ($m = 3$) pulses obtained using Eq.4.28 in Eq.5.10 and performing the integration numerically. In both cases, input pulses are assumed to be unchirped ($C = 0$). The fiber length and the peak power are chosen such that $\phi_{max} = 4.5\pi$.

The qualitative differences between the two spectra can be understood by referring to Figure 5.1, where the SPM-induced chirp is shown for the Gaussian and super-Gaussian pulses.

We notice that Fig.5.3 exhibit five peaks in the case of the silica fiber, and two peaks in Titanium sapphire. This is so because the chirp is nearly zero over the central region in Fig.5.1 for such a pulse, as a consequence of the nearly uniform intensity of a super-Gaussian pulse for $|T| < T_0$. The frequency chirp occurs

mainly near the leading and trailing edges. As these edges become steeper, the tails in Fig.5.3 extend over a longer frequency range but, at the same time, carry less energy because chirping occurs over small time duration.

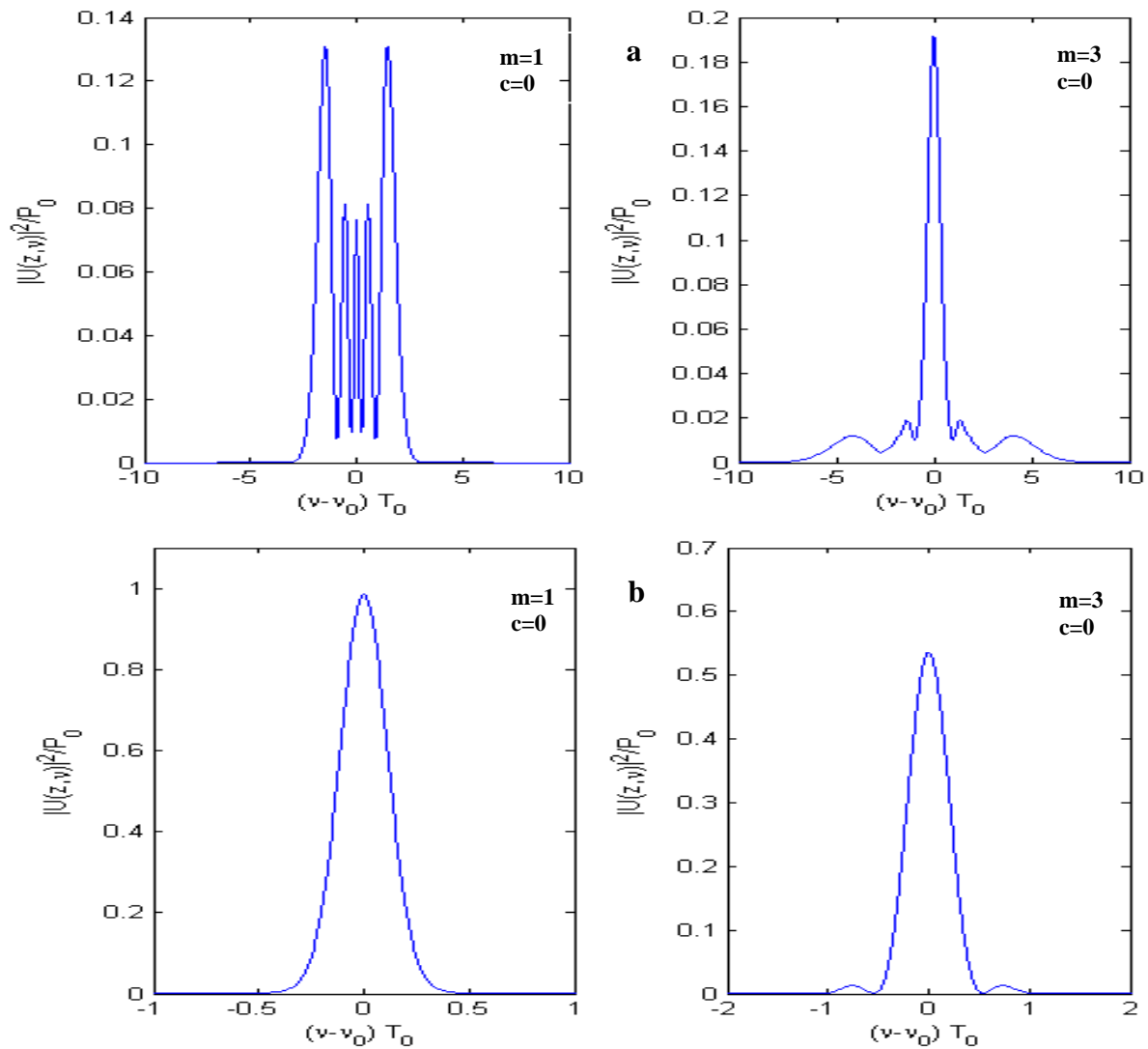


Figure.5.3: Comparison of SPM-broadened spectra for unchirped Gaussian and super-Gaussian pulses at a peak power corresponding to $\phi_{max} = 4.5$. a) Silica fiber (after[16]) and b) Titanium sapphire.

A positive chirp increases the number of spectral peaks while the opposite occurs in the case of a negative chirp in silica fiber. This can be understood by noting that the SPM-induced frequency chirp is linear and positive (frequency increases with increasing T) over the central portion of a Gaussian pulse (see Fig.5.1). Thus, it adds with the initial chirp for $C > 0$, resulting in an enhanced oscillatory

structure. The outermost peaks in Fig.5.4 for $C = -5$ are due to the residual chirp near the leading and trailing edges. In the case of titanium sapphire the pulse remains unchanged except for a creation of two peaks in the leading and trailing edges of the pulse. The spectral range is about three times larger for negative chirp and there is a creation of two peaks.

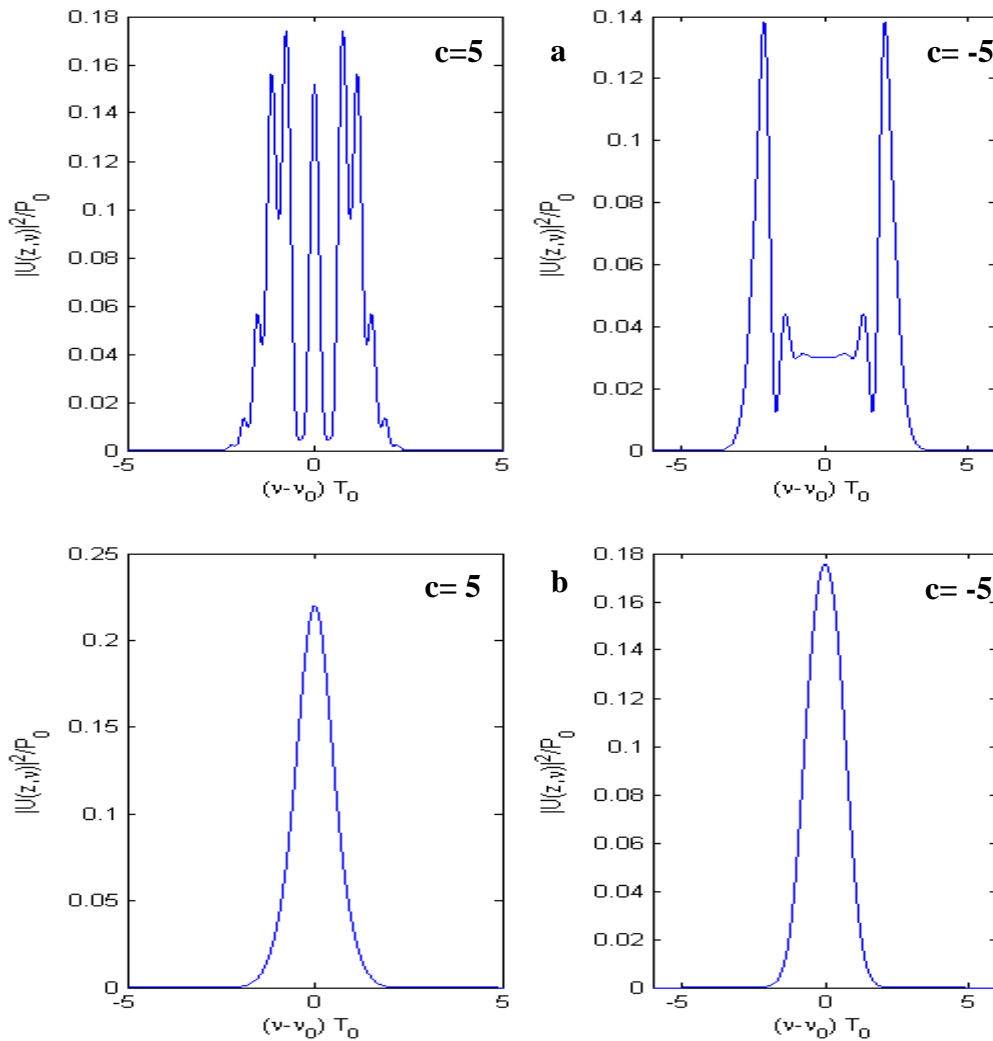


Figure 5.4: Effect of initial frequency chirp on SPM-broadened spectra of a chirped Gaussian pulse for $C = 5$ and $C = -5$. The two spectra should be compared with the left spectrum in Fig. 5.3 where $C = 0$. In all cases $\phi_{max} = 4.5\pi$. a) silica fiber and b) Titanium sapphire (after[16]).

For positive values of the chirp parameter C , the pulse spectrum at the fiber output can become narrower than that of initially unchirped pulses. These results

can be understood qualitatively by noting that the spectrum narrows as long as the SPM-induced chirp compensates the initial chirp.

5.2 Effect of Group-Velocity Dispersion

The SPM effects discussed in Section 5.1 describe the propagation behavior realistically only for relatively long pulses ($T_0 > 100$ ps) for which the dispersion length L_D is much larger compared with both the fiber length L and the nonlinear length L_{NL} . As pulses become shorter and the dispersion length becomes comparable to the fiber length, it becomes necessary to consider the combined effects of GVD and SPM [6]. New qualitative features arise from an interplay between GVD and SPM. In the anomalous-dispersion regime of an optical fiber, the two phenomena can cooperate in such a way that the pulse propagates as an optical soliton (Chapter VI). In the normal-dispersion regime, the combined effects of GVD and SPM can be used for pulse compression. This section considers the temporal and spectral changes that occur when the effects of GVD are included in the description of SPM [7-9].

5.2.1 Pulse Evolution

The starting point is the nonlinear Schrödinger (NLS) Eq.3.47 or its other form given in Eq.4.4. The later equation can be written in a normalized form as

$$i \frac{\partial U}{\partial \xi} = \text{sgn}(\beta_2) \frac{1}{2} \frac{\partial^2 U}{\partial \tau^2} - N^2 e^{-\alpha z} |U|^2 U, \quad (5.11)$$

where ξ and τ represent the normalized distance and time variables defined as

$$\xi = z/L_D, \quad \tau = T/T_0, \quad (5.12)$$

and the parameter N is introduced by using

$$N^2 = \frac{L_D}{L_{NL}} \equiv \frac{\gamma P_0 T_0^2}{|\beta_2|}. \quad (5.13)$$

The physical significance of N will become clear in Chapter.VI where the integer values of N are found to be related to the soliton order. The practical significance of the parameter N is that solutions of Eq.5.11 obtained for a specific N value are

applicable to many practical situations through the scaling law of Eq.5.13. As it is evident from Eq.5.13, N governs the relative importance of the SPM and GVD effects on pulse evolution along the fiber. Dispersion dominates for $N \ll 1$ while SPM dominates for $N \gg 1$. For values of $N \sim 1$, both SPM and GVD play an equally important role during pulse evolution. In Eq.5.11, $sgn(\beta_2) = \pm 1$ depending on whether GVD is normal ($\beta_2 > 0$) or anomalous ($\beta_2 < 0$). The split-step Fourier method of Section 3.4 can be used to solve Eq.5.11 numerically.

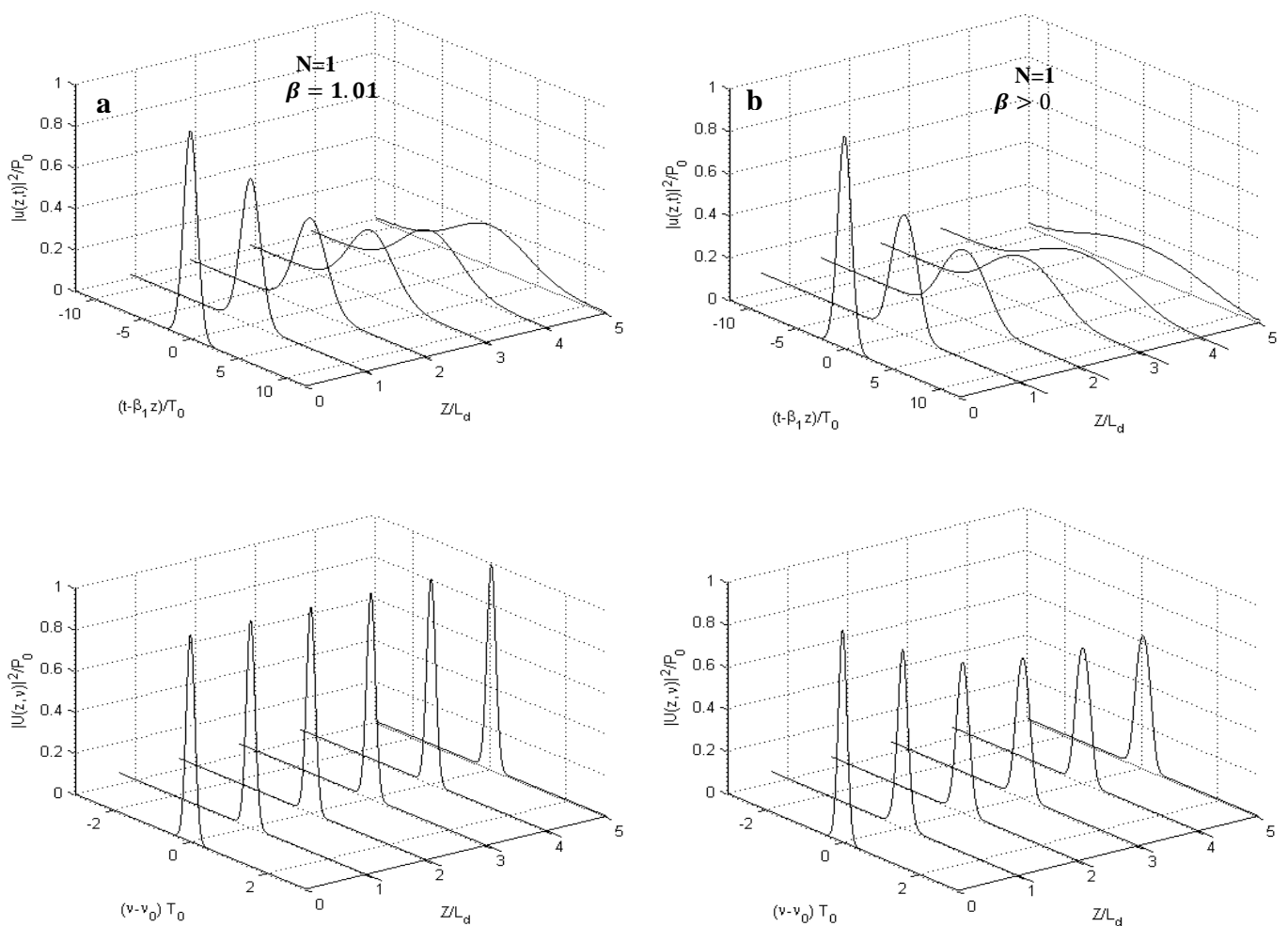


Figure 5.5: Evolution of pulse shapes and optical spectra over a distance of $5L_D$ for an initially unchirped Gaussian pulse propagating in the normal-dispersion regime of the fiber. a) for Titanium sapphire, and b) fiber silica (after[16]).

Fig.5.5 shows evolution of the shape and the spectrum of an initially unchirped Gaussian pulse in the normal-dispersion regime of a fiber using $N = 1$

and $\alpha = 0$. The qualitative behavior is quite different from that expected when either GVD or SPM dominates. In particular, the pulse broadens much more rapidly compared with the $N = 0$ case (no SPM). This can be understood by noting that SPM generates new frequency components that are red-shifted near the leading edge and blue-shifted near the trailing edge of the pulse.

As the red components travel faster than the blue components in the normal-dispersion regime, SPM leads to an enhanced rate of pulse broadening compared with that expected from GVD alone.

This in turn affects the spectral broadening as the SPM-induced phase shift Φ_{NL} becomes less than that occurring if the pulse shape were to remain unchanged. Indeed, $\Phi_{max} = 5$ at $z = 5L_D$, and a two-peak spectrum is expected in the absence of GVD. The single-peak spectrum for $z/L_D = 5$ in Figure.5.5 implies that the effective Φ_{max} is below π because of pulse broadening.

5.2.2 Optical Wave Breaking

Eq5.11 suggests that the effects of SPM should dominate over those of GVD for values of $N \gg 1$, at least during the initial stages of pulse evolution. In fact, by introducing a new distance variable as $Z = N^2\xi = z/L_{NL}$, Eq.5.11 can be written as

$$i \frac{\partial U}{\partial Z} - \frac{d}{2} \frac{\partial^2 U}{\partial \tau^2} + |U|^2 U, \quad (5.14)$$

here fiber losses are neglected and $d = \beta_2/(\gamma P_0 T_0^2)$ is a small parameter. Using the transformation

$$U(z, T) = \sqrt{\rho(z, T)} \exp\left(i \int_0^T v(z, T) dT\right), \quad (5.15)$$

in Eq.5.14, the pulse-propagation problem reduces approximately to a fluid dynamics problem in which the variables ρ and v play, respectively, the role of density and velocity of a fluid [10]. In the optical case, these variables represent the power and chirp profiles of the pulse. For a square-shape pulse, the pulse-propagation problem becomes identical to the one related to “breaking of a dam” and can be solved analytically [11].

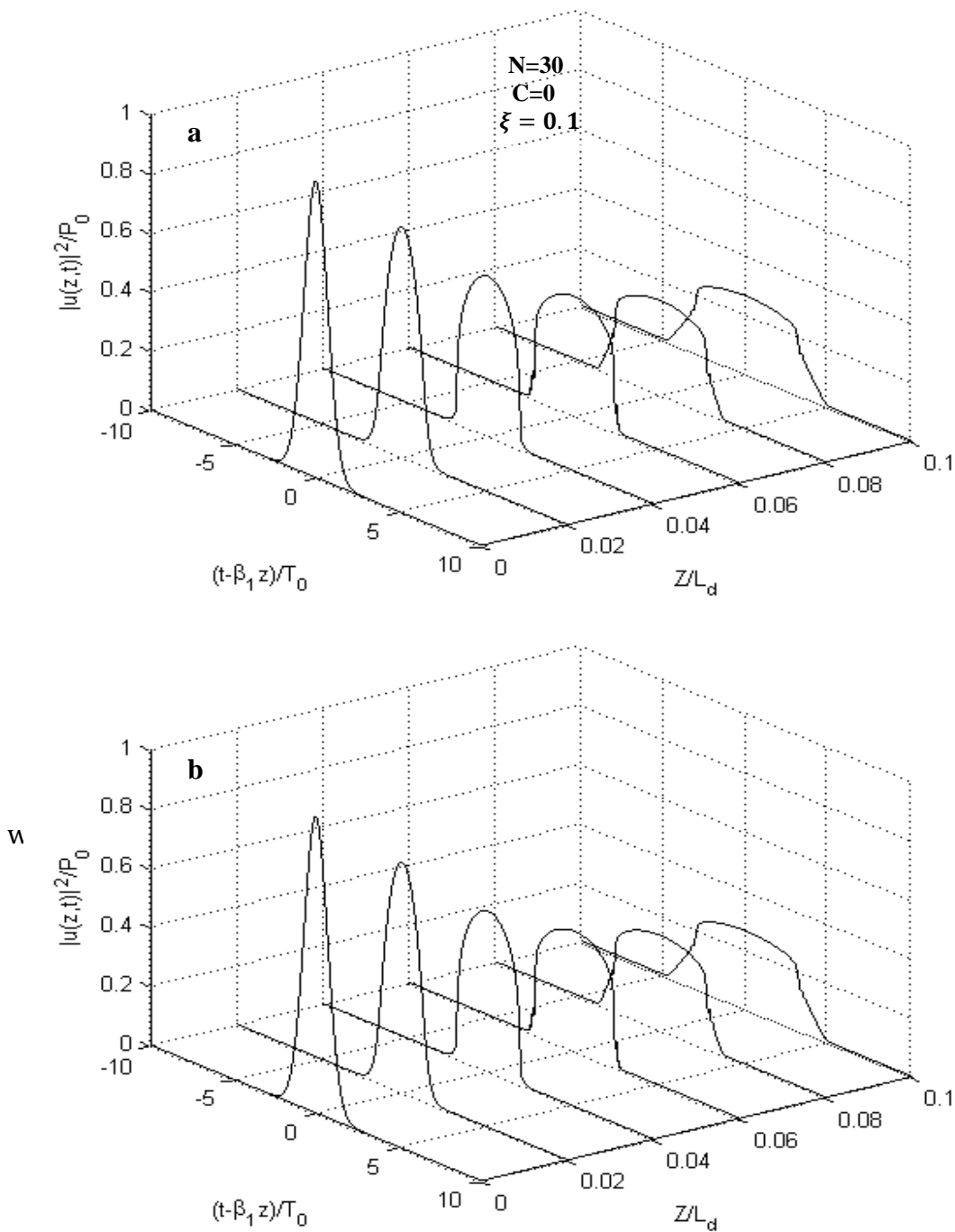


Figure 5.6: Evolution of an initially unchirped Gaussian pulse for $N = 30$ at $z/L_D = 0.1$ in the normal-dispersion regime a) Titanium sapphire, b) silica fiber (after [16]).

The approximate solution, although useful, does not account for a phenomenon termed *Optical Wave Breaking* [12-13]. It turns out that GVD cannot

be treated as a small perturbation even when N is large. The reason is that, because of a large amount of the SPM-induced frequency chirp imposed on the pulse, even weak dispersive effects lead to significant pulse shaping. In the case of normal dispersion ($\beta_2 > 0$), the pulse becomes nearly rectangular with relatively sharp leading and trailing edges and is accompanied by a linear chirp across its entire width. It is this linear chirp that can be used to compress the pulse by passing it through a dispersive delay line.

The GVD-induced pulse shaping has another effect on pulse evolution. It increases the importance of GVD because the second derivative in Eq.5.11 becomes larger near the pulse edges. As a consequence, the pulse develops a fine structure near its edges. Figure 5.6 shows the pulse evolution for $N = 30$ for the case of an initially unchirped Gaussian pulse. The oscillatory structure near pulse edges is already present at $z/L_D = 0.06$. Further increase in z leads to a broadening of the pulse tails. Fig.5.7 shows the pulse shape and the spectrum at $z/L_D = 0.08$.

The noteworthy feature is that rapid oscillations near pulse edges are always accompanied by the side lobes in the spectrum. The central multipeak part of the spectrum is also considerably modified by GVD. In particular, the minima are not as deep as expected from SPM alone.

The physical origin of temporal oscillations near the pulse edges is related to Optical Wave Breaking [44]. Both GVD and SPM impose frequency chirp on the pulse as it travels down the fiber. However, as seen from Eqs.(4.20) and (5.9), although the GVD-induced chirp is linear with time, the SPM-induced chirp is far from being linear across the entire pulse. Because of the nonlinear nature of the composite chirp, different parts of the pulse propagate at different speeds. In particular, in the case of normal GVD ($\beta_2 > 0$), the red-shifted light near the leading edge travels faster and overtakes the unshifted light in the forward tail of the pulse. The opposite occurs for the blue-shifted light near the trailing edge. In both cases, the leading and trailing regions of the pulse contain light at two

different frequencies that interfere. The phenomenon of Optical Wave Breaking can also be understood as a four-wave-mixing process. Nonlinear mixing of two different frequencies w_1 and w_2 in the pulse tails creates new frequencies at $2w_1 - w_2$ and $2w_2 - w_1$. The spectral sidelobes in Fig.5.7 represent these new frequency components.

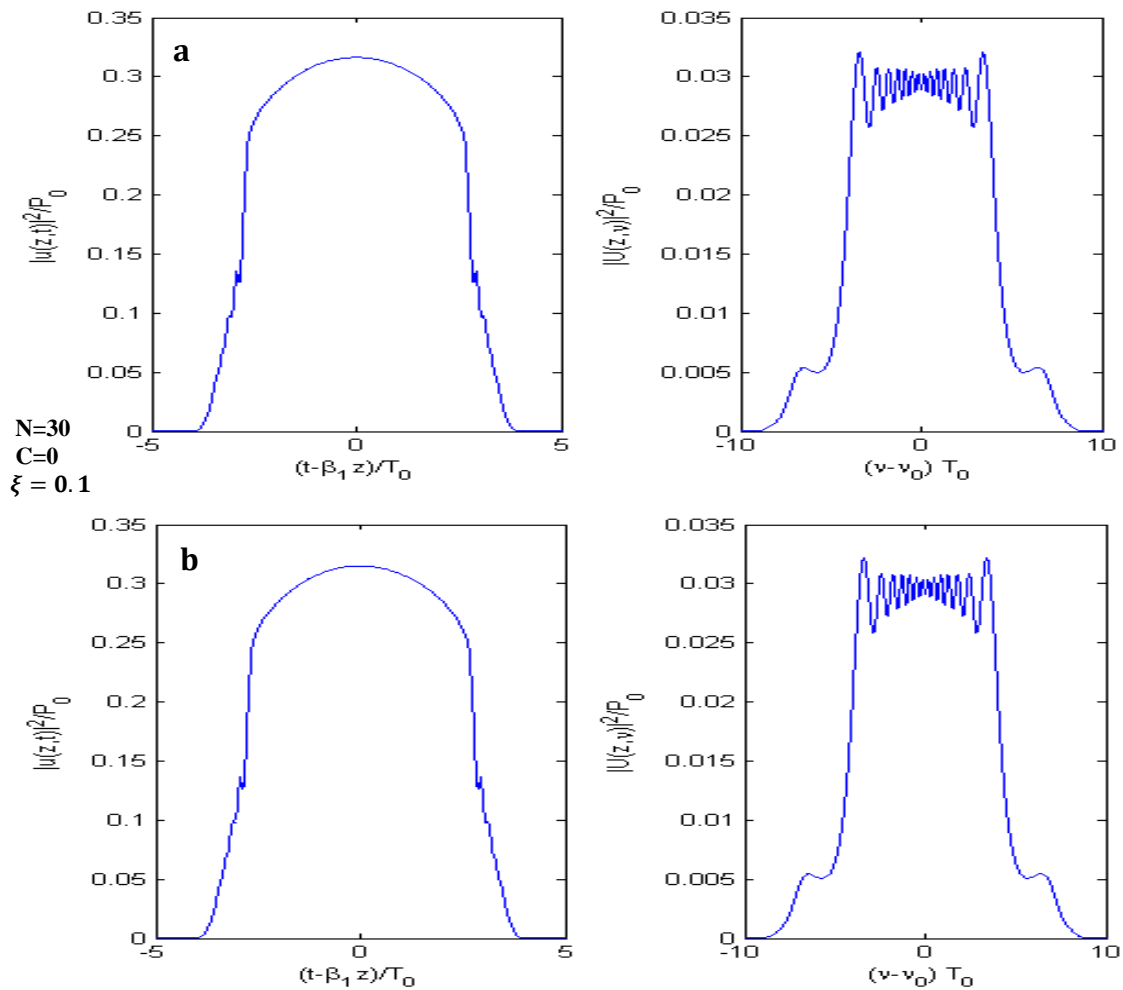


Figure 5.7: Shape and spectrum of an initially unchirped ($C = 0$) Gaussian pulse at $z/L_D = 0.08$. All parameters are identical to those of Fig.5.6. Spectral sidelobes and temporal structure near pulse edges are due to Optical Wave Breaking. a) Titanium sapphire, and b) silica fiber (after[16]).

Temporal oscillations near pulse edges and the spectral sidelobes are manifestations of the same phenomenon. The results shown in Figs. 5.6 and 5.7

are obtained for an unchirped pulse ($C = 0$). Pulses emitted from practical laser sources are often chirped and may follow quite a different evolution pattern depending on the sign and magnitude of the chirp parameter.

Fig.5.8 shows the pulse shape and the spectrum under conditions identical to those of Fig.5.7 except for the chirp parameter, which has a value $C = 20$. A comparison of the two figures illustrates how much an initial chirp can modify the propagation behavior.

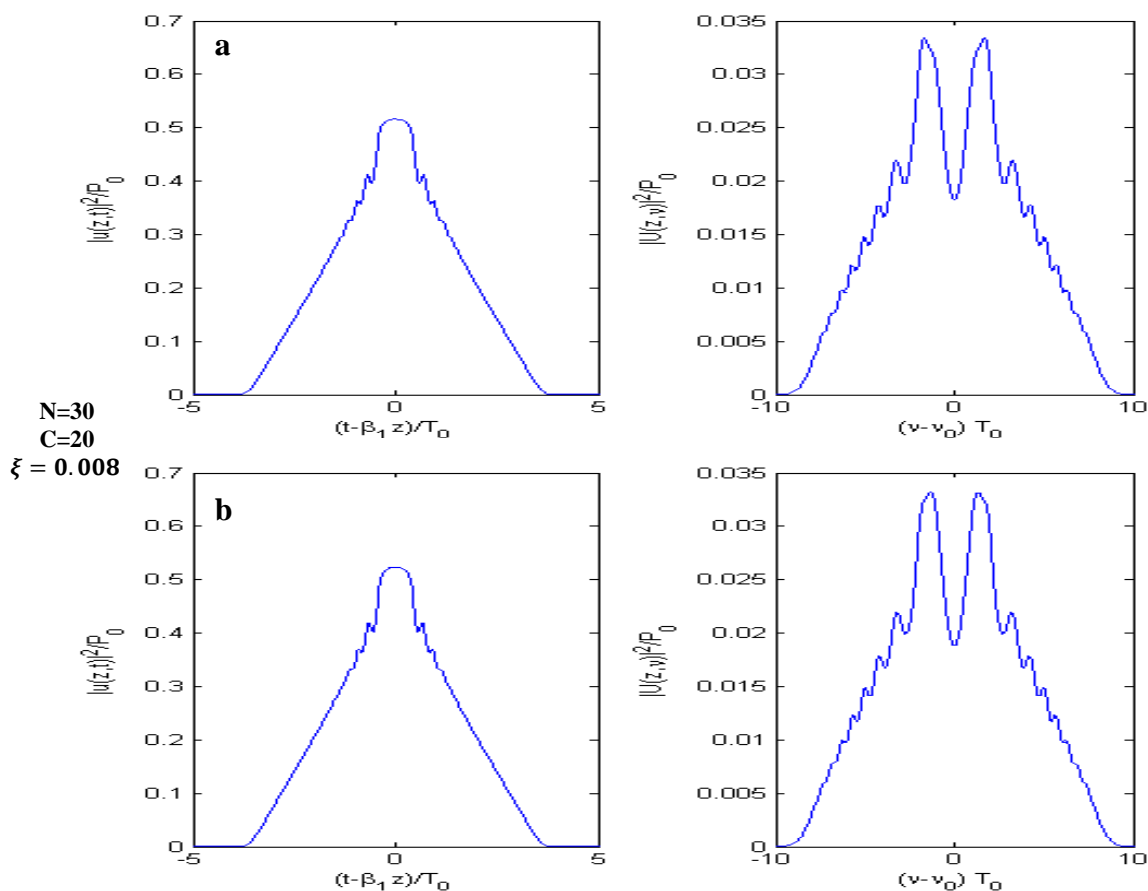


Figure 5.8: Pulse shape and spectrum under conditions identical to those of Fig. 5.7 except that the input Gaussian pulse is chirped with $C = 20$. a) silica fiber (after[16])and b) Titanium sapphire.

For an initially chirped pulse, the shape becomes nearly triangular rather than rectangular. At the same time, the spectrum exhibits an oscillatory structure in the wings while the central SPM-like structure (seen in Fig.5.7 for the case of

an unchirped pulse) has almost disappeared. These changes in the pulse shape and spectrum can be understood qualitatively by recalling that a positive initial chirp adds to the SPM-induced chirp. As a result, Optical Wave Breaking sets in earlier for chirped pulses. Pulse evolution is also sensitive to fiber losses. For an actual comparison between theory and experiment, it is necessary to include both the chirp and losses in numerical simulations. The spectral sidelobes associated with the Optical Wave Breaking were indeed found to be correlated with the generation of new frequencies near the pulse edges.

5.2.3 Effect of Third-Order Dispersion

In the case of an ultrashort pulse, it is necessary to include the effects of third-order dispersion (TOD) on SPM-induced spectral broadening [14–16]. The pulse propagation equation is obtained from Eq.3.46 by setting $\beta_2 = 0$ and neglecting the higher-order nonlinear terms. If we introduce the dispersion length L'_D from Eq.4.31 and define $\xi' = z/L'_D$ as the normalized distance, we obtain

$$i \frac{\partial U}{\partial \xi'} = \text{sgn}(\beta_3) \frac{i}{6} \frac{\partial^3 U}{\partial \tau^3} - \bar{N}^2 e^{-\alpha z} |U|^2 U, \quad (5.16)$$

where

$$\bar{N}^2 = \frac{L'_D}{L_{NL}} = \frac{\gamma P_0 T_0^3}{|\beta_3|} \quad (5.17)$$

Similar to Eq.5.11, the parameter \bar{N} governs the relative importance of the GVD and SPM effects during pulse evolution; GVD dominates for $\bar{N} \ll 1$ while SPM dominates for $\bar{N} \gg 1$. Eq.5.16 can be solved numerically using the split-step Fourier method of Section 3.4. In the following discussion we assume $\beta_3 > 0$ and neglect fiber losses by setting $\alpha = 0$.

Fig.5.9 shows the shape and the spectrum of an initially unchirped Gaussian pulse at $\xi' = 5$ for the case $\bar{N} = 1$. The pulse shape should be compared with that shown in Figure 4.5 where SPM effects were absent ($\bar{N} = 0$). The effect of SPM is to increase the number of oscillations seen near the trailing edge of the

pulse. At the same time, the intensity does not become zero at the oscillation minima. The effect of GVD on the spectrum is also evident in Fig5.9.

In the absence of GVD, a symmetric two-peak spectrum is expected (similar to the one shown in Figure 5.2 for the case $\phi_{max} = 1.5\pi$ (since $\phi_{max} = 5$ for the parameter values used in Fig.5.9)). The effect of TOD is to introduce spectral asymmetry without affecting the two-peak structure. Pulse evolution exhibits qualitatively different features for large values of N . As an example, Fig. 5.10 shows the shape and spectrum of an initially

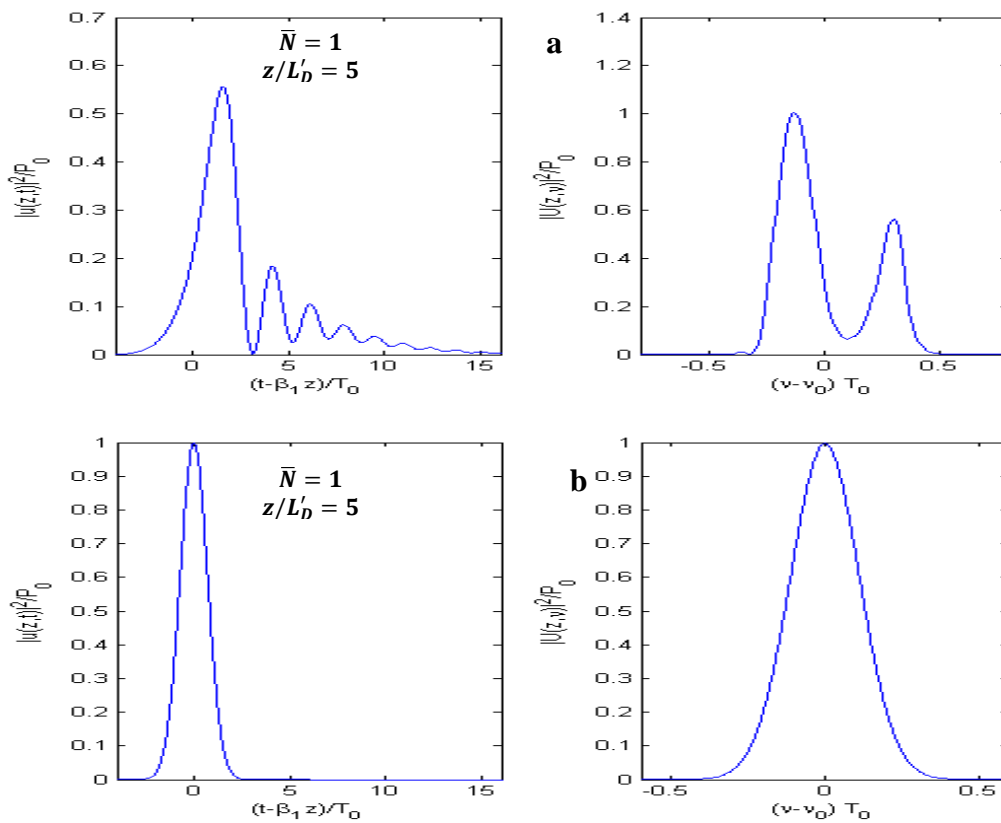


Figure 5.9: Pulse shape and spectrum of unchirped Gaussian pulses propagating exactly at the zero-dispersion wavelength with $\bar{N} = 1$ and $z = 5L'_D$. a) Titanium sapphire, and b) silica fiber (after[16]),

unchirped Gaussian pulse at $\xi' = 0.1$ for the case $\bar{N} = 10$. The pulse develops an oscillatory structure with deep modulation. Because of rapid temporal variations,

the third derivative in Eq.5.16 becomes large locally, and the TOD effects become more important as the pulse propagates inside the fiber.

The most noteworthy feature of the spectrum is that the pulse energy becomes concentrated in two spectral bands, a feature common for all values of $\bar{N} \geq 1$. As one of the spectral bands lies in the anomalous-dispersion regime, the pulse energy in that band can form a soliton. The energy in the other spectral band, lying in the normal-dispersion regime of the fiber, disperses with propagation. The soliton-related features are discussed later in Chapter.VI.

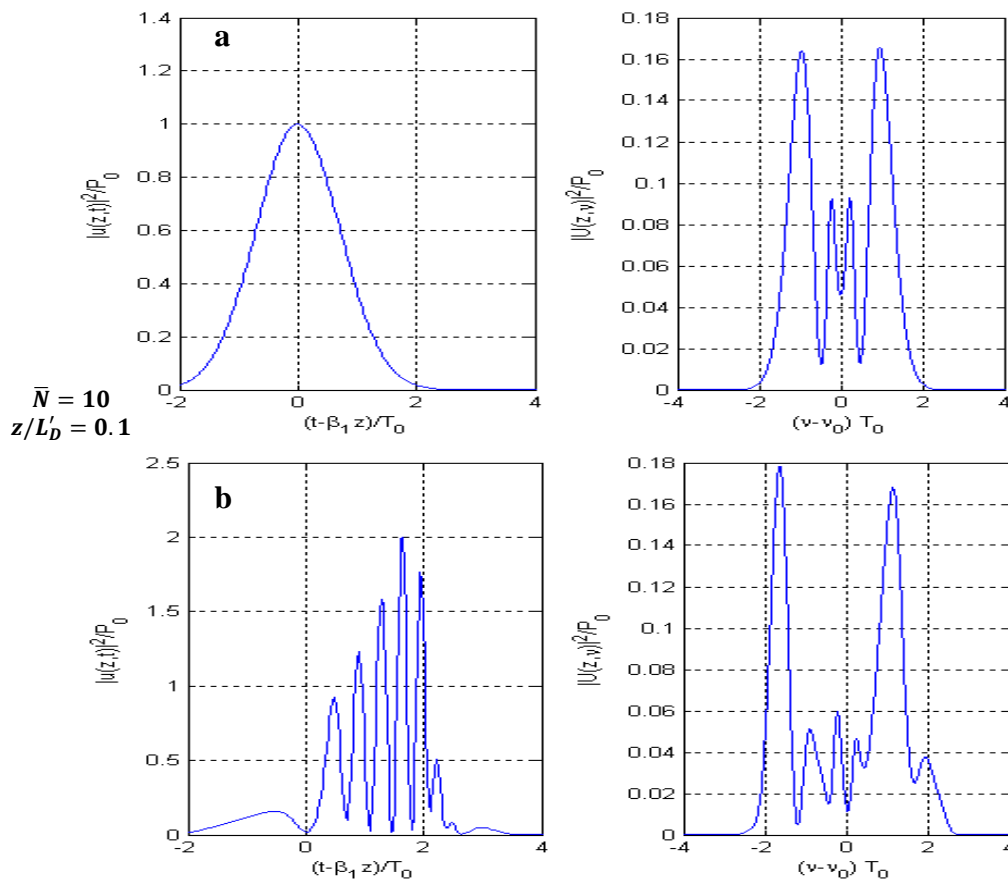


Figure 5.10: Pulse shape and spectrum under conditions identical to those of Fig. 5.9 except that $\bar{N} = 10$ and $z/L'_D = 0.1$. a) Titanium sapphire, and b) silica fiber (after[16]),

In dispersion-managed fiber links, β_2 is large locally but nearly vanishes on average. The effects of TOD play an important role in such links, especially for short optical pulses. The spectral and temporal evolution depends on whether the Dispersion-Compensating Fiber (DCF) is placed before or after the standard fiber (pre- or post-compensation). In the case of post-compensation, the pulse develops an oscillating tail because of TOD and exhibits spectral narrowing.

5.3 Higher-Order Nonlinear Effects

The discussion of SPM so far is based on the simplified propagation Eq.3.46. For ultrashort optical pulses ($T_0 < 1$ ps), it is necessary to include the higher-order nonlinear effects through Eq.3.46. If Eq.4.3 is used to define the normalized amplitude U , this equation takes the form

$$\frac{\partial U}{\partial z} + i \frac{\text{sgn}(\beta_2)}{2L_D} \frac{\partial^2 U}{\partial \tau^2} = \frac{\text{sgn}(\beta_3)}{6L'_D} \frac{\partial^3 U}{\partial \tau^3} + i \frac{e^{-\alpha z}}{L_{NL}} \left(|U|^2 U + is \frac{\partial}{\partial \tau} (|U|^2 U) - \tau_R U \frac{\partial |U|^2}{\partial \tau} \right), \quad (5.18)$$

Where L_D , L'_D , and L_{NL} are the three length scales defined as

$$L_D = \frac{T_0^2}{|\beta_2|}, \quad L'_D = \frac{T_0^3}{|\beta_3|}, \quad L_{NL} = \frac{1}{\gamma P_0}. \quad (5.19)$$

The parameters s and τ_R govern the effects of self-steepening and intrapulse Raman scattering, respectively, and are defined as

$$s = \frac{1}{w_0 T_0}, \quad \tau_R = \frac{T_R}{T_0}. \quad (5.23)$$

Both of these effects are quite small for picosecond pulses but must be considered for ultrashort pulses with $T_0 < 1$ ps.

5.3.1 Self-Steepening

Self-steepening results from the intensity dependence of the group velocity [17-18]. Its effects on SPM were first considered in liquid nonlinear media [2] and later extended to optical fibers [19-20]. Self-steepening leads to an asymmetry in the SPM-broadened spectra of ultrashort pulses [21].

Before solving Eq.5.18 numerically, it is instructive to consider the dispersionless case by setting $\beta_2 = \beta_3 = 0$. Eq.5.18 can be solved analytically in this specific case if we also set $\tau_R = 0$. Defining a normalized distance as $Z = z/L_{NL}$ and neglecting fiber losses ($\alpha = 0$), Eq.5.18 becomes

$$\frac{\partial U}{\partial Z} + s \frac{\partial}{\partial \tau} (|U|^2 U) = i|U|^2 U. \quad (5.21)$$

Using $U = \sqrt{I} \exp(i\phi)$ in Eq. 5.21 and separating the real and imaginary parts, we obtain the following two equations:

$$\frac{\partial I}{\partial Z} + 3sI \frac{\partial I}{\partial \tau} = 0, \quad (5.22)$$

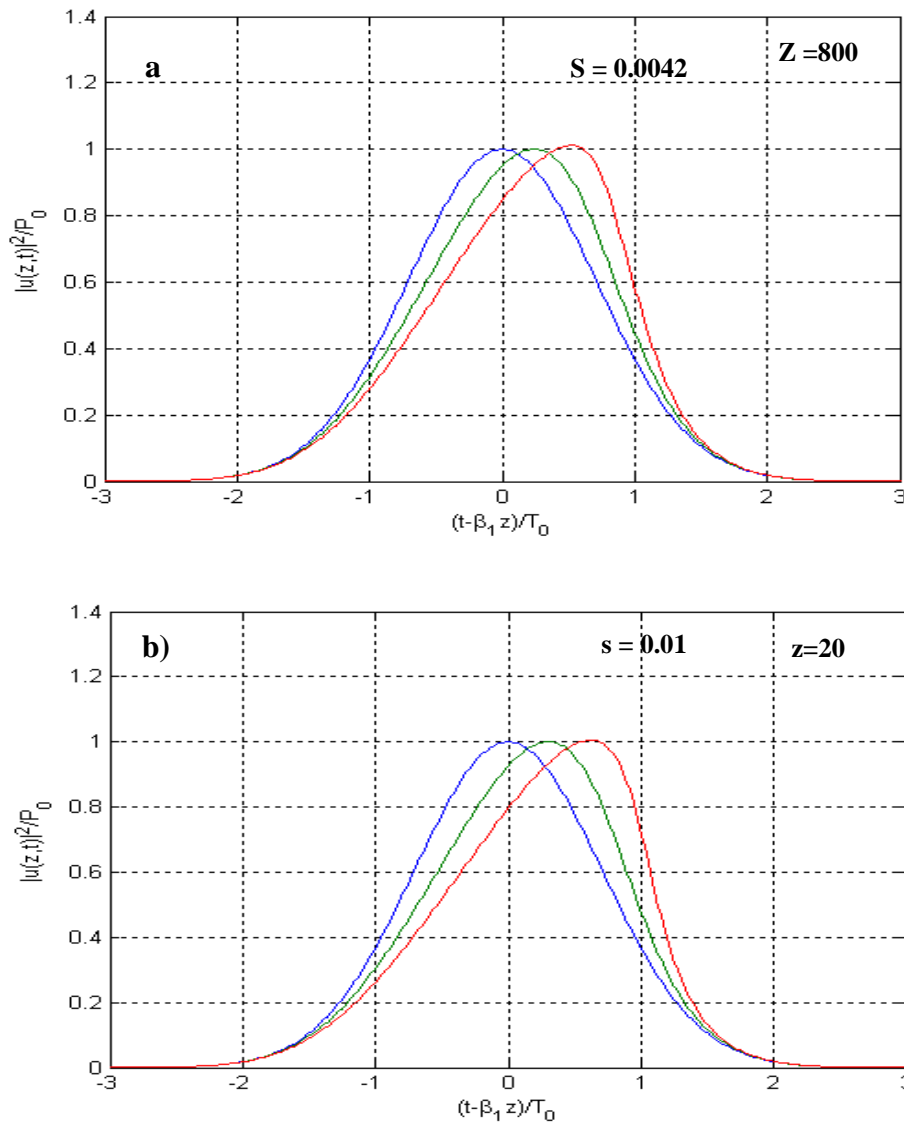
$$\frac{\partial \phi}{\partial Z} + sI \frac{\partial \phi}{\partial \tau} = I. \quad (5.23)$$

Since the intensity Eq.5.22 is decoupled from the phase Eq.5.23, it can be solved easily using the method of characteristics. Its general solution is given by [18]

$$I(Z, \tau) = f(\tau - 3sIZ), \quad (5.24)$$

where we used the initial condition $I(0, \tau) = f(\tau)$, where $f(\tau)$ describes the pulse shape at $z = 0$. Eq.5.24 shows that each point τ moves along a straight line from its initial value, and the slope of the line is intensity dependent. This feature leads to pulse distortion. As an example, consider the case of a Gaussian pulse for which

$$I(0, \tau) \equiv f(\tau) = \exp(-\tau^2). \quad (5.25)$$



From Eq.5.24, the pulse shape at a distance Z is obtained by using

$$I(Z, \tau) = \exp[-(\tau - 3sIZ)^2]. \tag{5.26}$$

The implicit relation for $I(Z, \tau)$ should be solved for each τ to obtain the pulse shape at a given value of Z . Figure 5.11 shows the calculated pulse shapes at $sZ = 25$, for $s = 0.0042$. As the pulse propagates inside the Titanium sapphire, it becomes asymmetric, with its peak shifting toward the trailing edge. As a result, the trailing edge becomes steeper and steeper with increasing Z .

Physically, the group velocity of the pulse is intensity dependent such that the peak moves at a lower speed than the wings.

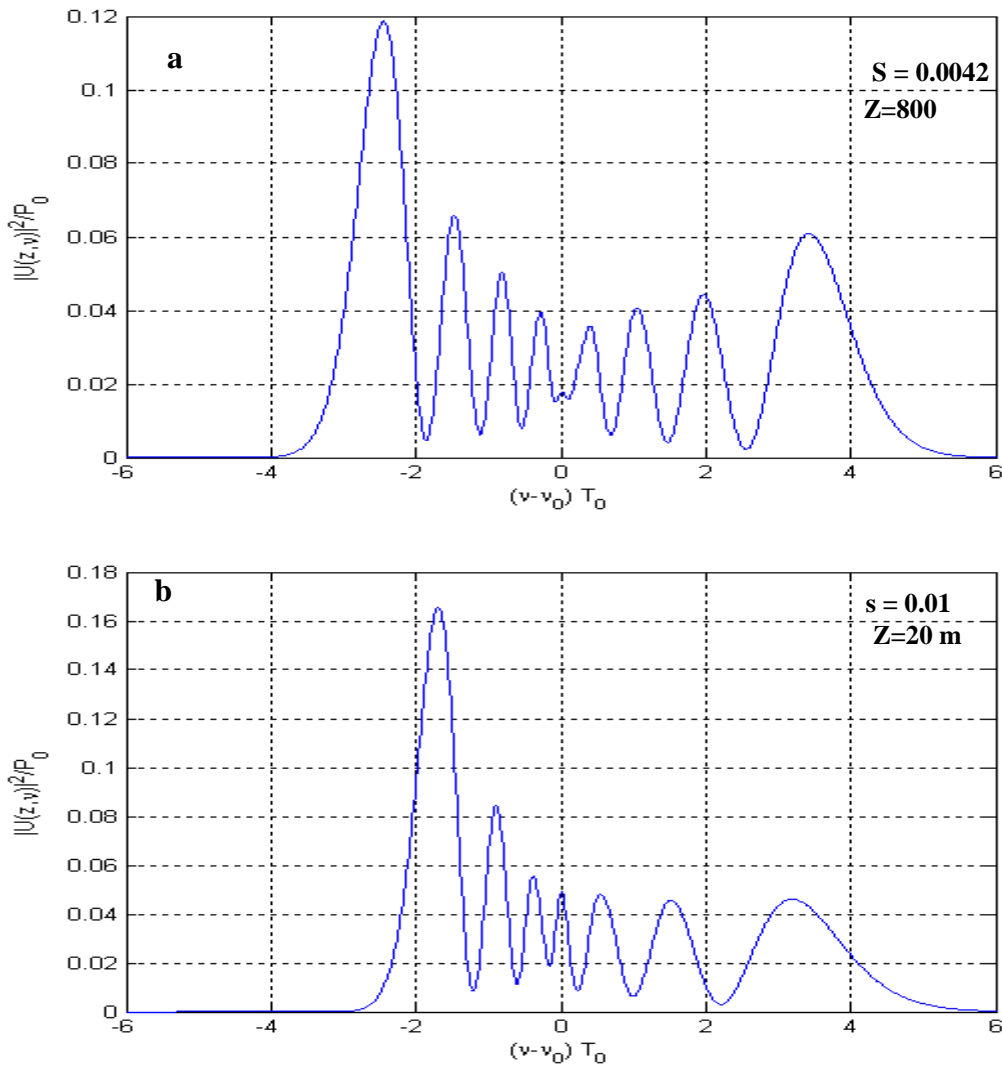


Figure 5.12: a) Spectrum of a Gaussian pulse at a distance $z = 0.2L_{NL}/s$ where $s = 0.01$ and L_{NL} is the nonlinear length. Self-steepening is responsible for the asymmetry in the SPM-broadened spectrum. The effects of GVD are neglected for a) Titanium sapphire, and b) silica fiber (after [16]).

As a result, significant self-steepening of the pulse can occur in a few-centimeter long fiber. Optical shocks with an infinitely sharp trailing edge never occur in practice because of the GVD.

As the pulse edge becomes steeper, the dispersive terms in Eq.5.18 become increasingly more important and cannot be ignored.

Self-steepening also affects SPM-induced spectral broadening. In the dispersionless case, $\phi(z, \tau)$ is obtained by solving Eq.5.23. It can then be used to calculate the spectrum using

$$S(\omega) = \left| \int_{-\infty}^{\infty} [I(z, \tau)]^{1/2} \exp[i\phi(z, \tau) + i(\omega - \omega_0)\tau] d\tau \right|^2. \quad (5.27)$$

Figure 5.12 shows the calculated spectrum at $sz/L_{NL} = 0.105$ for $s = 0.0042$. The most notable feature is the spectral asymmetry—the red-shifted peaks are more intense than the blue-shifted ones. The spectrum is asymmetric simply because the pulse shape is asymmetric. A steeper trailing edge of the pulse implies larger spectral broadening on the blue side as SPM generates blue components near the trailing edge (see Fig. 5.1).

In the absence of self-steepening ($s = 0$), a symmetric six-peak spectrum is expected because $\phi_{max} \approx 6.4\pi$ for the parameter values used in Fig.5.12 for silica fiber, and two peak spectrum for titanium sapphire. Self-steepening stretches the blue portion. The amplitude of the high-frequency peaks decreases because the same energy is distributed over a wider spectral range.

5.3.2 Effect of GVD on Optical Shocks

The spectral features seen in Fig. 5.12 are considerably affected by GVD, which cannot be ignored when short optical pulses propagate inside titanium sapphire. The pulse evolution in this case is studied by solving Eq.5.18 numerically. Figure 5.13 shows the pulse shapes and the spectra at $z/L_D = 0.2$ and 0.4 in the case of an initially unchirped Gaussian pulse propagating with normal dispersion ($\beta_2 > 0$) and $\beta_3 = 0$.

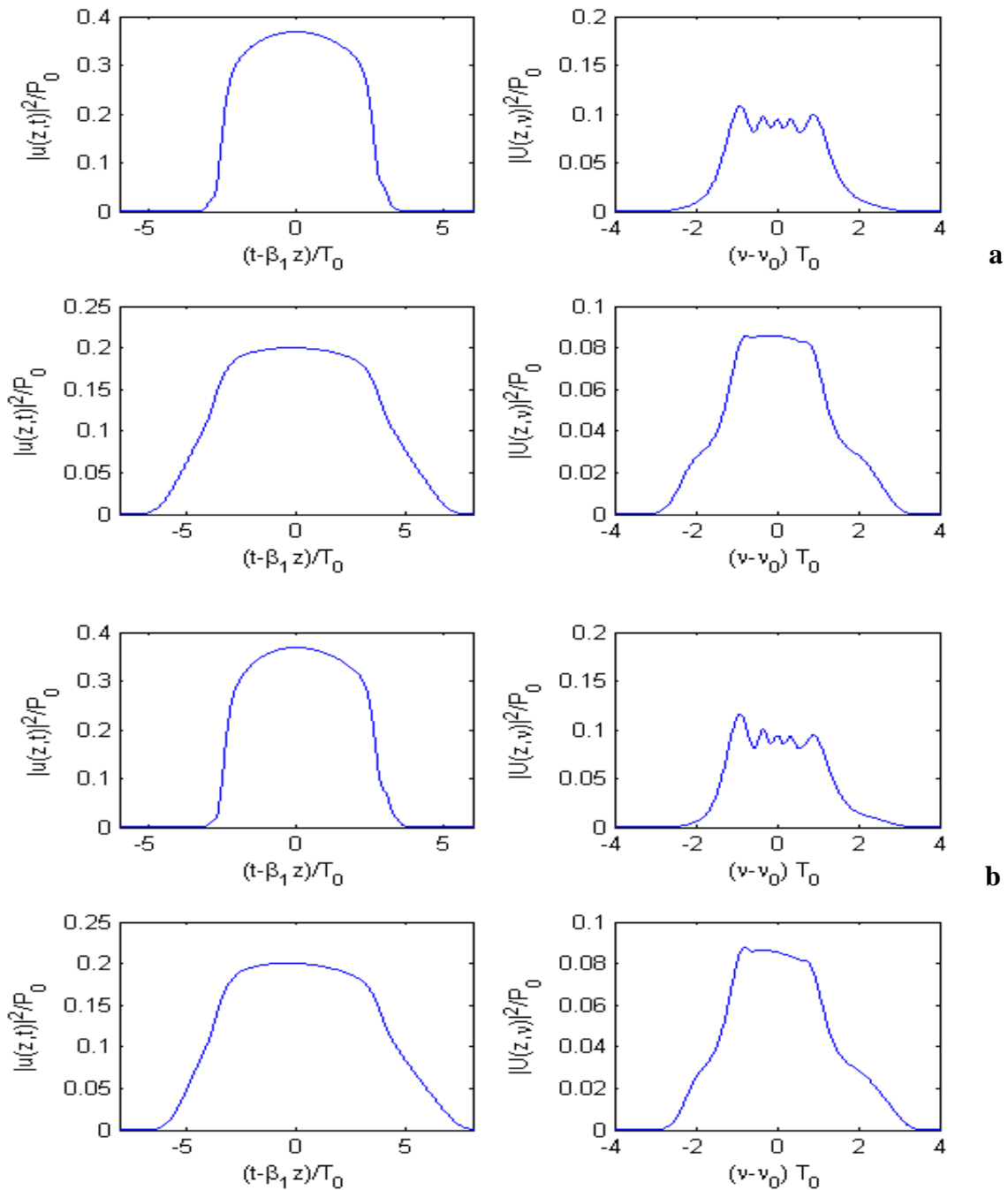


Figure 5.13: Pulse shapes and spectra at $z/L_D = 0.2$ (upper row $\beta_2 = 0$) and (lower row $\beta_2 = 1.01$) for a Gaussian pulse propagating in the normal-dispersion regime of the fiber. The other parameters are $\alpha = 0, \beta_3 = 0, s = 0.0042, \beta_2 = 0$ a) for Titanium sapphire, and, b) for silica fiber (after [16]).

The parameter N defined in Eq.5.13 is taken to be 10, resulting in $L_D = 100L_{NL}$. In the absence of GVD ($\beta_2 = 0$), the pulse shape and the spectrum

shown in the upper row of Fig. 5.13 reduce to those shown in Figs. 5.11 and 5.12 in the case of $sz/L_{NL} = 0.105$. A direct comparison shows that both the shape and spectrum are significantly affected by GVD even though the propagation distance is only a fraction of the dispersion length ($z/L_D = 0.2$).

The lower row of Fig. 5.13 shows the pulse shape and spectrum at $\beta_2 = 1.01$, where the qualitative changes induced by GVD are self-evident. It is the GVD that dissipates the shock by broadening the steepened trailing edge, a feature clearly seen in the asymmetric pulse shapes of Fig. 5.13. Although the pulse spectra do not exhibit deep oscillations (seen in Fig. 5.12 for the dispersionless case), the longer tail on the blue side is a manifestation of self-steepening. With a further increase in the propagation distance z , the pulse continues to broaden while the spectrum remains nearly unchanged.

5.3.3 Intrapulse Raman Scattering

The discussion so far has neglected the last term in Eq. 5.18 that is responsible for intrapulse Raman scattering. In the case of optical fibers, this term becomes quite important for ultrashort optical pulses ($T_0 < 1$ ps) and should be included in modeling pulse evolution of such short pulses in optical fibers [21]. The effects of intrapulse Raman scattering are most dramatic in the context of solitons, where they lead to new phenomena such as decay and self-frequency shift of solitons (see Chapter VI).

5.4 Chapter summary

The SPM and other nonlinear effects such as stimulated Raman scattering and four-wave mixing, occurring simultaneously inside optical fibers, can broaden the spectrum of an ultrashort pulse so much that it may extend over 100 nm or more. Such extreme spectral broadening is called supercontinuum, a phenomenon that attracted considerable attention during the 1990's because of its potential applications.

References

- [1] F. Shimizu, *Phys. Rev. Lett.* 19, 1097 (1967).
- [2] T. K. Gustafson, J. P. Taran, H. A. Haus, J. R. Lifshitz, and P. L. Kelley, *Phys. Rev.* 177, 306 (1969).
- [3] R. Cubeddu, R. Polloni, C. A. Sacchi, and O. Svelto, *Phys. Rev. A* 2, 1955 (1970).
- [4] R. R. Alfano and S. L. Shapiro, *Phys. Rev. Lett.* 24, 592 (1970); *Phys. Rev. Lett.* 24, 1217 (1970).
- [6] C. H. Lin and T. K. Gustafson, *IEEE J. Quantum Electron.* 8, 429 (1972).
- [5] E. P. Ippen, C. V. Shank, and T. K. Gustafson, *Appl. Phys. Lett.* 24, 190 (1974).
- [6] R. A. Fisher and W. K. Bischel, *J. Appl. Phys.* 46, 4921 (1975).
- [7] H. Nakatsuka, D. Grischkowsky, and A. C. Balant, *Phys. Rev. Lett.* 47, 910 (1981).
- [8] D. Grischkowsky and A. C. Balant, *Appl. Phys. Lett.* 41, 1 (1982).
- [9] J. Botineau and R. H. Stolen, *J. Opt. Soc. Am.* 72, 1592 (1982).
- [10] Y. Kodama and S. Wabnitz, *Opt. Lett.* 20, 2291 (1995).
- [11] Y. Kodama and S. Wabnitz, *Electron. Lett.* 31, 1761 (1995).
- [12] W. J. Tomlinson, R. H. Stolen, and A. M. Johnson, *Opt. Lett.* 10, 457 (1985).
- [13] A. M. Johnson and W. M. Simpson, *J. Opt. Soc. Am. B* 2, 619 (1985).
- [14] K. J. Blow, N. J. Doran, and E. Cummins, *Opt. Commun.* 48, 181 (1983).
- [15] V. A. Vysloukh, *Sov. J. Quantum Electron.* 13, 1113 (1983).
- [16] G. P. Agrawal and M. J. Potasek, *Phys. Rev. A* 33, 1765 (1986).
- [17] L. A. Ostrovskii, *Sov. Phys. JETP* 24, 797 (1967).
- [18] N. Tzoar and M. Jain, *Phys. Rev. A* 23, 1266 (1981).
- [19] R. L. Fork, C. V. Shank, C. Herlimann, R. Yen, and W. J. Tomlinson, *Opt. Lett.* 8, 1 (1983).
- [20] G. Yang and Y. R. Shen, *Opt. Lett.* 9, 510 (1984).
- [21] W. Hodel and H. P. Weber, *Opt. Lett.* 12, 924 (1987).

CHAP VI

GENERALIZED NONLINEAR SCHRODINGER EQUATION IN TITANIUM SAPPHIRE

$$i \frac{\partial u}{\partial \xi} + \frac{1}{2} \frac{\partial^2 u}{\partial \tau^2} + |u|^2 u$$
$$= i\delta_3 \frac{\partial^3 u}{\partial \tau^3} - is \frac{\partial}{\partial \tau} (|u|^2 u) + \tau_R u \frac{\partial |u|^2}{\partial \tau},$$

A fascinating manifestation of the fiber nonlinearity occurs through optical solitons, formed as a result of the interplay between the dispersive and nonlinear effects. The word soliton refers to special kinds of wave packets that can propagate undistorted over long distances. Solitons have been discovered in many branches of physics. In the context of optical fibers, not only are solitons of fundamental interest but they have also found practical applications in the field of fiber-optic communications. This chapter is devoted to the study of pulse propagation in optical fibers in the regime in which both the group velocity dispersion (GVD) and self-phase modulation (SPM) are equally important and must be considered simultaneously.

The chapter is organized as follows. Section 6.1 considers the phenomenon of modulation instability. Section 6.2 discusses the fibers solitons phenomenon. Higher-order nonlinear effects such as self-steepening and intrapulse Raman scattering are the focus of Section 6.3. Finally section 6.4 discusses the ultrashort pulses propagation.

6.1 Modulation Instability

Many nonlinear systems exhibit an instability that leads to modulation of the steady state as a result of an interplay between the nonlinear and dispersive effects [1-7]. This phenomenon is referred to as the *modulation instability* and was studied during the 1960s in such diverse fields as fluid dynamics [2-4], nonlinear optics [5-7] and plasma physics [8]. In the context of optical fibers, modulation instability requires anomalous dispersion and manifests itself as a breakup of the CW or quasi-CW radiation into a train of ultrashort pulses. This section discusses modulation instability in optical fibers as an introduction to soliton theory.

6.1.1 Linear Stability Analysis

Consider the propagation of CW light inside an optical fiber. The starting point is the simplified propagation Eq.3.46.

If fiber losses are ignored, this equation takes the form

$$i \frac{\partial A}{\partial z} = \frac{\beta_2}{2} \frac{\partial^2 A}{\partial T^2} - \gamma |A|^2 A, \quad (6.1)$$

and is referred to as the nonlinear Schrödinger (NLS) equation in the soliton literature. As discussed in Section 3.3, $A(z, T)$ represents the amplitude of the pulse envelope, β_2 is the GVD parameter, and the nonlinear parameter γ is responsible for SPM. In the case of CW radiation, the amplitude A is independent of T at the input end of the fiber, $z = 0$. Assuming that $A(z, T)$ remains time-independent during propagation inside the fiber, Equation 6.1 is readily solved to obtain the steady-state solution

$$\bar{A} = \sqrt{P_0} \exp(i\Phi_{NL}), \quad (6.2)$$

where P_0 is the incident power and $\Phi_{NL} = \gamma P_0 z$ is the nonlinear phase shift induced by SPM. Eq.6.2 implies that *CW* light should propagate through the fiber unchanged except for acquiring a power-dependent phase shift (and for reduction in power in the presence of fiber losses).

The effect of higher-order dispersive and nonlinear effects such as self-steepening and intrapulse Raman scattering can also be included using Eq.3.46 in place of Eq.6.1 as the starting point. The third-order dispersion β_3 does not affect the gain spectrum of modulation instability. When optical pulses with widths smaller than 100 ps are used, modulation instability can be initiated by SPM.

6.2 Fiber Solitons

The occurrence of modulation instability in the anomalous-GVD regime of optical fibers is an indication of a fundamentally different character of Eq.6.1 when $\beta_2 < 0$. It turns out that this equation has specific pulse-like solutions that either do not change along the fiber length or follow a periodic evolution pattern. Such solutions are known as optical solitons. The history of solitons, in fact, dates back to 1834, the year in which *Scott Russell* observed a heap of water in a canal that propagated undistorted over several kilometers. Here is a quote from his report published in 1844 [9-11]:

Such waves were later called solitary waves. However, their properties were not understood completely until the inverse scattering method was developed. The term *soliton* was coined in 1965 to reflect the particle-like nature of those solitary waves that remained intact even after mutual collisions. Since then, solitons have been discovered and studied in many branches of physics including optics. In the context of optical fibers, the use of solitons for optical communications was first suggested in 1973.

6.2.1 Fundamental Soliton

The first-order soliton ($N = 1$) corresponds to the case of a single eigenvalue. It is referred to as the fundamental soliton because its shape does not change on propagation. We obtain the following general form of the fundamental soliton:

$$u(\xi, \tau) = \operatorname{sech}(\tau) \exp(i\xi/2) \quad (6.3)$$

The solution in Eq.6.3 can also be obtained by solving the NLS equation directly. It is this feature of the fundamental solitons that makes them attractive for optical communication systems. The peak power P_0 required to support the fundamental soliton is obtained by setting $N = 1$ and is given by

$$P_0 = \frac{|\beta_2|}{\gamma T_0^2} \approx \frac{3.11|\beta_2|}{\gamma T_{FWHM}^2} \quad (6.4)$$

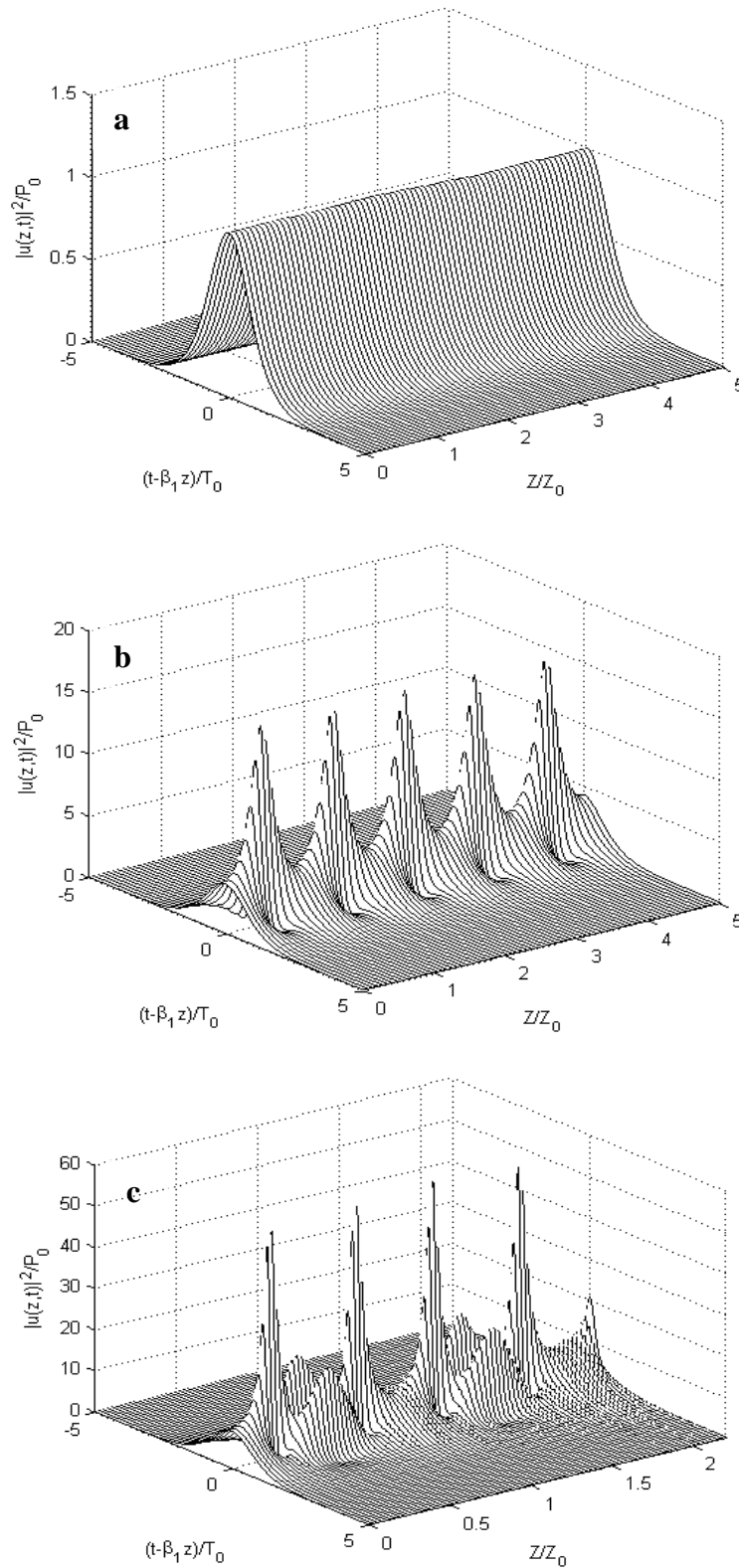


Figure 6.1 Temporal evolution over one soliton period for: a) $N=1$, b) $N=2$, and c) $N=3$ (after [27])

where the FWHM of the soliton is defined using $T_{FWHM} \approx 1.76T_0$ from Eq.4.27.

6.2.2 Higher-order Soliton

6.2.2.1 Second-order Soliton

A Second-order soliton is described in [25]:

$$u(\xi, \tau) = \frac{4[\cosh(3\tau) + 3\exp(4i\xi)\cosh(\tau)]\exp(i\xi/2)}{[\cosh(4\tau) + 4\cosh(2\tau) + 3\cos(4\xi)]} \tag{6.5}$$

where the soliton order N is an integer.

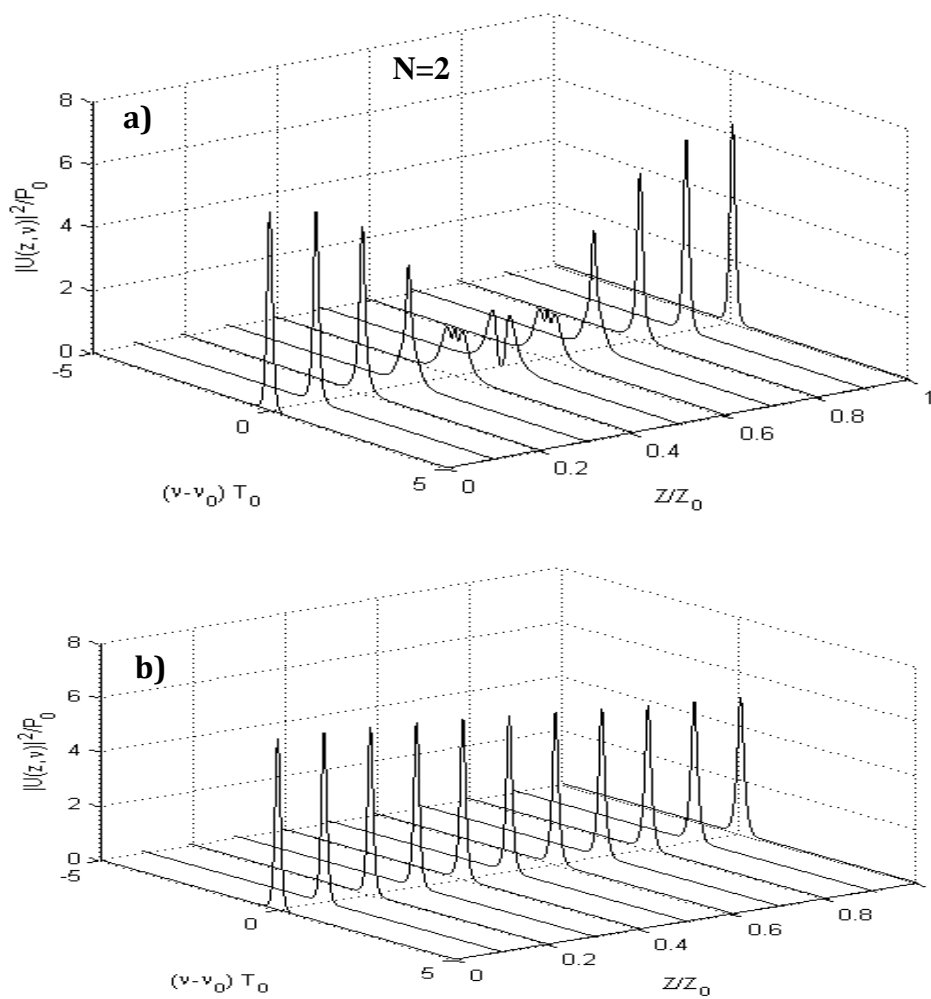


Figure 6.2: Spectral evolution over one soliton period for the third-order soliton. b) For Titanium sapphire, and a) For silica fiber (after [27])

An interesting property of the aforementioned solution is that $|u(\xi, \tau)|^2$ is periodic in ξ with the period $\xi_0 = \frac{\pi}{2}$ rad. In fact, this periodicity occurs for all higher-order solitons. Using the definition $\xi = z/L_D$ from Eq.5.12, the soliton period z_0 in real units becomes

$$z_0 = \frac{\pi}{2} L_D = \frac{\pi T_0^2}{2 |\beta_2|} \approx \frac{T_{FWHM}^2}{2 |\beta_2|} \tag{6.6}$$

6.2.2.2 Third-Order Soliton

Periodic evolution of a third-order soliton over one soliton period is shown in Fig.6.3. As the pulse propagates along the fiber, it first contracts to a fraction of its initial width, splits into two distinct pulses at $z_0/2$, and then merges again to recover the original shape at the end of the soliton period at $z = z_0$. This pattern is repeated over each section of length z_0 .

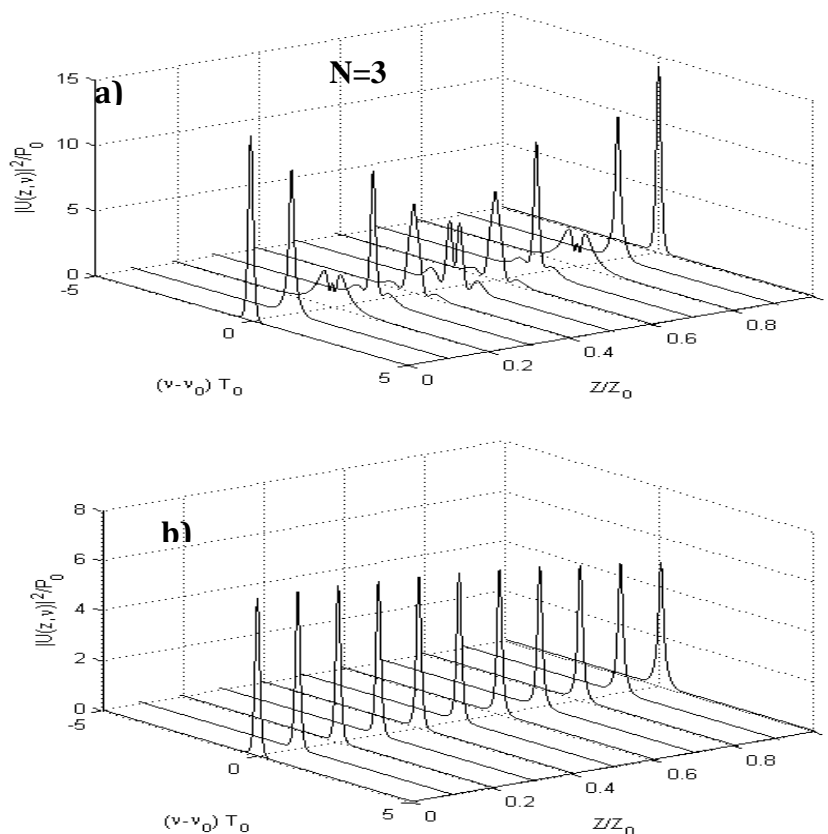


Figure 6.3: Spectral evolution over one soliton period for the third-order soliton. a) for silica fiber [27], and b) for Titanium sapphire.

To understand the origin of periodic evolution for higher-order solitons, it is helpful to look at changes in the pulse spectra shown in Figure 6.3 for the $N = 3$ soliton. The temporal and spectral changes result from an interplay between SPM and GVD. The SPM generates a frequency chirp such that the leading edge of soliton is red-shifted while its trailing-edge is blue-shifted from the central frequency. The SPM-induced spectral broadening is clearly seen in Fig. 6.3 for $z/z_0 = 0.2$ with its typical oscillatory structure. In the absence of GVD, the pulse shape would have remained unchanged. Only the central portion of the pulse contracts because the chirp is nearly linear only over that part. However, as a result of a substantial increase in the pulse intensity near the central part of the pulse, the spectrum changes significantly as seen in Figure 6.3 for $z/z_0 = 0.3$. It is this mutual interaction between the GVD and SPM effects that is responsible for the evolution pattern seen in Fig.6.1.

In the case of a fundamental soliton ($N = 1$), GVD and SPM balance each other in such a way that neither the pulse shape nor the pulse spectrum changes along the fiber length. In the case of higher-order solitons, SPM dominates initially but GVD soon catches up and leads to pulse contraction, seen in Fig.6.1.

6.3 Higher-Order Effects

The properties of optical solitons considered so far are based on the NLS Eq.6.1. As discussed in Section 3.3, when input pulses are so short that $T_0 < 5 ps$, it is necessary to include higher-order nonlinear and dispersive effects through Eq.3.46. In terms of soliton units introduced in Section 6.2, Eq.3.46 takes the form:

$$i \frac{\partial u}{\partial \xi} + \frac{1}{2} \frac{\partial^2 u}{\partial \tau^2} + |u|^2 u = i \delta_3 \frac{\partial^3 u}{\partial \tau^3} - i s \frac{\partial}{\partial \tau} (|u|^2 u) + \tau_R u \frac{\partial |u|^2}{\partial \tau}, \quad (6.7)$$

where the pulse is assumed to propagate in the region of normal GVD ($\beta_2 > 0$) and fiber losses are neglected ($\alpha = 0$). The parameters δ_3 , s , and τ_R govern,

respectively, the effects of third-order dispersion (TOD), self-steepening, and intrapulse Raman scattering. Their explicit expressions are

$$\delta_3 = \frac{\beta_3}{6|\beta_2|T_0} \quad s = \frac{1}{w_0 T_0} \quad \tau_R = \frac{T_R}{T_0}. \quad (6.8)$$

All three parameters vary inversely with the pulse width and are negligible for $T_0 \gg 1$ ps. They become appreciable for femtosecond pulses.

As an example: $\delta_3 \approx 0.0024$, $s \approx 0.0042$, and $\tau_R \approx 0.001$ for a 50 fs pulse ($T_0 \approx 30$ fs) propagating at 0.8 μm in Titane- sapphire, if we take $T_R = 3$ fs.

6.3.1 Third-Order Dispersion

When optical pulses propagate relatively far from the zero-dispersion wavelength of an optical fiber, the TOD effects on solitons are small and can be treated perturbatively. To study such effects as simply as possible, let us set $s = 0$ and $\tau_R = 0$ in Eq.6.7 and treat the δ_3 term as a small perturbation [13].

Physically speaking, the TOD slows down the soliton and, as a result, the soliton peak is delayed by an amount that increases linearly with distance. This TOD-induced delay is negligible in most fibers for picosecond pulses for distances as large as $\xi = 100$ as long as β_2 is not nearly zero.

Eq.6.7 cannot be used in this case because the normalization scheme used for it becomes inappropriate. Normalizing the propagation distance to $L'_D = T_0^3/|\beta_3|$ through $\xi' = z/L'_D$, we obtain the following equation:

$$i \frac{\partial u}{\partial \xi'} - \text{sgn}(\beta_3) \frac{i}{6} \frac{\partial^3 u}{\partial \tau^3} + |u|^2 u = 0, \quad (6.9)$$

Where $u = \tilde{N}U$, where \tilde{N} is defined by

$$\tilde{N}^2 = \frac{L'_D}{L_{NL}} = \frac{\gamma P_0 T_0^3}{|\beta_3|} \quad (6.10)$$

Figure.6.4 shows the pulse shape and the spectrum at $\xi' = 3$ for $\tilde{N} = 2$ and compares them with those of the input pulse at $\xi' = 0$. The most striking feature is the spectrum splitting into two well-resolved spectral peaks [14]. These peaks correspond to the outermost peaks of the SPM-broadened spectrum (see Fig.5.2). As the red-shifted peak lies in the anomalous-GVD regime, pulse energy in that spectral band can form a soliton.

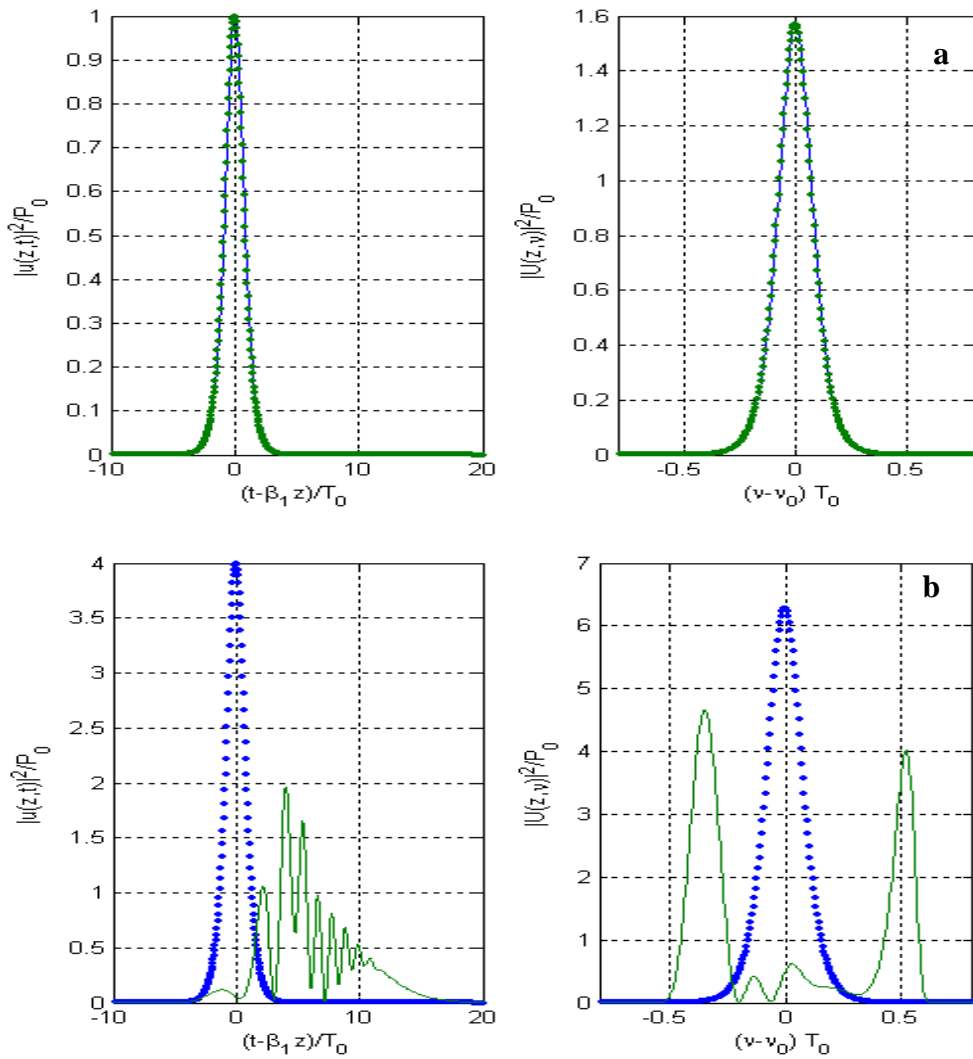


Figure 6.4: Pulse shape and spectrum at $z/L'_D = 3$ of a hyperbolic secant pulse propagating at the zero-dispersion wavelength with a peak power such that $\tilde{N} = 2$. Dotted curves show for comparison the initial profiles at the fiber input for a) Titanium sapphire, and b) silica fiber (after [27]).

The energy in the other spectral band disperses away simply because that part of the pulse experiences normal GVD. It is the trailing part of the pulse that disperses away with propagation because SPM generates blue-shifted components near the trailing edge. The pulse shape in Fig.6.4 shows a long trailing edge with oscillations that continues to separate away from the leading part with increasing ξ' . The important point to note is that, because of SPM-induced spectral broadening, the input pulse does not really propagate at the

zero-dispersion wavelength even if $\beta_2 = 0$ initially. In fact, the pulse creates its own $|\beta_2|$ through SPM.

In general, solitons at the zero-dispersion wavelength require less power than those occurring in the anomalous-GVD regime. This can be seen by comparing Eq.5.13 and Eq.6.10. To achieve the same values of N and \tilde{N} , the required power is smaller by a factor of $T_0|\beta_2/\beta_3|$ for pulses propagating at the zero-dispersion wavelength.

6.3.2 Self-Steepening

The phenomenon of self-steepening has been studied extensively [15,16]. Since it has already been covered in Section 5.3, its impact on solitons is discussed only briefly. To isolate the effects of self-steepening governed by the parameter s , it is useful to set $\delta_3 = 0$ and $\tau_R = 0$ in Eq. 6.7. Pulse evolution inside fibers is then governed by

$$i \frac{\partial u}{\partial \xi} + \frac{1}{2} \frac{\partial^2 u}{\partial \tau^2} + |u|^2 u + is \frac{\partial}{\partial \tau} (|u|^2 u) = 0. \quad (6.11)$$

As discussed in Section 5.3, self-steepening creates an optical shock on the trailing edge of the pulse in the absence of the GVD effects. This phenomenon is due to the intensity dependence of the group velocity that results in the peak of the pulse moving slower than the wings. The GVD dissipates the shock and smoothes the trailing edge considerably. However, self-steepening would still manifest through a shift of the pulse center.

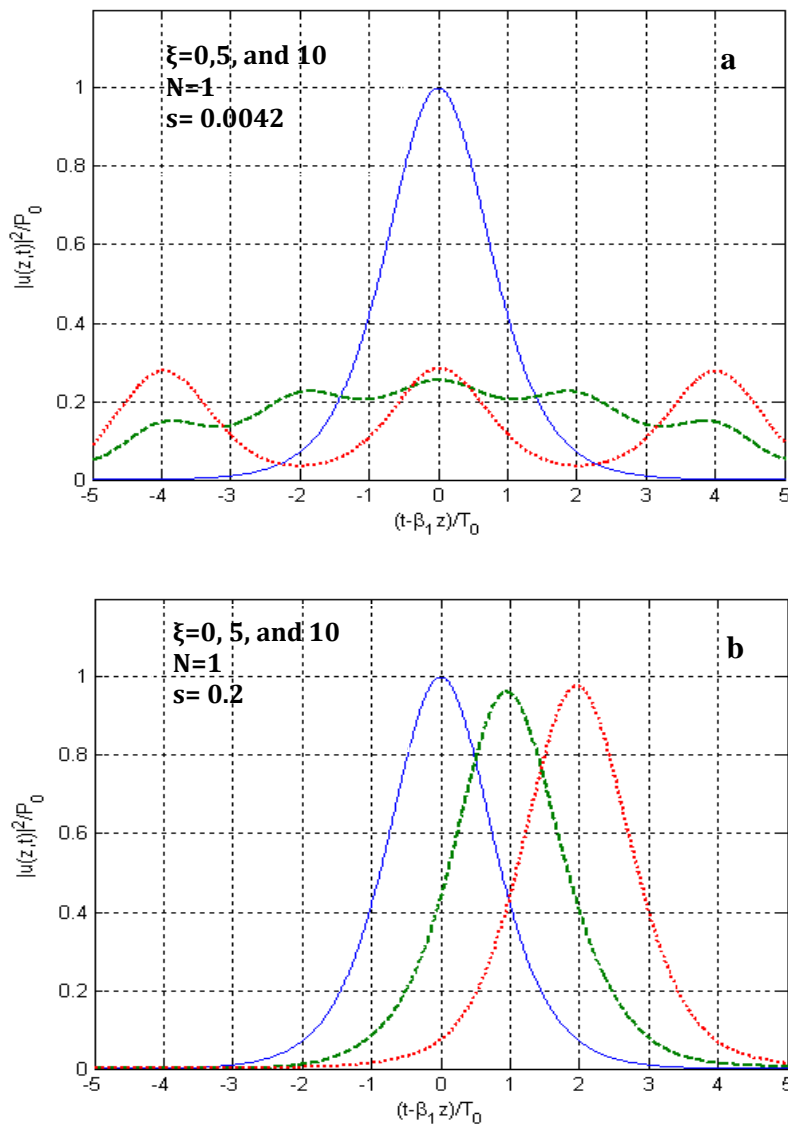


Figure.6.5:Pulse shapes at $\xi = 5$ and 10 for a fundamental soliton in the presence of self-steepening ($s = 0.041$). Dashed curves show the initial shape for comparison. The solid curves coincide with the dashed curve when $s = 0$. a) for Titanium sapphire, and b) for silica fiber (after [27]).

The self-steepening-induced shift is shown in Fig.6.5, where pulse shapes at $\xi = 0, 5$, and 10 are plotted for $s = 0.2$ and $N = 1$ by solving Eq.6.11 for silica fiber numerically with the input $u(0, \tau) = \text{sech}(\tau)$. As the peak moves slower than the wings for $s \neq 0$, it is delayed and appears shifted toward the trailing side in the case of silica fiber. Although the pulse broadens slightly with propagation,

it nonetheless maintains its soliton nature. The group velocity changes as a result of the shift. The delay of the peak seen in Fig. 6.5 is due to this change in the group velocity. In the limit $s = 0$, it reduces to the hyperbolic secant form of Eq. 6.3.

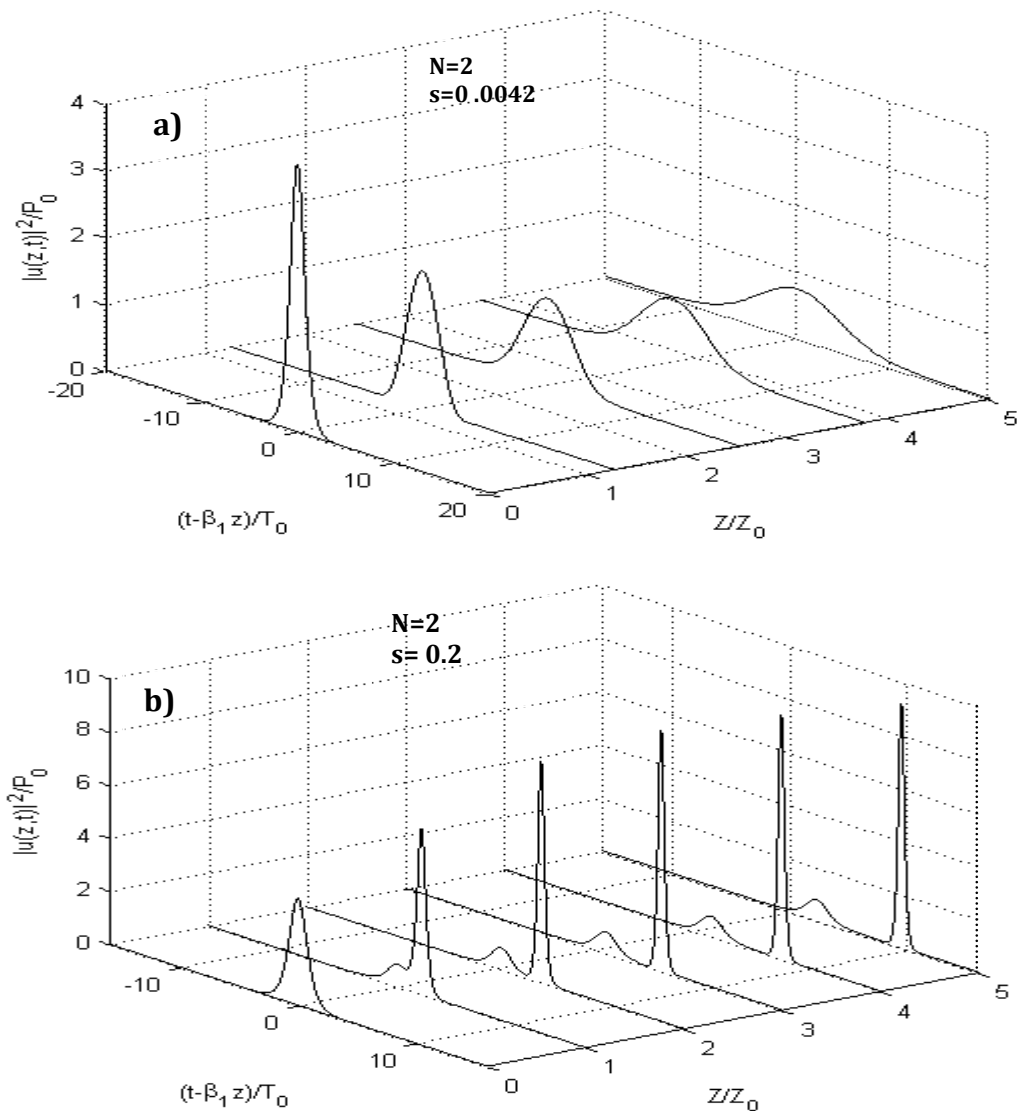


Figure.6.6: Decay of a second-order soliton ($N = 2$) induced by self-steepening ($s = 0.2$). Pulse evolution over five soliton periods is shown. a) for titanium sapphire, and b) for silica fiber (after [27]).

The effect of self-steepening on higher-order solitons is remarkable in that it leads to breakup of such solitons into their constituents, a phenomenon referred to as soliton decay. Figure 6.6 shows this behavior for a second-order soliton ($N = 2$) using $s = 0.2$. For this relatively large value of s , the two solitons have separated from each other within a distance of two soliton periods and continue to move apart with further propagation inside the fiber (see figure 6.6b: silica fiber).

A qualitatively similar behavior occurs for smaller values of s except that a longer distance is required for the breakup of solitons. In the absence of self-steepening ($s = 0$), the two solitons form a bound state because both of them propagate at the same speed (the eigenvalues have the same real part). The effect of self-steepening is to break the degeneracy so that the two solitons propagate at different speeds. As a result, they separate from each other, and the separation increases almost linearly with the distance [16].

In the case of the titanium sapphire the phenomenon of self steepening is governed by the group velocity dispersion and the pulse does not present the wave shock.

6.3.3 Intrapulse Raman Scattering

Intrapulse Raman scattering plays the most important role among the higher-order nonlinear effects. Its effects on solitons are governed by the last term in Eq.6.11 and were observed experimentally in 1985. The need to include this term became apparent when a new phenomenon, called the soliton self-frequency shift, was observed in 1986 [17] and explained using the delayed nature of the Raman response [18]. Since then, this higher-order nonlinear effect has been studied extensively [19]. To isolate the effects of intrapulse Raman scattering, it is useful to set $\delta_3 = 0$ and $s = 0$ in Eq.6.11. Pulse evolution inside fibers is then governed by:

$$i \frac{\partial u}{\partial \xi} + \frac{1}{2} \frac{\partial^2 u}{\partial \tau^2} + |u|^2 u = \tau_R u \frac{\partial |u|^2}{\partial \tau}. \quad (6.13)$$

For pulse widths ~ 1 ps or shorter, the spectral width of the pulse is large enough that the Raman gain can amplify the low frequency (red) spectral components of the pulse, with high-frequency (blue) components of the same pulse acting as a pump. The process continues along the fiber, and the energy from blue components is continuously transferred to red components. Such an energy transfer appears as a red shift of the soliton spectrum, with the shift increasing with distance.

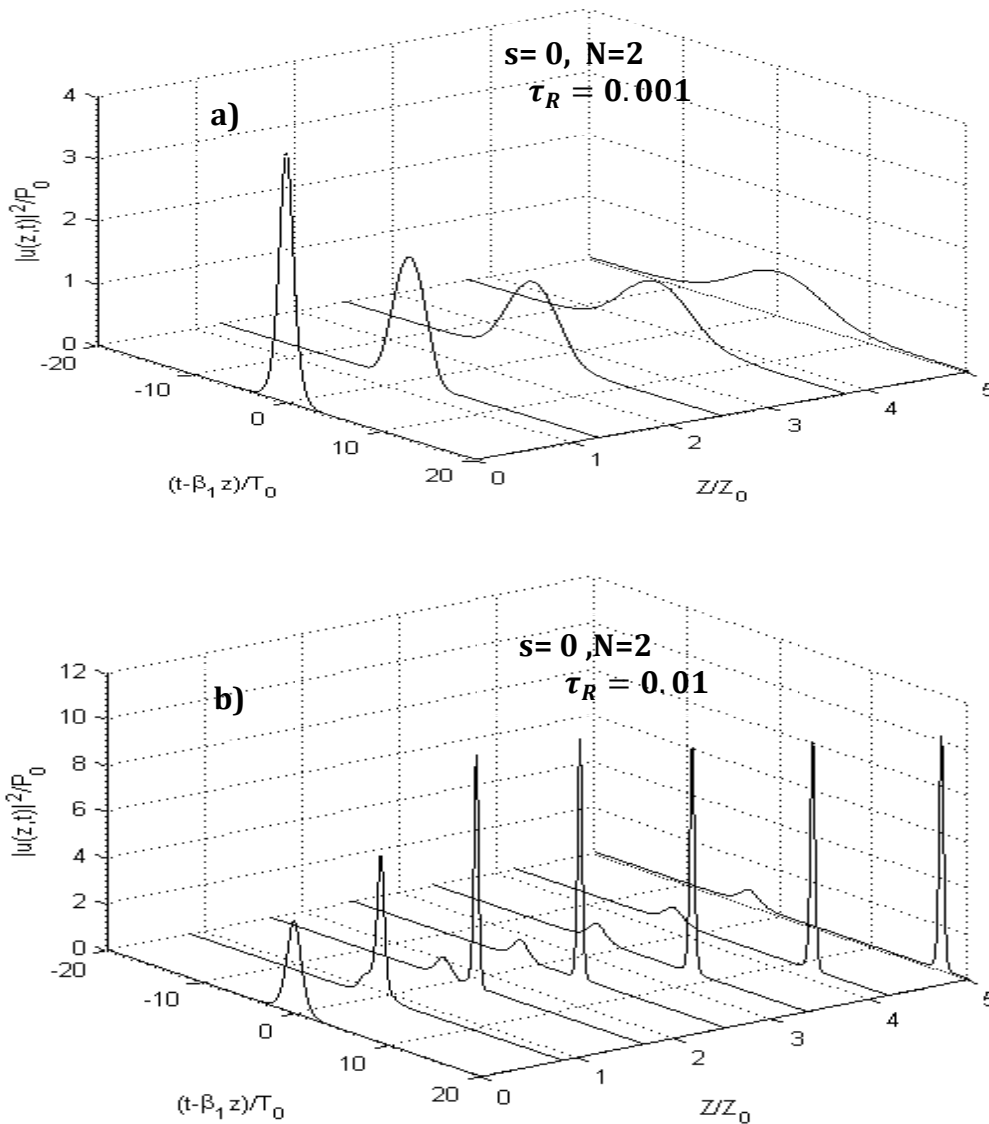


Figure 6.7: Decay of a second-order soliton ($N = 2$) induced by intrapulse Raman scattering ($\tau_R = 0.01$), a) for titanium sapphire, and b) for silica fiber (after [27]).

The effect of intrapulse Raman scattering on higher-order solitons is similar to the case of self-steepening. In particular, even relatively small values of τ_R lead to the decay of higher-order solitons into its constituents [20]. Figure 6.7 shows such a decay for a second-order soliton ($N = 2$) by solving Eq.6.13 numerically with $\tau_R = 0.01$. A comparison of Figures 6.6 and 6.7 shows the similarity and the differences for two different higher-order nonlinear mechanisms. An important difference is that relatively smaller values of τ_R compared with s can induce soliton decay over a given distance. For example, if $s = 0.01$ is chosen in Fig.6.6, the soliton does not split over the distance $z = 5L_D$. This feature indicates that the effects of τ_R are likely to dominate in practice over those of self-steepening (case of silica fiber).

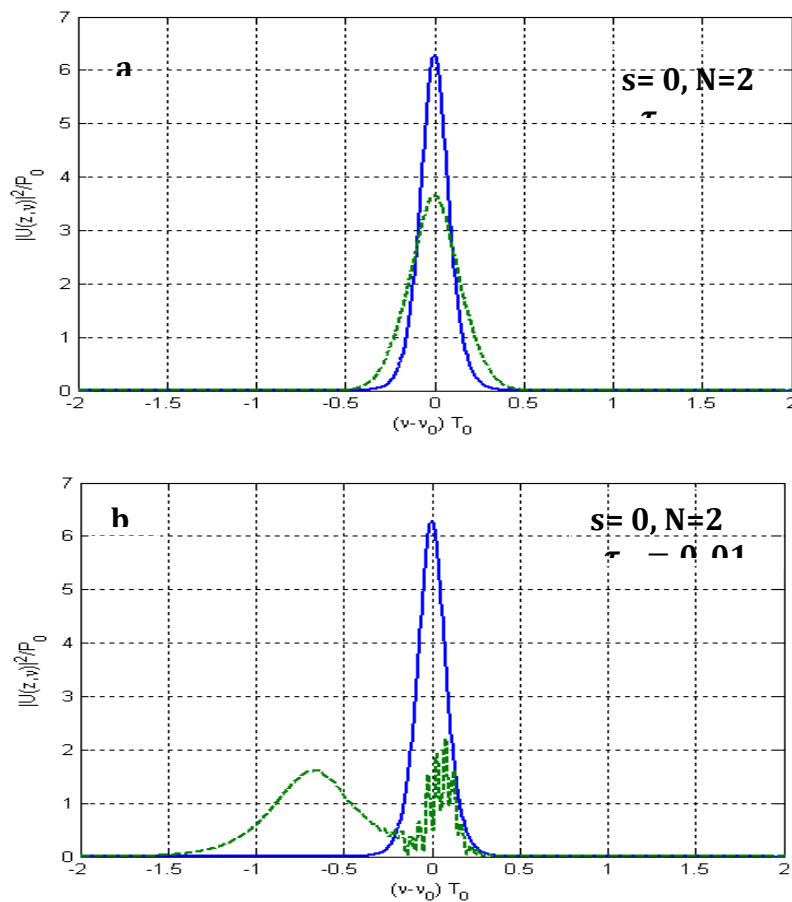


Figure 6.8: Pulse spectrum at $z/z_0 = 5$ for parameter values identical to those of Fig. 6.7. Dashed curves show the spectrum of input pulses. a) for Titanium sapphire, and b) for silica fiber (after [27]).

Another important difference seen in Figs. 6.6 and 6.7 is that both solitons are delayed in the case of self-steepening, while in the Raman case the low-intensity soliton is advanced and appears on the leading side of the incident pulse. This behavior can be understood qualitatively from Fig. 6.8 where the pulse spectrum at $z = 5z_0$ is compared with the input spectrum for the second-order soliton (whose evolution is shown in Fig. 6.7). The most noteworthy feature is the huge red shift of the soliton spectrum, about four times the input spectral width for $\tau_R = 0.01$ and $z/z_0 = 5$. The red-shifted broad spectral peak corresponds to the intense soliton shifting toward the right in Fig. 6.7, whereas the blue-shifted spectral feature corresponds to the other peak moving toward the left in that Figure. Because the blue-shifted components travel faster than the red-shifted ones, they are advanced while the others are delayed with respect to the input pulse. This feature of the Raman term can be understood by noting that the Raman-induced spectral red shift does not preserve pulse energy because a part of the energy is dissipated through the excitation of molecular vibrations.

In the case of the titanium sapphire the phenomenon of intra pulse Raman scattering is governed by the group velocity dispersion and the pulse does not present the wave shock.

6.4 Propagation of Femtosecond Pulses

For femtosecond pulses having widths $T_0 < 1$ ps, it becomes necessary to include all the higher-order terms in Eq. 6.17 because all three parameters δ_3 , s , and τ_R become non-negligible. Evolution of such ultrashort pulses in optical fibers is studied by solving Eq. 6.7 numerically. As an example, Fig. 5.9 shows the pulse shapes and spectra when a second-order soliton is launched at the input end of a fiber after choosing $\delta_3 = 0.0024$, $s = 0.0042$, and $\tau_R = 0.001$. These values are appropriate for a 50 fs pulse ($T_0 = 30$ fs) propagating in the 0.8 μm region of Titane-sapphire.

Soliton decay occurs within a soliton period, and the main peak shifts toward the trailing side at a rapid rate with increasing distance. This temporal shift is due to the decrease in the group velocity occurring as a result of the red shift of the soliton spectrum. A shift in the carrier frequency of the soliton changes its speed because $v_g = (d\beta/d\omega)^{-1}$ is frequency-dependent.

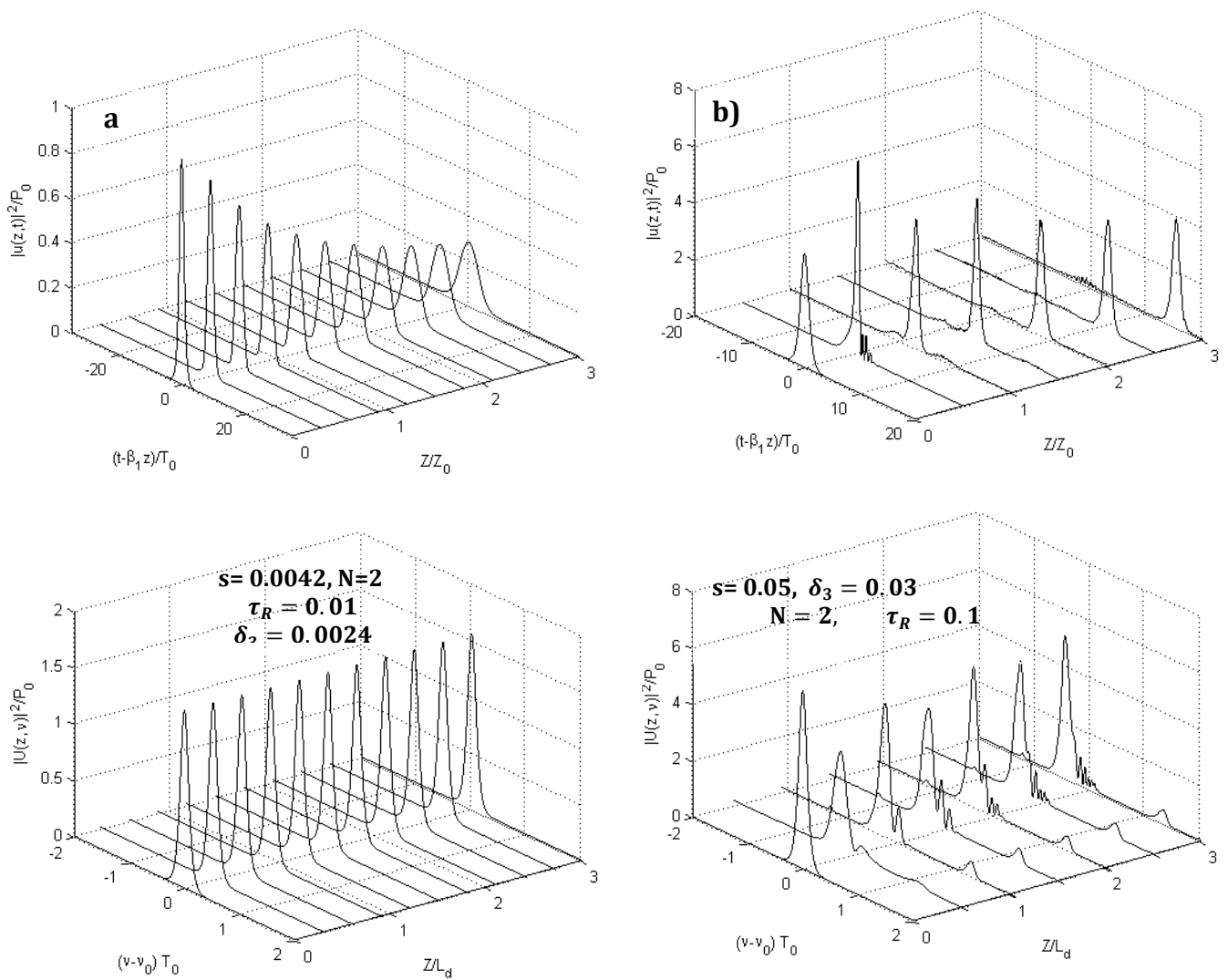


Figure 6.9: Evolution of pulse shapes and spectra a) for titanium sapphire, and b) for silica fiber (after [27]).

When the input peak power is large enough to excite a higher-order soliton such that $N \gg 1$, the pulse spectrum evolves into several bands, each corresponding to the splitting of a fundamental soliton from the original pulse. The combined effect of TOD, self-steepening, and intrapulse Raman scattering on a higher-order soliton is to split it into its constituents. In fact, the TOD can itself lead to soliton decay even in the absence of higher-order nonlinear effects when the parameter δ_3 exceeds a threshold value [22].

An interesting question is whether Eq.6.7 permits shape-preserving, solitary-wave solutions under certain conditions. Several such solutions have been found using a variety of techniques. In most cases, the solution exists only for a specific choice of parameter combinations. From a practical standpoint, such solutions of Eq.6.7 are rarely useful because it is hard to find fibers whose parameters satisfy the required constraints.

As successful as Eq.6.7 is in modeling the propagation of femtosecond pulses in optical fibers, it is still approximate. As discussed in Appendix B, a more accurate approach should use Eq.B.25, where $R(t)$ takes into account the time-dependent response of the fiber nonlinearity. The delayed nature of the molecular response not only leads to the soliton self-frequency shift but also affects the interaction between neighboring solitons. Equation 3.46 has been used to study numerically how intrapulse stimulated Raman scattering affects the evolution of femtosecond optical pulses in optical fibers for silica fiber [21].

The titanium sapphire smooth the two phenomena of self steepening and intra pulse Raman scattering, but remain the effects of group velocity dispersion accompanied in the propagation of an ultrashort lasers pulse.

References

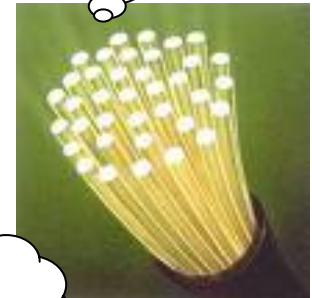
- [1] L. A. Ostrovskii, *Sov. Phys. Tech. Phys.* 8, 679 (1964); *Sov. Phys. JETP* 24,797 (1967).
- [2] G. B. Whitham, *Proc. Roy. Soc.* 283, 238 (1965)
- [3] G. B. Whitham, *J. Fluid Mech.* 27, 399 (1967).
- [4] T. B. Benjamin and J. E. Feir, *J. Fluid Mech.* 27, 417 (1967).
- [5] V. I. Bespalov and V. I. Talanov, *JETP Lett.* 3, 307 (1966).
- [6] V. I. Karpman, *JETP Lett.* 6, 277 (1967).
- [7] V. I. Karpman and E. M. Krushkal, *Sov. Phys. JETP* 28, 277 (1969).
- [8] T. Taniuti and H. Washimi, *Phys. Rev. Lett.* 21, 209 (1968).
- [9] J. Scott Russell, Report of 14th Meeting of the British Association for Advancement of Science, York, September 1844, pp. 311–390.
- [10] M. J. Ablowitz and P. A. Clarkson, *Solitons, Nonlinear Evolution Equations, and Inverse Scattering* (Cambridge University Press, New York, 1991).
- [11] J. T. Taylor (ed.), *Optical Solitons—Theory and Experiment*, (Cambridge University Press, New York, 1992).
- [12] H. A. Haus and M. N. Islam, *IEEE J. Quantum Electron.* QE-21, 1172 (1985).
- [13] H. Hasegawa and Y. Kodama, *Solitons in Optical Communications* (Oxford University Press, New York, 1995).
- [14] G. P. Agrawal and M. J. Potasek, *Phys. Rev. A* 33, 1765 (1986).
- [15] N. Tzoar and M. Jain, *Phys. Rev. A* 23, 1266 (1981).
- [16] E. A. Golovchenko, E. M. Dianov, A. M. Prokhorov, and V. N. Serkin, *JETP Lett.* 42, 87 (1985); *Sov. Phys. Dokl.* 31, 494 (1986).
- [17] F. M. Mitschke and L. F. Mollenauer, *Opt. Lett.* 11, 659 (1986);
- [18] J. P. Gordon, *Opt. Lett.* 11, 662 (1986).
- [19] Y. Kodama and A. Hasegawa, *IEEE J. Quantum Electron.* QE-23, 510 (1987).
- [20] K. Tai, A. Hasegawa, and N. Bekki, *Opt. Lett.* 13, 392 (1988).
- [21] P. V. Mamyshev and S. V. Chernikov, *Sov. Lightwave Commun.* 2, 97 (1992).
- [22] P. K. A. Wai, C. R. Menyuk, Y. C. Lee, and H. H. Chen, *Opt. Lett.* 11, 464 (1986).
- [23] T. Brabec and F. Krausz, *Phys. Rev. Lett.* 78, 3282 (1997).
- [24] J. K. Ranka and A. L. Gaeta, *Opt. Lett.* 23, 534 (1998).
- [25] J. Satsuma and N. Yajima, *Prog. Theor. Phys. Suppl.* 55, 284 (1974).
- [26] W. P. Zhong and H. J. Luo, *Chin. Phys. Lett.* 17, 577 (2000).
- [27] G. P. Agrawal “*Nonlinear Fiber Optics*” Third edition, University of Rochester (2001)

GENERAL CONCLUSION

Now, do you think
that I can be a useful
material?



Yes, a lot,
welcome to
the Telecom
world



Thank you
for this
solution



Not what, but is
it remains much
of work

The work described in this thesis charts the progress towards identifying novel waveguides such as titanium-doped sapphire for guiding the ultrashort laser pulse propagation. Titanium-doped sapphire is a material that has a simple energy level diagram, a high absorption cross section and is very widely vibronically broadened. These characteristics make sapphire a successful insulating substrate for micro-electronic components. Furthermore, it is an excellent material for optical windows.

The progress in the field of ultrashort laser pulse generation has been rapid and continuous, and has a long lifetime ahead. Laser powers should increase and intensities should be regularly pushed over 10^{21} W/cm². Research continues into discoveries for new gain media in the hope of improving on the excellent Ti: Sa and will continue for as long as ultrashort laser pulses remain useful, which judging by the numerous and varied applications, will be for many years to come. Of course, as technology continues to develop, more applications will be found for it. The laser should become cheaper to build as technologies and design improve, making them more compact and cheaper to buy as further applications call for them.

For an understanding of the nonlinear phenomena in optical fibers, it is necessary to consider the theory of electromagnetic wave propagation in dispersive nonlinear media. From Maxwell's equations, which describe the propagation of an electric field, we obtain the generalized nonlinear Schrodinger equation that describes the ultrashort laser pulse propagation through a titane sapphire waveguide.

Firstly, we consider the pulse propagation problem by treating fibers as linear optical media. We discuss the conditions under which the GVD effects dominate over the nonlinear effects by introducing two length scales associated with GVD and SPM. The dispersion induced pulse broadening discussed in detail is due to the lowest order GVD term proportional to β_2 . Although the contribution of this term dominates in most cases of practical interest, it is sometimes necessary to include the third order term proportional to β_3 in this expansion. The TOD distorts the pulse such that it becomes asymmetric with an oscillatory structure near one of its edges. The effect of third order dispersion is to make the intensity profile asymmetric and introduce a long oscillating

tail in leading or trailing edges of the pulses. The dispersion compensation technique has also been used for femtosecond optical pulses. When both β_2 and β_3 are nearly compensated, propagation of femtosecond optical pulses is limited by the fourth order dispersive effects governed by the parameter β_4 .

Then, we consider the pulse propagation problem by treating fibers as nonlinear optical media. An interesting manifestation of the intensity dependence of the refractive index in nonlinear optical media occurs through self phase modulation, a phenomenon that leads to spectral broadening of optical pulses. The SPM induced spectral broadening is a consequence of the time dependence of ϕ_{NL} . This can be understood by noting that a temporally varying phase implies that the instantaneous optical frequency differs across the pulse from its central value ω_0 . The chirp induced by SPM increases in magnitude with the propagated distance. In other words, new frequency components are generated continuously as the pulse propagates down the fiber. These SPM generated frequency components broaden the spectrum over its initial width at $z=0$. The number of peaks depends on ϕ_{max} and increases linearly with it. As mentioned before, the shape of the SPM broadened spectrum depends on the pulse shape and on the initial chirp if the input pulse is chirped. Next, we introduce new qualitative features, that arise from an interplay between GVD and SPM. In the anomalous dispersion regime of an optical fiber, the two phenomena can cooperate in such a way that the pulse propagates as an optical soliton. In the normal regime, the combined effects of GVD and SPM can be used for pulse compression.

Finally, we discuss the generalized nonlinear Schrodinger equation form for an ultrashort laser pulse. We define two other phenomena: the self steepening and the intrapulse Raman scattering effects. The self steepening results from the intensity dependence of the group velocity. This effect, as a result the trailing edge becomes steeper and steeper with increasing distance. Physically, the group velocity of the pulse is intensity-dependent such that the peak moves at a lower speed than the wings. The self steepening of the pulse eventually creates an optical shock, analogous to the development of an acoustic shock on the leading edge of a sound wave.

The intrapulse Raman scattering plays the most important role among the higher order nonlinear effects. Its effects on solitons are governed by the last term in GNLSE. Physically, the red shift can be understood in terms of stimulated Raman scattering. For pulse widths $\sim 1\text{ps}$ or shorter, the spectral width of the pulse is large enough that Raman gain can amplify the low frequency (red) spectral components of the pulse, with high frequency (blue) components of the same pulse acting as a pump. The process continues along the fiber, and the energy from blue components is continuously transferred to red components.

For pulses shorter than 20fs even the use of this equation becomes questionable because of the slowly varying envelope approximation, made in its derivation. Because such short pulses can be generated by modern mode-locked lasers, attempts have been made to improve upon this approximation while still working with the pulse envelope. For supershort pulses containing only a few cycles, it eventually becomes necessary to abandon the concept of the pulse envelope and solve Maxwell's equation directly.

APPENDICES
LISTS OF PUBLICATIONS
SIGLES AND ACRONYMS

A.1 Analytical expression of the temporal pulse crossing a dispersive medium

One considers an isotropic transparent medium characterized by an index of refraction $n(w)$. In a preoccupation with a simplicity, one supposes that the electric field entering medium has it an envelope of Gaussian form:

$$E(t) = E(t_0) \exp(jw_0 t) \exp\left[-\frac{(t-t_0)^2}{\tau_0^2}\right],$$

By using the remarkable integral $\int_{-\infty}^{+\infty} \exp[-ax^2 + bx] dx = \sqrt{\frac{\pi}{a}} \cdot \exp\left(\frac{b^2}{a}\right)$,

And transformation of Fourier formulates it: $S(w) = \frac{1}{\sqrt{2\pi}} \int_{-\infty}^{+\infty} E(t) \exp(-jw_0 t) dt$

The spectrum of this impulse is calculated

$$\begin{aligned} S(w) &= \frac{1}{\sqrt{2\pi}} \int_{-\infty}^{+\infty} E(t_0) \exp(-jw_0 t) \exp\left[-\frac{(t-t_0)^2}{\tau_0^2}\right] \exp(-jw t) dt \\ &= \frac{E(t_0)}{\sqrt{2\pi}} \int_{-\infty}^{+\infty} \exp\left[-\frac{(t-t_0)^2}{\tau_0^2}\right] \exp(j(w_0 - w)t) dt \\ &= \frac{E(t_0)}{\sqrt{2\pi}} \exp\left(-\frac{t_0^2}{\tau_0^2}\right) \int_{-\infty}^{+\infty} \exp\left[-\frac{t^2}{\tau_0^2}\right] \exp\left((j(w_0 - w) + 2\frac{t_0}{\tau_0^2})t\right) dt \\ &= \frac{E(t_0)}{\sqrt{2\pi}} \exp\left(-\frac{t_0^2}{\tau_0^2}\right) \sqrt{\pi} \tau_0 \exp\left[\left(\frac{j(w_0 - w) + \frac{2t_0}{\tau_0^2}}{2}\right)^2 \tau_0^2\right] \\ &= \frac{E(t_0)}{\sqrt{2\pi}} \tau_0 \exp\left[-\frac{(w - w_0)^2}{4} \tau_0^2\right] \exp[-jt_0(w - w_0)] \end{aligned}$$

Whose phase is modified during the propagation in the medium?

$$G(w) = S(w) \exp[-j\varphi(w)], \quad \varphi(w) = \frac{w}{c} n(w) \cdot L,$$

If the variation of the index of refraction $n(w)$ according to the pulsation is slow, the phase can be developed in Taylor series around w_0 :

$$\varphi(w) = \varphi(w_0) + a(w - w_0) + b(w - w_0)^2 + \dots,$$

$$a = \left. \frac{dk}{dw} \right|_{w_0} \cdot L, \quad b = \left. \frac{d^2k}{dw^2} \right|_{w_0} \cdot L.$$

At the exit of the transparent medium, the amplitude is given by the opposite transform of Fourier of $G(w)$:

$$\begin{aligned}
E^{sortie}(t) &= \frac{1}{\sqrt{2\pi}} \int_{-\infty}^{+\infty} G(w) \exp(jwt) dw \\
&= \frac{1}{\sqrt{2\pi}} \int_{-\infty}^{+\infty} S(w) \exp(jwt) \exp[-j\varphi(w_0) - ja(w-w_0) - jb(w-w_0)^2] dw \\
&= \frac{1}{\sqrt{2\pi}} \frac{E(t_0)}{\sqrt{2}} \exp[-j\varphi(w_0)] \int_{-\infty}^{+\infty} \exp\left[-\frac{(w-w_0)^2}{4} \tau_0^2 - jb(w-w_0)^2\right] \\
&\quad \times \exp[-ja(w-w_0)] \exp(jwt) \exp[-jt_0(w-w_0)] dw \\
&= \frac{1}{\sqrt{2\pi}} \frac{E(t_0)}{\sqrt{2}} \tau_0 \exp\left[-jt_0 w_0 - j\varphi(w_0) - \frac{w_0^2}{4} \tau_0^2 - jbw_0^2 + jaw_0\right] \\
&\quad \times \int_{-\infty}^{+\infty} \exp\left[-\left(\frac{\tau_0^2}{4} - jb\right) w^2\right] \exp\left[-2\left(\frac{w_0}{4} \tau_0^2 - jbw_0 + j\frac{a}{2} - j\frac{t}{2} + j\frac{t_0}{2}\right) w\right] dw \\
E^{sortie} &= \frac{1}{\sqrt{2\pi}} \frac{E(t_0)}{\sqrt{2}} \tau_0 \exp\left[it_0 w_0 - j\varphi(w_0) - \frac{w_0^2}{4} \tau_0^2 - jbw_0^2 + jaw_0\right] \left(\frac{\pi}{\frac{\tau_0^2}{4} + jb}\right)^{1/2} \\
&\quad \times \exp\left[\frac{-\left(\frac{\tau_0^2}{4} + jb\right) w_0 - \frac{j}{2}(t-t_0-a)^2}{\frac{\tau_0^2}{4} + jb}\right] \\
&= \frac{1}{2} E(t_0) \frac{\tau_0}{\left(\frac{\tau_0^2}{4} + jb\right)^{1/2}} \exp[-j\varphi(w_0)] \exp[-j(-t_0-a)w_0] \exp\left[-\left(\frac{\tau_0^2}{4} + jb\right) w_0^2\right] \\
&\quad \times \exp\left\{\frac{\left(\frac{\tau_0^2}{4} + jb\right)^2 w_0^2 + j\left(\frac{\tau_0^2}{4} + jb\right) w_0(-t_0-a) - \frac{1}{4}(-t_0-a)^2}{\frac{\tau_0^2}{4} + jb}\right\} \\
&= \frac{\tau_0}{\tau} E(t_0) \exp\left[-\frac{j}{2} \arctg\left(\frac{4b}{\tau_0^2}\right)\right] \exp[-j\varphi(w_0)] \exp\left[\frac{(t-t_0-a)^2}{\tau_0^2 + ajb}\right], \\
\text{with } \left(\frac{\tau_0^2}{4} + jb\right)^{1/2} &= \left(\frac{\tau_0^4}{16} + b^2\right)^{1/4} \exp\left[\frac{j}{2} \arctg\left(\frac{4b}{\tau_0^2}\right)\right], \quad \text{et } \tau^4 = \tau_0^4 + 16b^2
\end{aligned}$$

The electric field at exit of the medium is written then

$$E^{sortie} = \frac{\tau_0}{\tau} E(t_0) \exp[-j(\varphi + \phi(w_0))] \exp(jw_0 t) \exp\left\{-\frac{(t-t_0-a)^2}{\tau_0^2 + 4jb}\right\},$$

$$\text{avec } \phi = \frac{1}{2} \arctg\left(\frac{4b}{\tau_0^2}\right).$$

$$\begin{aligned} E^{sortie} &= \frac{\tau}{\tau_0} E(t_0) \exp[-j(\varphi(w_0) + \phi)] \exp(jw_0 t) \exp\left[-\frac{(\tau_0^2 - 4jb)(t-t_0-a)^2}{\tau_0^4 + 16b^2}\right] \\ &= \frac{\tau}{\tau_0} E(t_0) \exp[-j(\varphi(w_0) + \phi)] \exp(jw_0 t) \exp\left[-\frac{\tau_0^2}{\tau_0^4 + 16b^2}(t-t_0-a)^2\right] \\ &\quad \times \exp\left[4jb \frac{(t-t_0-a)^2}{\tau_0^4 + 16b^2}\right] \\ &= \frac{\tau}{\tau_0} E(t_0) \exp\left[-\frac{\tau_0^2}{\tau^4}(t-t_0-a)^2\right] \exp[-j(\varphi(w_0) + \phi)] \exp(jw_0 t) \times \exp\left[\frac{4jb}{\tau^4}(t-t_0-a)^2\right] \end{aligned}$$

This gives the following expression for the intensity at exit of the medium:

$$\begin{aligned} |E^{sortie}(t)|^2 &= \frac{\tau_0^2}{\tau^2} E^2(t_0) \exp\left[-2\frac{\tau_0^2}{\tau^4}(t-t_0-a)^2\right], \\ &= \frac{\tau_0^2 E^2(t_0)}{4\sqrt{\frac{\tau_0^4}{16} + b^2}} \exp\left[-\frac{\tau_0^2(t-t_0-a)^2}{8\left(\frac{\tau_0^4}{16} + b^2\right)}\right] \end{aligned}$$

The duration with middle height of the impulse after passage in the medium is worth

$$\Delta t^{sortie} = 2\sqrt{\frac{8\left(\frac{\tau_0^4}{16} + b^2\right)}{\tau_0^2}} \cdot \sqrt{\ln 2}.$$

This duration compared with the duration $\Delta t^{entree} = \tau_0 \sqrt{2 \ln 2}$ incidental pulse is worth

$$\begin{aligned} \Delta t^{sortie} &= \frac{2}{\tau_0} \sqrt{\frac{\tau_0^4}{2} + 8b^2} \cdot \sqrt{\ln 2} = \frac{2}{\tau_0} \sqrt{\tau_0^4 \left(\frac{1}{2} + \frac{8b^2}{\tau_0^4}\right)} \cdot \sqrt{\ln 2} = \sqrt{1 + \frac{16b^2}{\tau_0^4}} \tau_0 \cdot \sqrt{2 \ln 2}, \\ \Delta t^{sortie} &= \sqrt{1 + \frac{4\left(\left.\frac{d^2k}{dw^2}\right|_{w_0} L\right)^2}{\tau_0^4}} \cdot \Delta t^{entree} \end{aligned}$$

A.2 Calculation of the electric field of the wavelet:

$$\begin{aligned}
\theta(t, z = 0) &= TF\{\theta(\Omega, z = 0)\} \\
&= \frac{1}{2\pi} \int_{-\infty}^{+\infty} \theta(\Omega, z = 0) \exp(j\omega t) d\omega \\
&= \frac{1}{2\pi} \sqrt{\frac{\pi}{\Gamma}} \exp\left[-\frac{(w - w_0)^2}{4\Gamma}\right] \cdot \exp\left[-\frac{(w - \Omega)^2}{4\gamma}\right] \cdot \exp(j\omega t) d\omega \\
&= \frac{1}{2\pi} \sqrt{\frac{\pi}{\Gamma}} \cdot \exp\left[-\frac{w_0^2}{4\Gamma} - \frac{\Omega^2}{4\gamma}\right] \int_{-\infty}^{+\infty} \exp\left[-\left(\frac{1}{4\Gamma} + \frac{1}{4\gamma}\right)w^2 + \left(\frac{2}{4\Gamma}w_0 + \frac{2}{4\gamma}\Omega + jt\right)w\right] d\omega \\
&= \frac{1}{2\pi} \sqrt{\frac{\pi}{\Gamma}} \cdot \exp\left[-\frac{w_0^2}{4\Gamma} - \frac{\Omega^2}{4\gamma}\right] \sqrt{\frac{\pi}{4\gamma\Gamma}} \cdot \exp\left[\frac{\left(\frac{1}{2\Gamma}w_0 + \frac{1}{2\gamma}\Omega + jt\right)^2}{\frac{\gamma + \Gamma}{\gamma\Gamma}}\right] \\
&= \sqrt{\frac{\gamma}{\gamma + \Gamma}} \cdot \exp\left[-\frac{w_0^2}{4\Gamma} - \frac{\Omega^2}{4\gamma}\right] \cdot \exp\left[\left(\frac{w_0}{2\Gamma} + \frac{\Omega}{2\gamma}\right) \cdot \frac{\Gamma\gamma}{\Gamma + \gamma}\right] \cdot \exp\left[-\frac{\Gamma\gamma}{\Gamma + \gamma}t^2\right] \exp\left[j\left(\frac{w_0\gamma + \Omega\Gamma}{\gamma + \Gamma}\right)\right].
\end{aligned}$$

A.3 Calculation of the electric field through a dispersive medium of index $n(\omega)$:

$$\begin{aligned}
\theta(\Omega, z = 0) &= \frac{1}{2\sqrt{\pi\gamma}} \cdot E(\omega) \cdot \exp\left[-\frac{(w - \Omega)^2}{4\gamma}\right] \\
\theta(\Omega, z) &= \frac{1}{2\sqrt{\pi\gamma}} \cdot E(\omega) \cdot \exp\left[-\frac{(w - \Omega)^2}{4\gamma}\right] \cdot \exp[j\phi(\omega)] \\
\theta(t, z) &= \frac{1}{2\pi} \cdot \frac{1}{2\sqrt{\pi\gamma}} \cdot \int_{-\infty}^{+\infty} E(\omega) \cdot \exp\left[-\frac{(w - \Omega)^2}{4\gamma}\right] \cdot \exp[j\phi(\omega)] \\
\theta(t, z) &= \frac{1}{2\pi} \cdot \frac{1}{2\sqrt{\pi\gamma}} \cdot \sqrt{\frac{\pi}{\Gamma}} \int_{-\infty}^{+\infty} \exp\left[-\frac{(w - w_0)^2}{4\Gamma}\right] \cdot \exp\left[-\frac{(w - \Omega)^2}{4\gamma}\right] \\
&\quad \cdot \exp\left[j\phi^{(0)} + j\phi^{(1)}(w - \Omega) + \frac{1}{2}j\phi^{(2)}(w - \Omega)^2\right] \cdot \exp(j\omega t) \cdot d\omega
\end{aligned}$$

Temporal intensity $\theta(t, z)$ associated the wavelet such as

$$\theta(t, z) = \frac{1}{2\pi} \int_{-\infty}^{+\infty} \theta(\Omega, z) \cdot \exp(j\omega t) d\omega$$

knowing that:

$$\begin{aligned}(w - w_0)^2 &= (w - w_0 + \Omega - \Omega)^2 \\ &= (w - \Omega)^2 + (\Omega - w_0)^2 + 2(w - \Omega)(\Omega - w_0)\end{aligned}$$

$$\begin{aligned}\phi(t, z) &= \frac{1}{2\pi} \frac{1}{2\sqrt{\pi\gamma}} \cdot \sqrt{\frac{\pi}{\Gamma}} \int_{-\infty}^{+\infty} \exp\left[-\frac{(w - \Omega)^2}{4\Gamma}\right] \cdot \exp\left[-\frac{(\Omega - w_0)^2}{4\Gamma}\right] \cdot \exp\left[\frac{(w - \Omega)(\Omega - w_0)}{2\Gamma}\right] \\ &\quad \cdot \exp\left[-\frac{(w - \Omega)^2}{4\gamma}\right] \exp(j\varphi^{(0)}) \exp j(w - \Omega)\varphi^{(1)} \cdot \exp \frac{1}{2} j(w - \Omega)^2 \cdot \varphi^{(2)} \cdot \exp(jwt) dw\end{aligned}$$

$$\phi(t, z) = \frac{1}{2\pi} \frac{1}{2\sqrt{\pi\gamma}} \cdot \sqrt{\frac{\pi}{\Gamma}} \exp\left[-\frac{(\Omega - w_0)^2}{4\Gamma}\right] \cdot \exp(j\varphi^{(0)}) \int_{-\infty}^{+\infty} e^{-\left[\frac{1}{4\Gamma} + \frac{1}{4\gamma} - \frac{1}{2}j\varphi^{(2)}\right](w - \Omega)^2} e^{-\left[\frac{(\Omega - w_0)}{2\Gamma} - j\varphi^{(1)}\right](w - \Omega)} \cdot e^{j\Omega w} dw$$

$$\begin{aligned}\phi(t, z) &= \frac{1}{2\pi} \frac{1}{2\sqrt{\pi\gamma}} \cdot \sqrt{\frac{\pi}{\Gamma}} \cdot e^{-\left[\frac{(\Omega - w_0)^2}{4\Gamma}\right]} \cdot e^{(j\varphi^{(0)})} \cdot e^{-\left[\frac{1}{4\Gamma} + \frac{1}{4\gamma} - \frac{1}{2}j\varphi^{(2)}\right]\Omega^2} \cdot e^{\left[\frac{(\Omega - w_0)}{2\Gamma} - j\varphi^{(1)}\right]\Omega} \\ &\quad \int_{-\infty}^{+\infty} e^{-\left[\frac{1}{4\Gamma} + \frac{1}{4\gamma} - \frac{1}{2}j\varphi^{(2)}\right]w^2} e^{\left[\frac{1}{4\Gamma} + \frac{1}{4\gamma} - \frac{1}{2}j\varphi^{(2)}\right]2\Omega \cdot w} \cdot e^{-\left[\frac{(\Omega - w_0)}{2\Gamma} - j\varphi^{(1)}\right]w} \cdot e^{j\Omega w} dw\end{aligned}$$

Exposant can be written:

$$A = -\frac{1}{4\Gamma(z)} w^2 + \left[\frac{\Omega}{2\Gamma(z)} - \frac{(\Omega - w_0)}{2\Gamma} + j\varphi^{(1)} + jt \right] w$$

$$\text{with: } \frac{1}{\Gamma(z)} = \frac{1}{\Gamma} + \frac{1}{\gamma} - 2j\varphi^{(2)}$$

And consequently the integral is written:

$$I = \sqrt{\pi 4\Gamma(z)} \cdot \exp\left[\frac{\Omega}{2\Gamma(z)} - \frac{(\Omega - w_0)}{2\Gamma} + j\varphi^{(1)} + jt \right]^2 \cdot \Gamma(z)$$

that is to say :

$$\begin{aligned}\theta(t, z) &= \frac{1}{2\sqrt{\pi\gamma}} \cdot \sqrt{\frac{\Gamma(z)}{\Gamma}} \cdot \exp(j\varphi^{(0)}) \cdot \exp\left(-\Gamma(z) \left[t + \frac{z}{V_g(\Omega)} \right]^2\right) \cdot \exp\left(-\frac{(\Omega - w_0)^2}{4\Gamma} \left[1 - \frac{\Gamma(z)}{\Gamma} \right]\right) \\ &\quad \exp j \left[\left(1 - \frac{\Gamma(z)}{\Gamma} \right) \Omega + \frac{\Gamma(z)}{\Gamma} \cdot w_0 \right] \left[t + \frac{z}{V_g(\Omega)} \right]\end{aligned}$$

B.1 Nonlinear Pulse Propagation

The study of most nonlinear effects in optical fibers involves the use of short pulses with widths ranging from $\sim 10\text{ns}$ ns to 10fs . When such optical pulses propagate inside a fiber, both dispersive and nonlinear effects influence their shape and spectrum. In this section we derive a basic equation that governs propagation of optical pulses in nonlinear dispersive fibers. The starting point is the wave Eq.3.7. This is generally not possible as Eq.3.35 is nonlinear because of the intensity dependence of ε_{NL} . In one approach, ε_{NL} is treated as a constant during the derivation of the propagation equation. The approach is justified in view of the slowly varying envelope approximation and the perturbative nature of P_{NL} . Substituting Equations.3.36–3.37 in Eq.3.35, the Fourier transform $\tilde{E}(r, w - w_0)$, defined as

$$\tilde{E}(r, w - w_0) = \int_{-\infty}^{+\infty} E(r, t) \cdot \exp[i(w - w_0)t] dt, \quad (\text{B.1})$$

is found to satisfy the Helmholtz equation

$$\nabla^2 \tilde{E} + \varepsilon(w) k_0^2 \tilde{E} = 0, \quad (\text{B.2})$$

where $k_0 = w/c$ and

$$\varepsilon(w) = 1 + \tilde{\chi}_{xx}^{(1)}(w) + \varepsilon_{NL} \quad (\text{B.3})$$

is the dielectric constant whose nonlinear part ε_{NL} is given by Eq.3.42. Similar to Eq.3.14, the dielectric constant can be used to define the refractive index \tilde{n} and the absorption coefficient $\tilde{\alpha}$. However, both \tilde{n} and $\tilde{\alpha}$ become intensity dependent because of ε_{NL} . It is customary to introduce

$$\tilde{n} = n + n_2 |E|^2, \quad \tilde{\alpha} = \alpha + \alpha_2 |E|^2. \quad (\text{B.4})$$

Using $\varepsilon = (\tilde{n} + i\tilde{\alpha}/2k_0)^2$ and Eq.3.42 and Eq.B.3, the nonlinear-index coefficient n_2 and the two-photon absorption coefficient α_2 are given by

$$n_2 = \frac{3}{8n} \text{Re}(\chi_{xxxx}^{(3)}), \quad \alpha_2 = \frac{3w_0}{4nc} \text{Im}(\chi_{xxxx}^{(3)}). \quad (\text{B.5})$$

The linear index n and the absorption coefficient α are related to the real and imaginary parts of $\tilde{\chi}_{xx}^{(1)}$ as in Eq.3.15 and Eq.3.16.

Eq.B.2 can be solved by using the method of separation of variables. If we assume a solution of the form

$$\tilde{E}(r, w - w_0) = F(x, y) \tilde{A}(z, w - w_0) \exp(i\beta z), \quad (\text{B.6})$$

where $\tilde{A}(z, w)$ is a slowly varying function of z and β_0 is the wave number to be determined later, Eq.B.2 leads to the following two equations for $F(x, y)$ and $\tilde{A}(z, w)$:

$$\frac{\partial^2 F}{\partial x^2} + \frac{\partial^2 F}{\partial y^2} + [\varepsilon(w)k_0^2 - \tilde{\beta}^2]F = 0, \quad (\text{B.7})$$

$$2i\beta_0 \frac{\partial \tilde{A}}{\partial z} + (\tilde{\beta}^2 - \tilde{\beta}_0^2)\tilde{A} = 0. \quad (\text{B.8})$$

In obtaining Eq.B.8, the second derivative $(\partial^2 \tilde{A})/\partial z^2$ was neglected since $\tilde{A}(z, w)$ is assumed to be a slowly varying function of z . The wave number β is determined by solving the eigenvalue Eq.B.7 for the fiber modes using a procedure similar to that used in Section 3.2. The dielectric constant $\varepsilon(w)$ in Eq. B.7 can be approximated by

$$\varepsilon = (n + \Delta n)^2 \approx n^2 + 2n\Delta n, \quad (\text{B.9})$$

where Δn is a small perturbation given by

$$\Delta n = n_2 |E|^2 + \frac{i\tilde{\alpha}}{2k_0}.$$

(B.10)

Eq.B.7 can be solved using first-order perturbation theory [11]. We first replace ε with n^2 and obtain the modal distribution $F(x, y)$, and the corresponding wave number $\beta(w)$. For a single-mode fiber, $F(x, y)$ corresponds to the modal distribution of the fundamental fiber mode HE_{11} given by Eq.B.6 and Eq.B.7, or by the Gaussian approximation Eq.B.8. We then include the effect of Δn in Eq.B.7. In the first-order perturbation theory, Δn does not affect the modal distribution $F(x, y)$. However, the eigenvalue $\tilde{\beta}$ becomes

$$\tilde{\beta}(w) = \beta(w) + \Delta\beta, \quad (\text{B.11})$$

where

$$\Delta\beta = \frac{k_0 \iint_{-\infty}^{+\infty} \Delta n |F(x, y)|^2 dx dy}{\iint_{-\infty}^{+\infty} \Delta n |F(x, y)|^2 dx dy} \quad (\text{B.12})$$

This step completes the formal solution of Eq.3.35 to the first order in perturbation P_{NL} . Using Eqs.3.36 and 3.46, the electric field $E(r, t)$ can be written as

$$E(r, t) = \frac{1}{2} \hat{x}[F(x, y)A(z, t) \exp[i(\beta_0 z - w_0 t)] + c. c.] \quad (\text{B.13})$$

where (z, t) is the slowly varying pulse envelope. The Fourier transform $\tilde{A}(z, w - w_0)$ of $A(z, t)$ satisfies Eq.B.8, which can be written as

$$\frac{\partial \tilde{A}}{\partial z} = i[\beta(w) + \Delta\beta - \beta_0]\tilde{A}, \quad (\text{B.14})$$

where we used Eq.B.11 and approximated $\tilde{\beta}^2 - \beta_0^2$ by $2\beta_0(\tilde{\beta} - \beta_0^2)$. The physical meaning of this equation is clear. Each spectral component within the pulse envelope acquires, as it propagates down the fiber, a phase shift whose magnitude is both frequency and intensity dependent. At this point, one can go back to the time domain by taking the inverse Fourier transform of Eq.B.14, and obtain the propagation equation for $A(z, t)$. However, as an exact functional form of $\beta(w)$ is rarely known, it is useful to expand $\beta(w)$ in a Taylor series about the carrier frequency w_0 as

$$\beta(w) = \beta_0 + (w - w_0)\beta_1 + \frac{1}{2}(w - w_0)^2\beta_2 + \frac{1}{6}(w - w_0)^3\beta_3 + \dots \quad (\text{B.15})$$

where

$$\beta_m = \left(\frac{d^m \beta}{dw^m} \right)_{w=w_0} \quad m = 1, 2, \dots \quad (\text{B.16})$$

The cubic and higher-order terms in this expansion are generally negligible if the spectral width $\Delta w \ll w_0$. We substitute Eq.B.15 in Eq.B.14 and take the inverse Fourier transform by using

$$A(z, t) = \frac{1}{2\pi} \int_{-\infty}^{+\infty} \tilde{A}(z, w - w_0) \exp[-i(w - w_0)t] dw. \quad (\text{B.17})$$

During the Fourier-transform operation, $w - w_0$ is replaced by the differential operator $i(\partial/\partial t)$. The resulting equation for $A(z, t)$ becomes

$$\frac{\partial A}{\partial z} = -\beta_1 \frac{\partial A}{\partial t} - \frac{i\beta_2}{2} \frac{\partial^2 A}{\partial t^2} + i\Delta\beta A. \quad (\text{B.18})$$

The term with $\Delta\beta$ includes the effect of fiber loss and nonlinearity. By using Eq. B.10 and Eq.B.12, $\Delta\beta$ can be evaluated and substituted in Eq.B.18. The result is

$$\frac{\partial A}{\partial z} + \beta_1 \frac{\partial A}{\partial t} + \frac{i\beta_2}{2} \frac{\partial^2 A}{\partial t^2} + \frac{\alpha}{2} A = i\gamma |A|^2 A, \quad (\text{B.19})$$

where the nonlinear parameter γ is defined as

$$\gamma = \frac{n_2 w_0}{c A_{eff}}. \quad (\text{B.20})$$

In obtaining Eq.B.19 the pulse amplitude A is assumed to be normalized such that $|A|^2$ represents the optical power. The quantity $\gamma|A|^2$ is then measured in units of m^{-1} if n_2 is expressed in units of m^2/W . The parameter A_{eff} is known as the effective core area and is defined as

$$A_{eff} = \frac{\left(\iint_{-\infty}^{+\infty} |F(x,y)|^2 dx dy\right)^2}{\iint_{-\infty}^{+\infty} |F(x,y)|^4 dx dy}. \quad (\text{B.21})$$

Its evaluation requires the use of modal distribution $F(x, y)$ for the fundamental fiber mode. Clearly A_{eff} depends on fiber parameters such as the core radius and the core-cladding index difference. If $F(x, y)$ is approximated by a Gaussian distribution as in Eq.3.34, $A_{eff} = \pi w^2$.

Eq.B.19 describes propagation of picosecond optical pulse in single-mode fibers. It is often referred to as the nonlinear Schrödinger (NLS) equation because it can be reduced to that form under certain conditions. It includes the effects of fiber losses through α , of chromatic dispersion through β_1 and β_2 , and of fiber nonlinearity through γ . Briefly, the pulse envelope moves at the group velocity $v_g \equiv 1/\beta_1$ while the effects of group-velocity dispersion (GVD) are governed by β_2 .

B.2 Higher-Order Nonlinear Effects

The starting point is again the wave Eq.3.35. Eq.3.10 describes a wide variety of third-order nonlinear effects, and not all of them are relevant to our discussion. For example, nonlinear phenomena such as third harmonic generation and four-wave mixing are unlikely to occur unless an appropriate phase-matching condition is satisfied. Nonresonant, incoherent (intensity-dependent) nonlinear effects can be included by assuming the following functional form for the third-order susceptibility:

$$\chi^{(3)}(t - t_1, t - t_2, t - t_3) = \chi^{(3)} R(t - t_1) \delta(t - t_2) \delta(t - t_3), \quad (\text{B.22})$$

where $R(t)$ is the nonlinear response function normalized in a manner similar to the delta function, i.e., $\int_{-\infty}^{+\infty} R(t) dt = 1$. By substituting Eq.B.22 in Eq.3.10 the nonlinear polarization is given by

$$P_{NL}(r, t) = \varepsilon_0 \chi^{(3)} E(r, t) \int_{-\infty}^t E(t - t_1) |E(r, t_1)|^2 dt_1 \quad (\text{B.23})$$

where it is assumed that the electric field and the induced polarization vectors point along the same direction. The upper limit of integration in Eq.B.23 extends only up to t because the response function $R(t - t_1)$ must be zero for $t_1 > t$ to ensure causality.

The analysis of Section 3.3.1 can still be used by working in the frequency domain. Using Eqs.3.34–3.36, \tilde{E} is found to satisfy

$$\begin{aligned} \nabla^2 \tilde{E} + n^2(w) k_0^2 \tilde{E} = & -ik_0 \alpha + \chi^{(3)} \frac{w^2}{c^2} \iint_{-\infty}^{\infty} \tilde{R}(w - w_1) \\ & \times \tilde{E}(w_1, z) \tilde{E}(w_2, z) \tilde{E}^*(w_1 + w_2 - w, z) dw_1 dw_2 \end{aligned} \quad (\text{B.24})$$

where $\tilde{R}(w)$ is the Fourier transform of $R(t)$. As before, one can treat the terms on the right-hand side as a small perturbation and first obtain the modal distribution by neglecting them. The effect of perturbation terms is to change the propagation constant for the fundamental mode by $\Delta\beta$ as in Eq.B.11 but with a different expression for $\Delta\beta$. One can then define the slowly varying amplitude $A(z, t)$ as in Eq.B.13 and obtain, after some algebra, the following equation for pulse evolution inside a single-mode fiber:

The following equation for pulse evolution inside a single-mode fiber:

$$\begin{aligned} & \frac{\partial A}{\partial z} + \frac{\alpha}{2} A + \beta_1 \frac{\partial A}{\partial t} + \frac{i\beta_2}{2} \frac{\partial^2 A}{\partial t^2} - \frac{\beta_3}{6} \frac{\partial^3 A}{\partial t^3} \\ = & i\gamma \left(1 + \frac{i}{w_0} \frac{\partial}{\partial t} \right) \left(A(z, t) \int_{-\infty}^{\infty} R(t') |A(z, t - t')|^2 dt' \right) \end{aligned} \quad (\text{B.25})$$

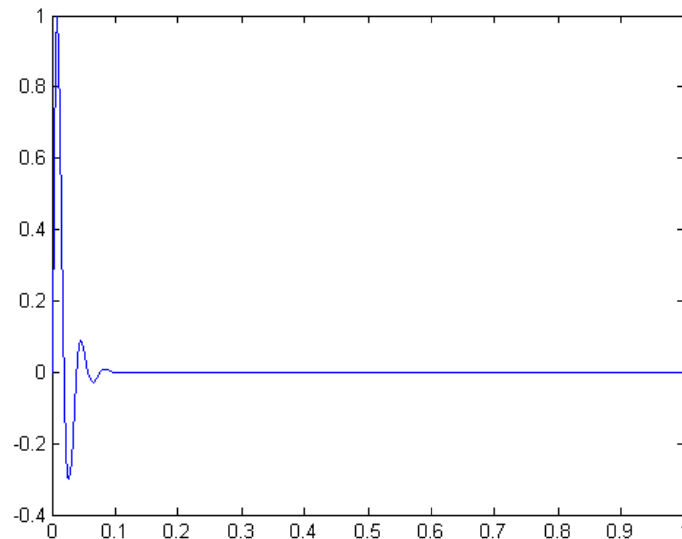


Fig: B.1 Temporal variation of the Raman response function obtained by using the actual Raman-gain spectrum of silica fibers.

where β_2 is the nonlinear parameter as defined in Eq.B.20. In general, the effective core area A_{eff} is also a function of ω because the mode distribution is frequency dependent. However, the variation of A_{eff} over the pulse spectrum is typically negligible and can be included in a straightforward manner.

The time derivative appearing on the right-hand side of Eq.B.25 results when Eq.3.38 is used in Eq.3.7 and the first-order time derivative of A_{eff} is retained in the analysis used for ultrashort pulses. This term is responsible for self-steepening and shock formation at a pulse edge and has been discussed extensively since 1967. This term also includes the nonlinear energy loss resulting from intrapulse Raman scattering. Eq.B.25 may be valid even when the slowly varying envelope approximation does not hold and can be used for pulses as short as a few optical cycles if enough higher-order dispersive terms are included. The response function $R(t)$ should include both the electronic and vibrational (Raman) contributions. Assuming that the electronic contribution is nearly instantaneous, the functional form of $R(t)$ can be written as

$$(B.26)$$

where f_R represents the fractional contribution of the delayed Raman response to nonlinear polarization P_{NL} . The Raman response function $h_R(t)$ is responsible for the Raman gain whose spectrum is given by

$$g_R(\Delta\omega) = \frac{\omega_0}{c n_0} f_R \chi^{(3)} \text{Im}[\tilde{h}_R(\Delta\omega)], \quad (\text{B.27})$$

where $\Delta\omega = \omega - \omega_0$ and Im stands for the imaginary part. The real part of $\tilde{h}_R(\Delta\omega)$ can be obtained from the imaginary part by using the Kramers–Kronig relations. Attempts have been made to determine an approximate analytic form of the Raman response function.

$$h_R(t) = \frac{\tau_1^2 + \tau_2^2}{\tau_1 \tau_2^2} \exp\left(-\frac{t}{\tau_2}\right) \sin\left(\frac{t}{\tau_1}\right). \quad (\text{B.28})$$

The parameters τ_1 and τ_2 are two adjustable parameters and are chosen to provide a good fit to the actual Raman-gain spectrum. Their appropriate values are $\tau_1 = 12.2 \text{ fs}$ and $\tau_2 = 32 \text{ fs}$. Eq.B.25 governs evolution of ultra-short pulses in optical fibers. Its accuracy has been verified by showing that it preserves the number of photons during pulse evolution if fiber loss is ignored by setting $\alpha = 0$. As the higher-order dispersion term (involving β_3) and the shock term (involving ω_0) are negligible for such pulses, Eq.B.25 reduces to Eq.B.19.

The pulse energy is not conserved in the presence of intrapulse Raman scattering because a part of the pulse energy is absorbed by silica molecules. Equation B.25 includes this source of nonlinear loss. It is easy to see that it reduces to the simpler equation obtained in Section 3.3.1 [Eq.B.19] for optical pulses much longer than the time scale of the Raman response function $h_R(t)$ because $R(t)$ for such pulses is replaced by the delta function $\delta(t)$. Noting that $h_R(t)$ becomes, nearly zero for $t > 1 \text{ ps}$ (see Fig. B.1), this replacement is valid for picoseconds pulses having widths much greater than 1 ps . As the higher-order dispersion term (involving β_3) and the shock term (involving ω_0) are negligible for such pulses, Eq.3.67 reduces to Eq.B.19. For pulses shorter than 5 ps but wide enough to contain many optical cycles (widths $\gg 10 \text{ fs}$), we can simplify Eq.B.25 using a Taylor-series expansion such that

$$|A(z, t - t')|^2 \approx |A(z, t)|^2 - t' \frac{\partial}{\partial t} |A(z, t)|^2. \quad (\text{B.29})$$

This approximation is reasonable if the pulse envelope evolves slowly along the fiber. Defining the first moment of the nonlinear response function as

$$T_R \equiv \int_{-\infty}^{\infty} t R(t) dt = f_R \int_{-\infty}^{\infty} t h_R(t) dt = f_R \left. \frac{d(\text{Im}\tilde{h}_R)}{d(\Delta\omega)} \right|_{\Delta\omega=0}, \quad (\text{B.30})$$

and noting that $\int_0^{\infty} R(t) dt = 1$, Eq. (C.25) can be approximated by

$$\frac{\partial A}{\partial z} + \frac{\alpha}{2} A + \frac{i\beta_2}{2} \frac{\partial^2 A}{\partial t^2} - \frac{\beta_3}{6} \frac{\partial^3 A}{\partial t^3} = i\gamma \left(|A|^2 A + \frac{i}{w_0} \frac{\partial}{\partial T} (|A|^2 A) - T_R A \frac{\partial |A|^2}{\partial T} \right), \quad (\text{B.31})$$

where a frame of reference moving with the pulse at the group velocity v_g (the so-called retarded frame) is used by making the transformation

$$T = t - \frac{z}{v_g} \equiv t - \beta_1 z. \quad (\text{B.32})$$

A second-order term involving the ratio T_R/w_0 was neglected in arriving at Eq.B.31 because of its smallness.

It is easy to identify the origin of the last three higher-order terms in Eq.B.31. The term proportional to β_3 results from including the cubic term in the expansion of the propagation constant in Eq.B.15. This term governs the effects of third-order dispersion and becomes important for ultrashort pulses because of their wide bandwidth. The term proportional to w_0^{-1} results from including the first derivative of P_{NL} . It is responsible for self-steepening and shock formation. The last term proportional to T_R in Eq.B.25 has its origin in the delayed Raman response, and is responsible for the self-frequency shift induced by intrapulse Raman scattering. By using Eq.B.27 and Eq.B.30, T_R can be related to the slope of the Raman gain spectrum that is assumed to vary linearly with frequency in the vicinity of the carrier frequency w_0 .

For pulses of width $T_0 > 5 ps$, the parameters $(w_0 T_0)^{-1}$ and T_R/T_0 become so small ($< 0,001$) that the last two terms in Eq.B.25 can be neglected. As the contribution of the third-order dispersion term is also quite small for such pulses

(as long as the carrier wavelength is not too close to the zero-dispersion wavelength), one can use the simplified equation

$$i \frac{\partial A}{\partial z} + i \frac{\alpha}{2} A - \frac{\beta_2}{2} \frac{\partial^2 A}{\partial T^2} - \gamma |A|^2 A = 0. \quad (\text{B.33})$$

This equation can also be obtained from Eq.B.19 by using the transformation given in Eq.3.46. In the special case of $\alpha = 0$, Eq.B.33 is referred to as the NLS equation because it resembles the Schrodinger equation with a nonlinear potential term (variable z playing the role of time). To extend the analogy further, Eq.B.25 is called the generalized (or extended) NLS equation. The NLS equation is a fundamental equation of nonlinear science and has been studied extensively in the context of solitons. Eq.B.33 is the simplest nonlinear equation for studying third order nonlinear effects in optical fibers. Eq.B.33 appears in optics in several different contexts. For example, the same equation holds for propagation of CW beams in planar waveguides when the variable T is interpreted as the spatial coordinate. The β_2 term in Eq.B.33 then governs beam diffraction in the plane of the waveguide. This analogy between “diffraction in space” and “dispersion in time” is often exploited to advantage since the same equation governs the underlying physics.

B.3 Numerical Methods

A numerical approach is therefore often necessary for an understanding of the nonlinear effects in optical fibers. A large number of numerical methods can be used for this purpose. The one method that has been used extensively to solve the pulse-propagation problem in nonlinear dispersive media is the split-step Fourier method. The relative speed of this method compared with most finite-difference schemes can be attributed in part to the use of the finite-Fourier-transform (FFT) algorithm. This section describes various numerical techniques used to study the pulse-propagation problem in optical fibers with emphasis on the split-step Fourier method and its modifications.

B.3.1 Split-Step Fourier Method

To understand the philosophy behind the split-step Fourier method, it is useful to write Eq.B.25 formally in the form

$$\frac{\partial A}{\partial z} = (\widehat{D} + \widehat{N})A, \quad (\text{B.34})$$

where \widehat{D} is a differential operator that accounts for dispersion and absorption in a linear medium and \widehat{N} is a nonlinear operator that governs the effect of fiber nonlinearities on pulse propagation. These operators are given by

$$\widehat{D} = -\frac{i\beta_2}{2} \frac{\partial^2}{\partial T^2} + \frac{\beta_3}{6} \frac{\partial^3}{\partial T^3} - \frac{\alpha}{2}, \quad (\text{B.35})$$

$$\widehat{N} = i\gamma \left(|A|^2 + \frac{i}{\omega_0 A} \frac{\partial}{\partial T} (|A|^2 A) - T_R \frac{\partial |A|^2}{\partial T} \right), \quad (\text{B.36})$$

In general, dispersion and nonlinearity act together along the length of the fiber. The split-step Fourier method obtains an approximate solution by assuming that in propagating the optical field over a small distance h , the dispersive and nonlinear effects can be pretended to act independently. More specifically, propagation from z to $z + h$ is carried out in two steps. In the first step, the nonlinearity acts alone, and $\widehat{D} = 0$ in Eq.B.34.

In the second step, dispersion acts alone, and $\widehat{N} = 0$ in Eq.B.36. Mathematically,

$$A(z + h, T) \approx \exp(h\widehat{D}) \exp(h\widehat{N}) A(z, T). \quad (\text{B.37})$$

The exponential operator $\exp(h\widehat{D})$ can be evaluated in the Fourier domain using the prescription

$$\exp(h\widehat{D})B(z, T) = F_T^{-1} \exp[h\widehat{D}(i\omega)] F_T B(z, T), \quad (\text{C.38})$$

where F_T denotes the Fourier-transform operation, $\widehat{D}(i\omega)$ is obtained from Eq.B.35 by replacing the differential operator $\partial/\partial T$ by $i\omega$, and ω is the frequency in the Fourier domain. As $\widehat{D}(i\omega)$ is just a number in the Fourier space, the evaluation of Eq.B.37 is straightforward. The use of the FFT algorithm makes numerical evaluation of Eq.B.37 relatively fast. It is for this reason that the split-

step Fourier method can be faster by up to two orders of magnitude compared with most finite-difference schemes. To estimate the accuracy of the split-step Fourier method, we note that a formally exact solution of Eq.B.34 is given by

$$A(z + h, T) = \exp[h(\widehat{D} + \widehat{N})] A(z, T), \quad (\text{B.39})$$

if \widehat{N} is assumed to be z independent. At this point, it is useful to recall the Baker-Hausdorff formula for two noncommuting operators \widehat{a} and \widehat{b} ,

$$\exp(\widehat{a})\exp(\widehat{b}) = \exp\left(\widehat{a} + \widehat{b} + \frac{1}{2}[\widehat{a}, \widehat{b}] + \frac{1}{12}[\widehat{a} - \widehat{b}, [\widehat{a}, \widehat{b}]] + \dots\right), \quad (\text{B.40})$$

where $[\widehat{a}, \widehat{b}] = \widehat{a}\widehat{b} - \widehat{b}\widehat{a}$. A comparison of Eqs. (B.37) and (B.39) shows that the split-step Fourier method ignores the noncommutating nature of the operators \widehat{D} and \widehat{N} . By using Eq.B.40 with $\widehat{a} = h\widehat{D}$ and $\widehat{b} = h\widehat{N}$ the dominant error term is found to result from the single commutator $\frac{1}{2}h^2[\widehat{D}, \widehat{N}]$. Thus, the splitstep Fourier method is accurate to second order in the step size h .

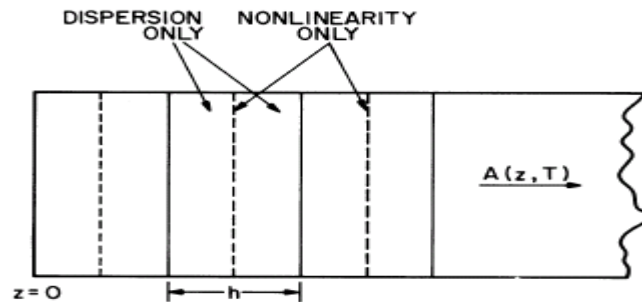


Fig: B.2 Schematic illustration of the symmetrized split-step Fourier method used for numerical simulations. Fiber length is divided into a large number of segments of width h . Within a segment, the effect of nonlinearity is included at the midplane shown by a dashed line.

The accuracy of the split-step Fourier method can be improved by adopting a different procedure to propagate the optical pulse over one segment from z to $z + h$. In this procedure Eq.B.37 is replaced by

$$A(z + h, T) \approx \exp\left(\frac{h}{2}\widehat{D}\right) \exp\left(\int_z^{z+h} \widehat{N}(z') dz'\right) \exp\left(\frac{h}{2}\widehat{D}\right) A(z, T). \quad (\text{B.41})$$

The main difference is that the effect of nonlinearity is included in the middle of the segment rather than at the segment boundary. Because of the

symmetric form of the exponential operators in Eq.B.41, this scheme is known as the symmetrized split-step Fourier method. The integral in the middle exponential is useful to include the z dependence of the nonlinear operator \hat{N} . If the step size h is small enough, it can be approximated by $\exp(h\hat{N})$, similar to Eq.B.37. The most important advantage of using the symmetrized form of Eq.B.41 is that the leading error term results from the double commutator in Eq.B.40 and is of third order in the step size h . This can be verified by applying Eq.B.40 twice in Eq.B.41. The accuracy of the split-step Fourier method can be further improved by evaluating the integral in Eq.B.41 more accurately than approximating it by $h\hat{N}(z)$.

A simple approach is to employ the trapezoidal rule and approximate the integral by

$$\int_z^{z+h} \hat{N}(z') dz' \approx \frac{h}{2} [\hat{N}(z) + \hat{N}(z+h)]. \quad (\text{B.42})$$

However, the implementation of Eq.B.42 is not simple because $\hat{N}(z+h)$ is unknown at the midsegment located at $z+h/2$. It is necessary to follow an iterative procedure that is initiated by replacing $\hat{N}(z+h)$ by $\hat{N}(z)$. Eq.B.41 is then used to estimate $A(z+h, T)$ which in turn is used to calculate the new value of $\hat{N}(z+h)$. Although the iteration procedure is time-consuming, it can still reduce the overall computing time if the step size h can be increased because of the improved accuracy of the numerical algorithm. Two iterations are generally enough in practice.

The implementation of the split-step Fourier method is relatively straightforward. As shown in Fig.B.2, the fiber length is divided into a large number of segments that need not be spaced equally. The optical pulse is propagated from segment to segment using the prescription of Eq.B.41. More specifically, the optical field $A(z, T)$ is first propagated for a distance $h/2$ with dispersion only using the FFT algorithm and Eq.B.38. At the midplane $z+h/2$, the field is multiplied by a nonlinear term that represents the effect of nonlinearity over the whole segment length h . Finally, the field is propagated the

remaining distance $h/2$ with dispersion only to obtain $A(z + h, T)$. In effect, the nonlinearity is assumed to be lumped at the midplane of each segment (dashed lines in Fig.B.2).

The split-step Fourier method has been applied to a wide variety of optical problems including wave propagation in atmosphere, graded-index fibers, semiconductor lasers, unstable resonators, and waveguide couplers. It is referred to as the beam-propagation method when applied to the propagation of CW optical beams in nonlinear media where dispersion is replaced by diffraction.

For the specific case of pulse propagation in optical fibers, the split-step Fourier method was first applied in 1973. Its use has become widespread since then because of its fast execution compared with most finite difference schemes.

Although the method is relatively straightforward to implement, it requires that step sizes in z and T be selected carefully to maintain the required accuracy. In particular, it is necessary to monitor the accuracy by calculating the conserved quantities such as the pulse energy (in the absence of absorption) along the fiber length. The optimum choice of step sizes depends on the complexity of the problem. Although a few guidelines are available, it may sometimes be necessary to repeat the calculation by reducing the step size to ensure the accuracy of numerical simulations. The time window should be wide enough to ensure that the pulse energy remains confined within the window. Typically, window size is 10–20 times the pulse width. In some problems, a part of the pulse energy may spread so rapidly that it may be difficult to prevent it from hitting the window boundary. This can lead to numerical instabilities as the energy reaching one edge of the window automatically reenters from the other edge (the use of the FFT algorithm implies periodic boundary conditions). It is common to use an “absorbing window” in which the radiation reaching window edges is artificially absorbed even though such an implementation does not preserve the pulse energy. In general, the split-step Fourier method is a powerful tool provided care is taken to ensure that it is used properly.

If the only a step h is taken along the waveguide z , then the linear and non-linear components can be treated separately resulting in only a small numerical error. These steps are illustrated in Figure 3.2.

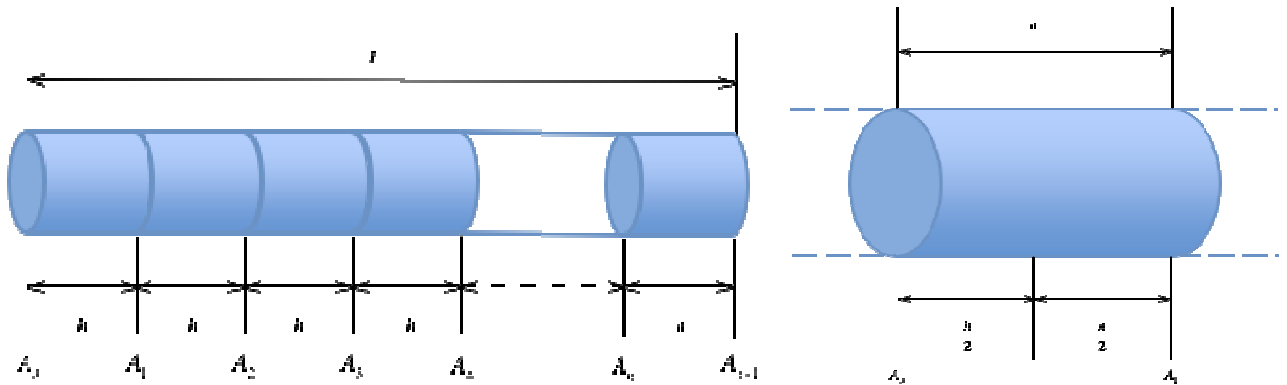


Fig. B.3 Principe of SSFM

In each step in the splits-step method there are three operations, involving the non-linear and linear components. The non-linear transfer function is applied from A_0 to $h/2$, then from $h/2$ to A_1 . The linear transfer function is then applied from A_0 to A_1 . This is illustrated in Figure B.4.

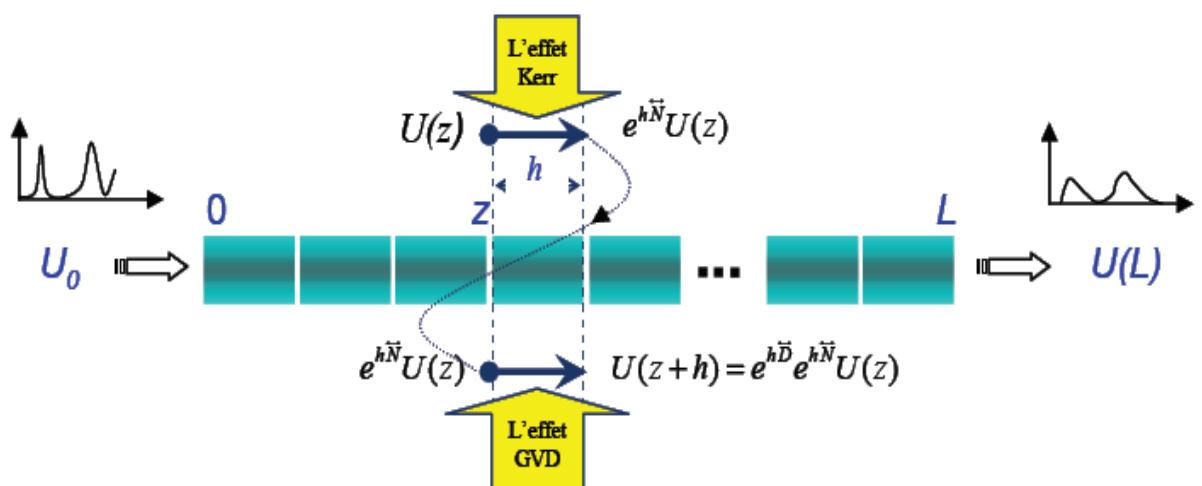


Fig.B.4: method schematization

LISTS OF PUBLICATIONS

Publications Internationale :

1. **Mounir KHELLADI**, Omar SEDDIKI, Fethi Tarik BENDIMERAD. "TIME-FREQUENCY DECOMPOSITION OF AN ULTRASHORT PULSE: WAVELET DECOMPOSITION". Radioengineering journal, April 2008.
2. **Mounir KHELLADI**, Omar SEDDIKI. " Modélisation d'impulsions lasers ultra brèves ». Journal Afrique Science 04 (2) (2008) 167-185 ISSN 1813-548X
3. **Mounir KHELLADI**, Omar SEDDIKI, Fethi Tarik. BENDIMERAD. "Nonlinear Effect of an ultrashort Laser Pulse Propagation in Ti:sapphire Crystal", Journal Computational and Theoretical Nanoscience, July 2009.

Communications Internationale :

1. **M. KHELLADI**, O.SEDDIKI, A.BELAID. « Analyse par ondelettes d'impulsions laser ultra-courtes » Cinquième Conférence Internationale sur la Science des Matériaux (CSM5), Beyrouth-Liban, 17-19 Mai 2006.
2. **M. KHELLADI**, O.SEDDIKI, Fethi Tarik BENDIMERAD, "ULTRASHORT LASER PULSES PROPAGATION IN CHALCOGENIDE FIBER: LINEAR REGIME", International Conference on Materials Informatics and DFT, University Abou Bekr Belkaid, Tlemcen, Algeria 11-13 October 2008.

SIGLES AND ACRONYMS

Sigles and Acronyms

AM : Amplitude Modulation

CW: Continuous Wave

CS₂ : Sulfure de Carbone

DSF : Dispersion Shifted Fiber

DODCI: 3.3'-DiethylOxaDicarboCyanine Iodide

FFT : Fast Fourier Transform

FWHM: Full-Width at Half-Maximum

FWM : Four-Wave Mixing

GVD : Group Velocity Dispersion

GDD: Group Delay Dispersion

He: Ne: Laser Helium Neon

KLM: Kerr Lens Mode-Locking

LASER : Light Amplification by Simulated Emission of Radiation

NLSE : NonLinear Schrödinger Equation

NRZ : Non-Return-to-Zero

NZDSF : Non-Zero Dispersion Shifted Fiber

Nd: YAG: Neodymium: Yttrium-Aluminum Garnet

Nd: YLF: Neodymium: Yttrium Lithium Fluoride

PMD : Polarization Mode Dispersion

SBS : Stimulated Brillouin Scattering

SMF : Single Mode Fiber

SPM : Self-Phase Modulation

SRS : Stimulated Raman Scattering-

SSF : Split-Step Fourier

SESAM: SEMiconductor Saturable Absorber Mirror

TE :Transverse Electric

TM: Transverse Magnetic

TOD: Third Order Dispersion

Ti: Al₂O₃: Titane Sapphire

WB: Wave Breaking

ZDW: Zero-Dispersion Wavelength

Abstract:

Wave propagation in dispersive nonlinear media has become a topic of intense research activities, in part stimulated by its potential application to optical fiber communication systems. Propagation of optical pulses in Titanium Sapphire is mainly influenced by the group velocity dispersion and the refractive index nonlinearity. Rapid progress in ultra short time laser technology has made it possible that optical pulses with durations comparable to the carrier oscillation cycle can be generated. The propagation of such ultra short and intense pulses is then affected by additional physical mechanisms, where especially higher order effects become important. Highly nonlinear operating conditions or the interplay between the different linear and nonlinear effects can result in dramatic changes of the temporal and spectral properties of the pulse.

The propagation of an ultra short pulse is governed by a generalized nonlinear Schrödinger equation (NLSE), which can be derived from the underlying Maxwell equations within the slowly varying envelope approximation. We solve numerically a generalized Schrodinger equation by using a split step Fourier method. Effects such as the impacts of group velocity dispersion (GVD), third order dispersion (TOD), self phase modulation (SPM), wave breaking (WB), self steepening (SS), and intrapulse stimulated Raman scattering (ISRS) are demonstrated in detail. Examples for the above effects are demonstrated, as well as their interplay in the context of soliton propagation. The numerical method therefore presents an advantage tool for describing the ultra short pulse laser propagation in Titanium sapphire.

Keywords: Titanium sapphire, ultra short laser pulse, Generalized Nonlinear Schrodinger Equation, Group Velocity Dispersion, Self Phase modulation, Soliton.